Digital Protection Algorithms for EHV Teed & Multi-Terminal Transmission Circuits

Thesis submitted in partial fulfillment of the requirements
for the award of the degree of

DOCTOR OF PHILOSOPHY

IN

ELECTRICAL ENGINEERING

by

BHUPATIRAJU RAVI KUMAR VARMA

(Roll No: 700738)

Supervisor

Prof. D.V.S.S. Siva Sarma

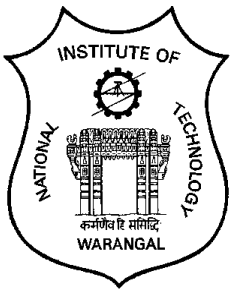

DEPARTMENT OF ELECTRICAL ENGINEERING

NATIONAL INSTITUTE OF TECHNOLOGY, WARANGAL

TELANGANA INDIA

MARCH 2017

DEPARTMENT OF ELECTRICAL ENGINEERING
NATIONAL INSTITUTE OF TECHNOLOGY
WARANGAL

CERTIFICATE

This is to certify that the dissertation work titled **"Digital Protection Algorithms for EHV Teed & Multi-terminal Transmission Circuits",** which is being submitted by Mr. B. Ravi Kumar Varma (Roll No. 700738), is a bonafide work submitted to National Institute of Technology, Warangal in partial fulfillment of the requirements for the award of the degree of **Doctor of Philosophy** in the Department of Electrical Engineering. To the best of our knowledge, the work has not been submitted elsewhere for the award of any degree.

Dr. D.V.S.S. Siva Sarma
(Supervisor)
Professor
Department of Electrical Engineering
National Institute of Technology
WARANGAL, TS, INDIA - 506004

Approval Sheet

This Thesis entitled **Digital Protection Algorithms for EHV Teed & Multi-terminal Transmission Circuits** by BHUPATIRAJU RAVI KUMAR VARMA is approved for the degree of Doctor of Philosophy.

Examiners

_____

_____

_____

Supervisors

_____

_____

_____

Chairman

_____

Date:

Declaration

This is to certify that the work presented in the thesis titled **Digital Protection Algorithms for EHV Teed & Multi-terminal Transmission Circuits** by Bhupatiraju Ravi Kumar Varma is a bonafide work done by me under the supervision of **Prof. D.V.S.S. Siva Sarma** and was not submitted elsewhere for the award of any degree.

I declare that this written submission represents my ideas in my own words and where others' ideas or words have been included, I have adequately cited and referenced the original sources. I also declare that I have adhered to all principles of academic honesty and integrity and have not misrepresented or fabricated or falsified any idea/data/fact/source in my submission. I understand that any violation of the above will be a cause for disciplinary action by the Institute and can also evoke penal action from the sources which have thus not been properly cited or from whom proper permission has not been taken when needed.

_____

(Signature)

BHUPATIRAJU RAVI KUMAR VARMA

(Name of the student)

(Roll No: 700738)

Date: 21-03-2017

Dedication

In the deep loving memory of my mother

Bhupatiraju Lakshmi Narasamma

Acknowledgements

I am extremely grateful to my supervisors **Professor P.V. Ramana Rao and Professor D.V.S.S. Siva Sarma** Department of Electrical Engineering, National Institute of Technology Warangal for their continuous guidance and support during the entire Ph.D. program. Their patience and concern during many confusing situations and tough times helped me to regain strength and optimism. I am profoundly influenced by their philosophical thinking, value systems and simplicity in life.

I would like to extend my heartfelt thanks to **Professor M. Sydulu** for his stimulating and insightful words that made me to choose NITW for my learning. His guidance, support and love throughout helped me to learn many things.

I wish to acknowledge my sincere gratitude to DSC members **Professor V.T. Somasekhar**, Head of the Department, **Professor. B.K. Murthy** and **Dr. C.B. Rama Rao** for their help, feedback, cooperation and encouragement during the course of my PhD work. I also thank all other faculty members of Department of Electrical Engineering for their help and support in my efforts. I consider NITW to be an abode of nice people and academic excellence and I am deeply indebted to NITW for giving me an opportunity to become a member of its family. I would like to express my sincere thanks to my fellow research scholars **Rama Devi, Varaprasad** and all others for their support.

I owe my deep sense of gratitude to the **Management** of **SRKR Engineering College** for their kind support and encouragement. I express my sincere thanks to my students **Kumarraja, Chaitanya, Nagaraju** for their help and support during my thesis work. I would like to extend my heartfelt thanks to my **colleagues at SRKR Engineering College** for their help and encouragement.

With tears in my eyes, I recall my mother late **Lakshmi Narasamma** and father **Ananda Swarupa Varma** for giving me this wonderful life and I am always indebted to them. I would like to express my love and gratitude to my brother **Suri**, **wife Jyothi**, **daughter Manasa, son Rahul** who stood by me with their patience and support. Finally, I

thank all my **relatives**, **friends**, and **well wishers** who helped me directly or indirectly in the successful completion of this work.

B Ravi Kumar Varma
Warangal, March 2017

ABSTRACT

Modern power grids are becoming complex interconnected power systems to facilitate optimal utilization of existing infrastructure and resources. In such grids, the EHV transmission lines carry bulk power and play a vital role in maintaining the grid integrity. Reliable protection of transmission lines involves quick fault detection, identification of the faulted section and fault classification features. In addition, digital line protection systems provide fault location capability also.

A multi-terminal line configuration poses additional protection problems due to non-availability of measurements at tap points. Traditional protection schemes for EHV three-terminal circuits are complex and the relaying speed of these schemes is not adequate to meet the requirements of the modern power grids. Fault location procedures become complex due to multiple sources feeding a fault and superimposed reflections of the fault signals. Further, the measurements taken from various terminals are generally unsynchronized and it is expensive to provide GPS based synchronization at all terminals. Therefore, high speed protection and accurate location are of significance. Transient based protection is an alternative approach suitable for high-speed fault clearance.

In this thesis work, new classification and location algorithms are developed for protection of teed (three-terminal) and multi-terminal transmission circuits which use new and simple transient based fault detection procedures. A transient based fault classification algorithm using Wavelet Transform for teed circuits is developed and a probabilistic neural network (PNN) classifier is added to improve its performance with double-line to ground faults.

Also, a hybrid fault location procedure for teed circuits using transients and Modified DFT Phasor Estimation is presented followed by a novel travelling wave based fault location scheme using S-Transform & ANNs. The above proposed hybrid method is extended to an EHV multi-terminal circuit with four terminals. Finally, a non-iterative fault Locator for general multi-terminal transmission lines using unsynchronized measurements is also proposed. Simulation results are presented to validate the performance of all the proposed techniques.

Table of Contents

List of Figures

List of Tables

List of Abbreviations

ANN	:	Artificial Neural Network
EHV	:	Extra High Voltage
GPS	:	Global Positioning System
PNN	:	Probabilistic Neural Network
DFT	:	Discrete Fourier Transform
SVM	:	Support Vector Machine
NETE	:	Normalized Effective Transient Energy
WAMS	:	Wide Area Measurements Systems
NERC	:	North American Electricity Reliability Council
TW	:	Travelling Wave
CT	:	Current Transformer
PT	:	Potential Transformer
AI	:	Artificial Intelligence
WSE	:	Wavelet Singular Entropy
FIA	:	Fault Inception Angle
FSEI	:	Fault Section Energy Index
DWT	:	Discrete Wavelet Transform
GRNN	:	Generalized Regression Neural Network
PMU	:	Phasor Measurement Unit
STFT	:	Short Term Fourier Transform
ST	:	S-Transform (Stockwell-Transform)
PDF	:	Probability Density Function
GVA	:	Giga Volt Amperes
MRA	:	Multi Resolution Analysis

List of Symbols

R_f	: Fault resistance	V_a, V_b, V_c	: Phase voltages
θ	: Fault inception angle	I_a, I_b, I_c	: Phase currents
δ	: Synchronization angle	ψ	: Transient energy
υ	: Wave propagation velocity	$h(n)$	: High pass filter
$D1$	: First level wavelet detail coefficients	$l(n)$	: Low pass filter
$W(a,b)$	: Continuous Wavelet Transform	Δt	: Sampling time
V_m	: Modal voltage	$TT(t,\tau)$	: Time-time transform
x	: Fault distance	$S(\tau, f)$	: S-transform
σ	: Smoothing parameter	$\|h(x)\|_p$	: p norm of a function
γ_k	: Modal propagation constant	Ψ_a, Ψ_b, Ψ_c	: NETE of phase voltages
Z_{0k}	: Modal surge impedance	$\Psi_{ab}, \Psi_{bc}, \Psi_{ca}$	: NETE of line voltages
R_0	: Zero sequence resistance	Z_{app}	: Apparent impedance
R_1	: Positive sequence resistance	Z_m	: Mutual Impedance
L_0	: Zero sequence inductance	Z_c	: Characteristic Impedance
L_1	: Positive sequence inductance	V_1	: Ground mode voltage
C_0	: Zero sequence capacitance	V_2, V_3	: Aerial mode voltages
C_1	: Positive sequence capacitance	$\Delta Q12$	: Change in reactive power
ω_0	: Fundamental frequency of the system	t_1, t_2, t_3	: Wave arrival times
V_d	: Direct axis voltage	I_{DFT}^{odd}	: Odd sample DFT
V_q	: Quadrature axis voltage	I_{DFT}^{even}	: Even sample DFT
τ	: Time constant of decaying dc	V_S	: Sending end voltages
Ψ_0	: NETE of zero sequence voltage	V_R	: Receiving end voltages
$f_A(X)$	: Probability density function	V_F	: Fault point voltages
$V_{A\Delta 1}$	: Incremental positive sequence voltage	T	: Clark's Transformation matrix

Chapter 1

Introduction

Electrical power has become an essential need for human beings. Economic prosperity, national security, and standard of living depend on reliable electric power systems [1]. An electric power system is expected to supply uninterrupted quality power to consumers economically with minimal environmental impact. Over the years, a steep increase in demand for electrical power due to rapid urbanisation and technological advancements created many complex interconnected power systems all over the world. These modern power grids face many challenges as they are forced to operate with optimal utilisation of existing resources and infrastructure. Economic reasons and stringent environmental regulations make it very difficult to add new power stations and transmission lines to meet the growing demand. An ever increasing and inevitable penetration of unpredictable and intermittent renewable sources like wind and solar will also pose new challenges to grid control and management. Also, significant power exchanges between regions triggered by open access and flexibility in the frequency of operation lead to complex operating scenarios like line overloading, voltage variations, inter-area oscillations. Under such complexities, carrying out security assessment on real time basis and responding to contingencies are critical for maintaining reliability and stability of the grid.

The occurrence of major blackouts in many major power systems around the world has shown the need for making existing grids safe, reliable and efficient to avoid huge economic losses. Recent advances in measurement, communications and analytic technologies have created a range of new options for improving such grids. The goal of such improvements is to make the power system less immune to catastrophic failures and to reduce the severity of after effects.

The power system operation is controlled by a mix of automatic feedback and manual control actions. Power system operation and control have become more complex, although it is aided by technologies like power electronics, computers and communications. Optimal utilisation of existing resources implies that system operation with large security margins will not be acceptable. This means that system operation will have to rely more on automation using adaptive estimation and control than on human experience. The recently evolving technologies like Wide Area Measurement Systems (WAMS) and advanced power electronics

are going to impact power system operation and control immensely. In particular, WAMS have the ability to address not just immediate reliability concerns but also other issues like enhancing real-time power transfer capability, advanced automatic corrective actions like adaptive islanding, power swing blocking/unblocking functions of distance relays, better visualisation through state measurements, decision support tools etc. However, to apply these new technologies optimally, there is a need to develop appropriate analytical tools.

1.1 System Components and Protection

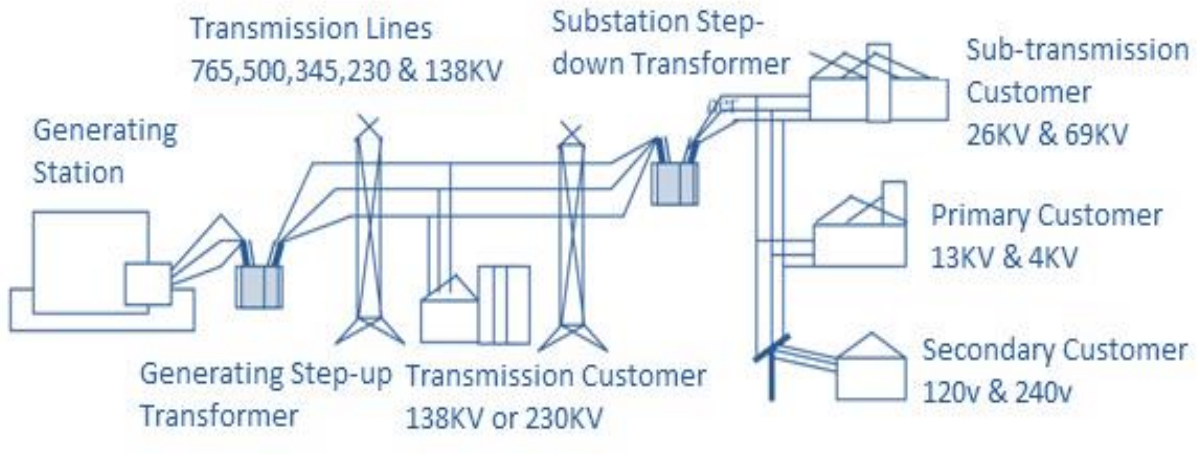

Fig. 1.1 A typical power system.

A typical power system as shown in Fig.1.1 contains many components like generators, transformers, transmission lines, distribution lines and loads that consume the generated power. Significantly, induction motors are the main loads in distribution and industrial power systems. Other power system equipment includes reactors, buses and capacitors. Most of this equipment undergoes abnormalities in their operating lifetime due to various reasons. For example, a worn out bearing may lead to overloading of a motor. A fallen or touching tree may cause a fault on overhead lines and a lightning strike can cause insulation failure. Also, the breakdown of insulators may occur due to environmental pollution. Under or over-frequency of a generator may cause mechanical damage to turbines which leads to tripping of an alternator. Therefore, it is necessary to contain these abnormal operating situations for the safety of the equipment as well as operating personnel. Hence, it is necessary to isolate and de-energize the faulty equipment. To conclude, the power system has to be monitored to protect it from abnormal operating conditions and this task is assigned to protective relaying schemes. It encompasses both apparatus protection and system protection.

Apparatus protection deals with fault detection in the apparatus and subsequent protection. System Protection is the art and science of detecting problems with power system components and isolating these components. It is concerned with the detection of system's proximity to the unstable region of operation and necessary control actions to restore stability and avoid damage to equipment. Control actions associated with system protection may be classified into preventive or emergency control actions. Further, loss of system stability may lead to partial or complete system blackouts. Different techniques employing under-frequency relays, out-of-step protection, islanding systems, the rate of change of frequency relays, reverse power flow relays, voltage surge relays etc. are used for system protection. Recently, Wide Area Measurement (WAM) systems are also being deployed for system protection by utilising modern communication facilities.

1.2 Transmission Line Protection and Fault Location

Modern power systems consist of thousands of high voltage transmission lines transmitting electrical power between generators and load centers. Major transmission line construction is of overhead type and therefore, is easily susceptible to various transient and permanent faults. These faults can lead to damage of the line itself and can cause power system instability. It is of the utmost importance that protective relay systems are capable of clearing all faults within the stipulated time, and exhibit a high degree of dependability and security. In the case of permanent faults, the line needs to be restored quickly by locating the fault accurately to make repairs.

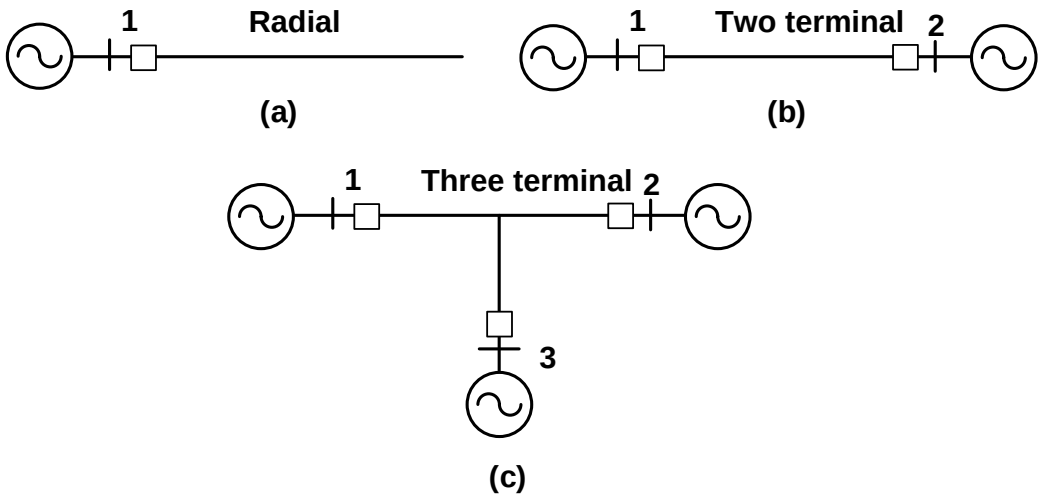

Fig. 1.2 Three types of line configurations. (a) Radial (one-terminal) (b) Two-terminal (c) Three-terminal

In practice, three types of line configurations are used within the power networks as shown in Fig.1.2 including radial (one-terminal), two-terminal, and multi-terminal type of which three-terminal (teed) is the most frequently encountered type.

Three-terminal and other multi-terminal line configurations are generally a compromise between economy and protection complexities which sometimes lead to reliability problems. There is an economic benefit in the construction of three terminal lines because it avoids the expense of a substation and typically reduces the transmission line miles. Also, there are other factors which influence the decision to configure a transmission line with three terminals such as right-of-way constraints, lead time and regulatory approvals.

A reliable transmission line protection scheme is expected to detect the internal faults precisely so that only the faulted line will be isolated and identify the exact fault type so that advanced single-pole tripping and reclosing procedures can be initiated [2]. The reliability of these two functions is very important for reducing the impact of faults on system stability.

The traditional line protection schemes use fundamental frequency components of the transient fault voltage and current signals and these schemes can be classified into two categories: Non-unit protection and Unit protection. The non-unit protection schemes use measured signals from one end of the transmission line whereas the unit protection schemes usually take data from many ends. The non-unit protection such as distance relay fails to protect the entire length of the line because it can not differentiate between internal and external faults occurring near zone boundaries. The unit protection such as pilot relaying requires a communication link to exchange the blocking or transfer tripping signals. In such schemes, the protection reliability highly depends on the reliability of the communication link. The fault type classification is also traditionally based on fundamental frequency components.

In view of the high-speed requirements of Extra High Voltage (EHV) transmission lines, Travelling Wave (TW) theory based techniques have been developed. These TW based relays can respond well within 5 ms whereas phasor based relays take at least half cycle time. In recent times, another new technique using high-frequency components of the fault generated transient signals is explored by several authors to improve the protection of lines. The principal goal of all these approaches is to quickly detect the internal fault and classify the fault accurately for possible single-pole tripping.

Another important aspect of line protection schemes is the fault location facility. Modern digital relays provide this additional feature to accurately locate the fault so that the repair crew can immediately reach the place of fault to restore service. Many fault location schemes are developed over the past few decades by applying different principles like fault loop impedance approach and travelling waves. The algorithms used in many techniques take measurements from multiple ends of the lines for accuracy in fault location.

Protection algorithms for teed and multi-terminal lines are further complicated because of lack of measurements at the tap points and multiple sources feeding the faults. In this thesis, work is done for improvements in the accuracy of fault classification and location in particular reference to teed and multi-terminal transmission circuits.

1.3 Protection Issues with Teed and Multi-terminal Lines

As per the NERC blackout report [3], most of the lines that tripped just before the cascade tripping were three-terminal lines. The three-terminal line configuration poses many challenges to conventional protection schemes like distance relaying, differential relaying. In the case of distance relaying, the third terminal causes under-reach for line faults beyond the tap point due to in-feed as shown in Fig.1.3.

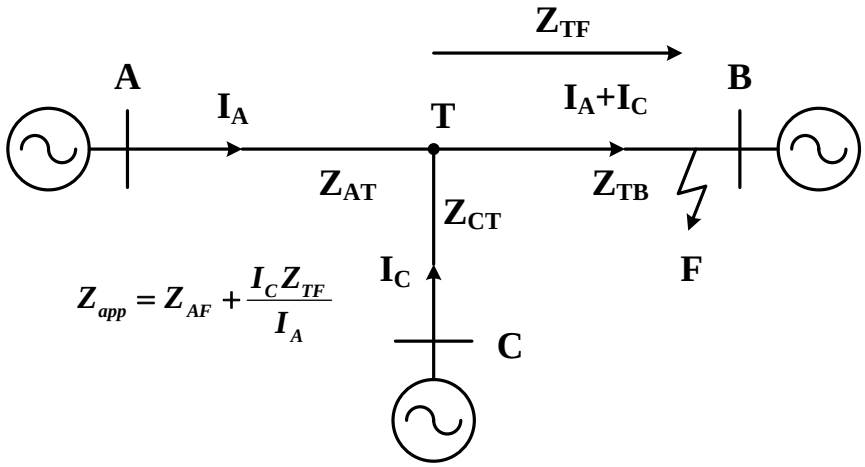

Fig. 1.3 Under-reach problem due to in-feed

On the other hand, an outfeed condition creates an overreaching problem for the distance relay. Therefore, the stepped-distance relaying for the protection of three-terminal line cannot provide simultaneous fault clearing at all terminals. The limitation of stepped-distance relaying for the protection of three-terminal line is overcome by using communication assisted distance protection schemes such as Direct Under-reaching Transfer

Trip (DUTT), Permissive Overreaching Transfer Trip (POTT) and Directional Comparison Blocking (DCB). The current differential scheme is also used for the protection of three-terminal lines which has faster response, but the scheme may fail if an outfeed condition arises due to an internal fault.

Travelling wave based schemes developed for three terminal lines also face difficulties because of multiple reflections between t-point, fault point and line terminations. Such reflections cause severe distortions in voltage and current waveforms at the line ends. The protection issue of three-terminal lines is further compounded if branch lengths are unequal. In an effort to overcome the difficulties with conventional methods and achieve high speed relaying, a third approach is developed which is based on the high-frequency components of measured voltage and current signals. Unlike conventional phasor based methods, the transient based schemes implemented in digital relays use short fault data windows to detect and classify faults quickly.

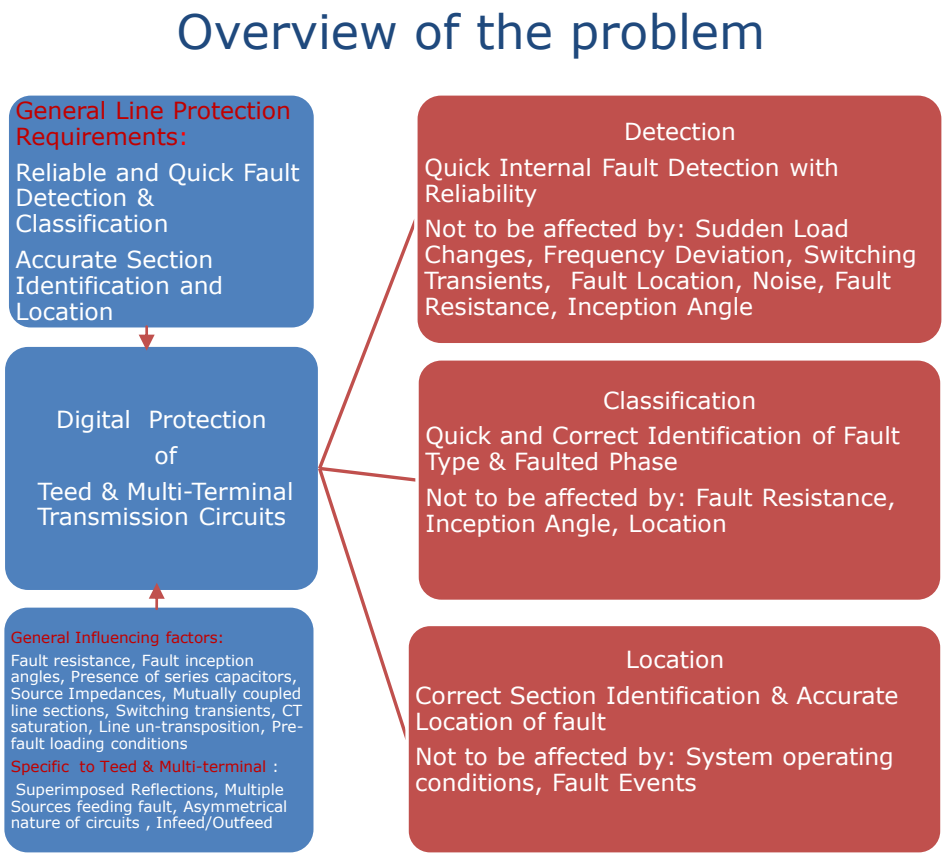

Fig. 1.4 Overview of the problem

Considering the fault location issues, the three terminal lines pose additional difficulties while extending techniques developed for two-terminal lines because of infeed/outfeed from the third terminal. The faulted leg needs to be identified first in such lines for finding the exact location within it. The multi-terminal line protection faces similar challenges as it contains many taps without measurements and multiple sources feeding the fault. Fault location is made further difficult when compared to three-terminal lines as it requires complex procedures to identify the faulted section. The above diagram (Fig.1.4) shows the overall view of the protection problems with teed and multi-terminal transmission circuits.

1.4 Literature Survey and the State of Art

A literature survey is presented in this section on three terminal Lines (Teed) and multi-terminal lines. With an initial briefing of the earlier traditional works till the year 2000, details of the subsequent contributions of different authors are presented for identifying current issues of concern.

1.4.1 Three-terminal Lines

In 1986, Agarwal and Johns [4] presented a Current differential scheme for the protection of three-terminal lines and it has faster response and is free from problems associated with a power swing. They developed another differential scheme [5] that uses both voltages and currents with emphasis on minimising the number of communication channels. In 1991, Aggarwal et al. [6] designed a microprocessor based current differential relay for EHV teed feeders. A high-speed digital signal processor is used for hardware implementation. The relay performance showed immunity to the outfeed, CT saturation and insensitive to variation in fault resistance.

In 1992, Girgis et al. [7] presented a fault location technique for three-terminal lines by computing the fundamental phasors. It was shown to be insensitive to fault resistance & source impedance variation and independent of fault type. The method considered synchronisation errors also. In 1993, Aggarwal et al. [8] developed a fault locator that utilises fault voltages and currents from all ends. It is based on superimposed components and modal transformation. The technique is insensitive to variations in fault resistance, source impedance, line configurations including line un-transposition. High performance is achieved with simulation results by considering transducer and hardware errors. In 1996, Carter et al.

[9] described a non-unit protection scheme for three-terminal lines by using fault generated high-frequency signals. The high-frequency signals are extracted by using a stack tuner and line trap which are tuned to the frequency band of 70-81 KHZ. The scheme performance shows its ability to discriminate between internal and external faults clearly. The results are not influenced by factors such as fault position, fault type and fault inception angle.

In 2002, Lin, Liu & Yu [10] proposed a fault locator for three-terminal lines by using synchronised voltage and current phasors from two ends only. Firstly, superimposed positive sequence quantities are used as inputs to identify the faulted leg and then both superimposed positive sequence quantities & post-fault positive sequence quantities are applied to locate a fault on a specific leg. This method requires synchronised measurements and fault type information.

In 2005, M.M. Eissa [11] proposed a scheme for EHV three-terminal lines by using wavelet transform. Haar basis function is applied to discriminate the polarities at each terminal and only one relay instead of two is located at the terminal that has two circuits as shown in Fig.1.5. The fault is detected by checking the difference between the pre-fault and post-fault values of the currents against a threshold. The relay at each end is identified as a tripping or blocking terminal. The technique is claimed to be effective for solving the problems of outfeed condition, no feeding at bus and high resistance faults. But, the details of simulation and results are not presented to justify the claims.

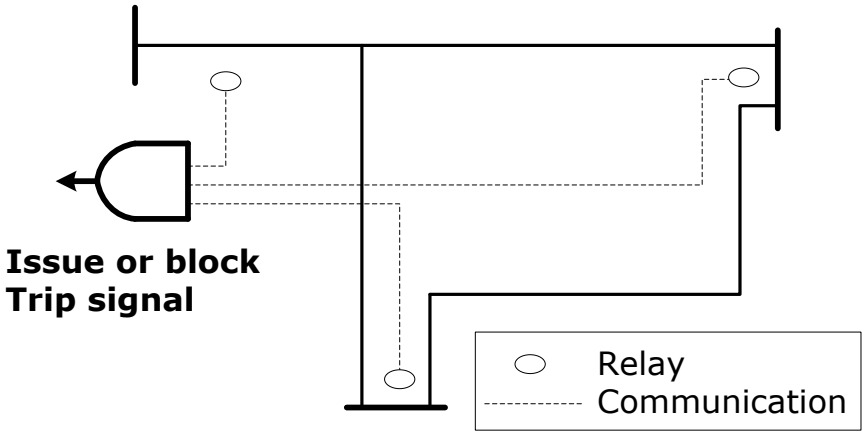

Fig. 1.5 Haar Wavelet transform based relaying scheme

In 2005, Evrensoglu and Ali Abur [12] presented a fault location method for teed circuits which is based on travelling waves. By processing the unsynchronized voltage measurements from all ends, the arrival times of travelling waves are calculated with wavelet transform. The technique is shown to be insensitive to the presence of series capacitors protected by MOV, random errors and mutual coupling. The location procedure includes

Clark modal transformation and the accuracy of the algorithm is proportional to the sampling frequency.

Due to coupling between capacitance and inductance effect of multiphase systems the travelling wave phenomenon is complicated. In such systems, mutual impedances between conductors influence the behavior of transients. By using modal transformation, the three phase system can be decoupled into three single phase system. Clark's transformation is generally used for fully transposed transmission lines

The phase voltage and currents in a three phase system can be expressed as

$$V_{ph} = T.V_m \tag{1.1}$$

$$I_{ph} = T.I_m \tag{1.2}$$

The transformation matrix T is given by

$$\begin{bmatrix} V_0 \\ V_1 \\ V_2 \end{bmatrix} = \frac{1}{\sqrt{3}} \begin{bmatrix} 1 & 1 & 1 \\ \sqrt{2} & -\frac{1}{\sqrt{2}} & -\frac{1}{\sqrt{2}} \\ 0 & \frac{\sqrt{3}}{\sqrt{2}} & -\frac{\sqrt{3}}{\sqrt{2}} \end{bmatrix} . \begin{bmatrix} V_a \\ V_b \\ V_c \end{bmatrix} \tag{1.3}$$

Where V_0 is a ground mode voltage, V_1, V_2 are aerial mode voltages. V_a, V_b and V_c are phase voltages.

The series impedance matrix of the transmission line is

$$Z = \begin{bmatrix} Z_{aa} & Z_{ab} & Z_{ac} \\ Z_{ba} & Z_{bb} & Z_{bc} \\ Z_{ca} & Z_{cb} & Z_{cc} \end{bmatrix} \tag{1.4}$$

The voltage and current are related to each other

$$V_{ph} = Z.I_{ph} \tag{1.5}$$

Using Transformation matrix T

$$T.V_m = Z_{mod}.T.I_m \tag{1.6}$$

$$V_m = T^{-1}.Z_{mod}.\ T.I_m == Z_{mod}.\ I_m \tag{1.7}$$

The Z_{mod} has the following form

$$Z_{mode} = \begin{bmatrix} Z_s + 2Z_m & 0 & 0 \\ 0 & Z_s - Z_m & 0 \\ 0 & 0 & Z_s - Z_m \end{bmatrix} \tag{1.8}$$

Where Z_s ($Z_s = Z_{aa} = Z_{bb} = Z_{cc}$) and Z_m ($Z_m = Z_{ab} = Z_{bc} = Z_{ac}$) are the self and mutual impedances of the line respectively.

The post-fault three-phase voltage signals of one cycle duration are transformed into their modal signals by using Clark's model. The first mode (mode-0) referred to as the ground mode is significant only during faults having a path to ground. The second mode (mode-1) and a third mode (mode-2) are known as the aerial modes which are present for any kind of fault. These modal signals are decomposed into low and high-frequency components using wavelets.

The flowchart shown in Fig.1.6 describes the overall procedure. The faulted line segment is identified by comparing the magnitudes of the squares of wavelet transform coefficients (WTC^2) of the aerial mode voltages for un-grounded faults and ground mode voltages for grounded faults at each terminal as shown in the flow chart. In the flow chart, A_i is the maximum of scale1, mode2 for ungrounded faults and scale1, mode0 for grounded faults. Identification of faulted section is carried out by comparison of A_i from all terminals.

The fault location for teed circuit is given as $x_i = \frac{(L(j)+L(i))-(v*(t(j)-t(i)))}{2}$,

where i=1, 2, 3 terminals, x_i is the fault distance in i^{th} section, L_j & L_i are the total line lengths of the faulted and un-faulted section, t_j & t_i are arrival times of the backward and forward travelling waves of un-faulted section and faulted line section, and v is the travelling wave velocity.

The algorithm is shown to be very accurate and unaffected by the presence of series capacitors and mutual coupling. However, this method requires high sampling rate and is influenced by low fault inception angles. Simulation results for effects of fault resistance and FIA are also not reported in the paper.

As per 2006 NERC report [3], the protection problems with three-terminal lines include Transmission line relay loadability, Sequential clearing for transmission line faults, Compromises in the ability of the protection to detect faults, Compromises in relay coordination between the three-terminal line protection and the protection of adjacent facilities. Increased complexity of associated communications system, susceptibility to false tripping for heavy transient loading conditions and stable power swings are other issues of importance. Communication assisted protection schemes like DUTT, Permissive Overreach Transfer Trip (POTT) and Directional Comparison Blocking (DCB) are found to be effective for three-terminal line protection.

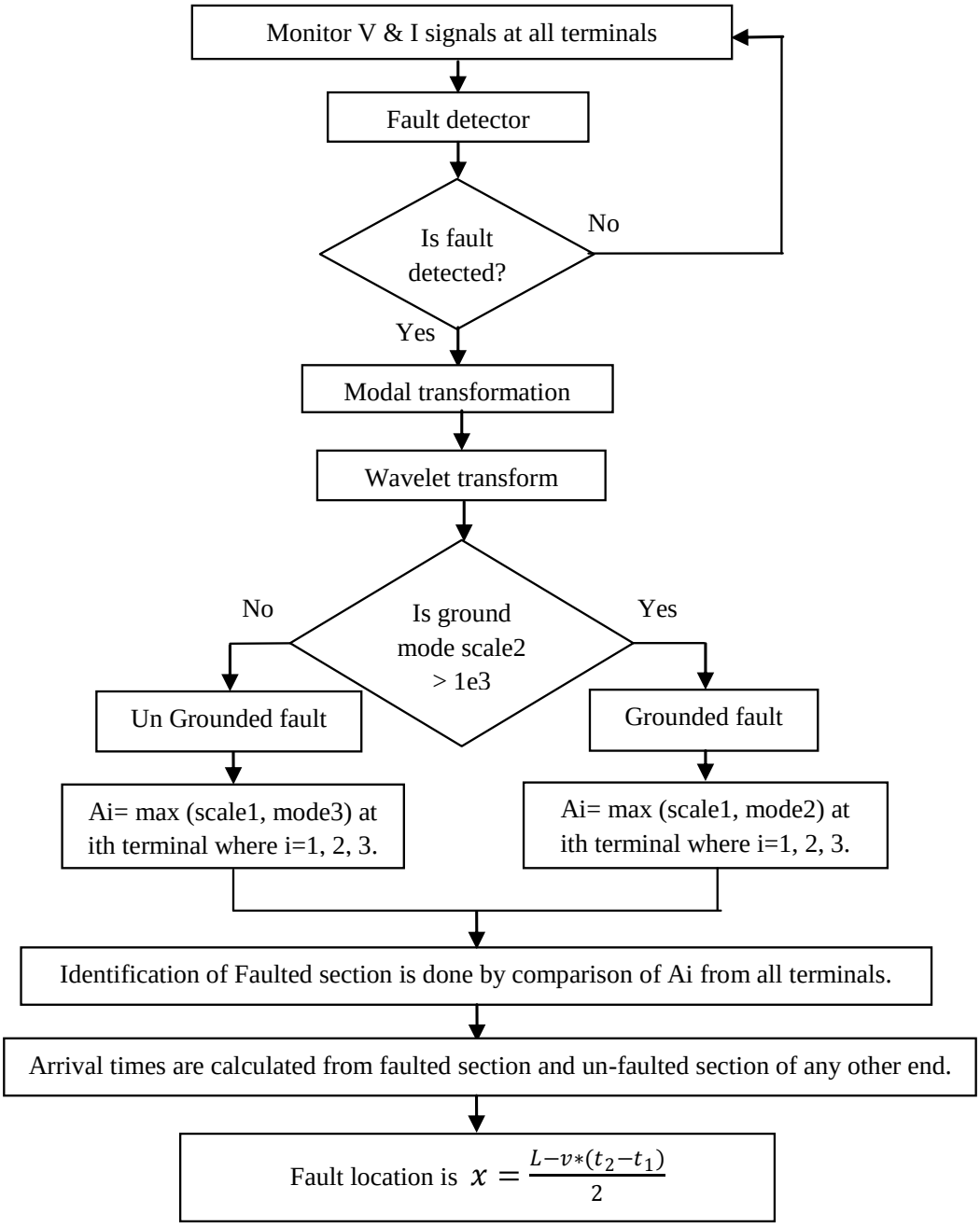

Fig. 1.6 Flow Chart for Fault Location using Travelling Wave based method

In 2007, a fault location method for current differential relays in three-terminal lines is proposed by Jan Izykowski et al. [13]. Three phase currents from all ends and a three-phase voltage signal from the local end are used as inputs to the locator. Using generalised fault-loop models, a set of three routines are formed and a valid routine is selected to identify the faulted section. Simulation results showed very high accuracy under different fault conditions. An elimination procedure is incorporated by considering section range, fault resistance and source impedance. Fig.1.7 shows the scheme of the fault locator using current differential

relays. The technique is suitable for three terminal lines protected by current differential relays and CT saturation leads to large errors.

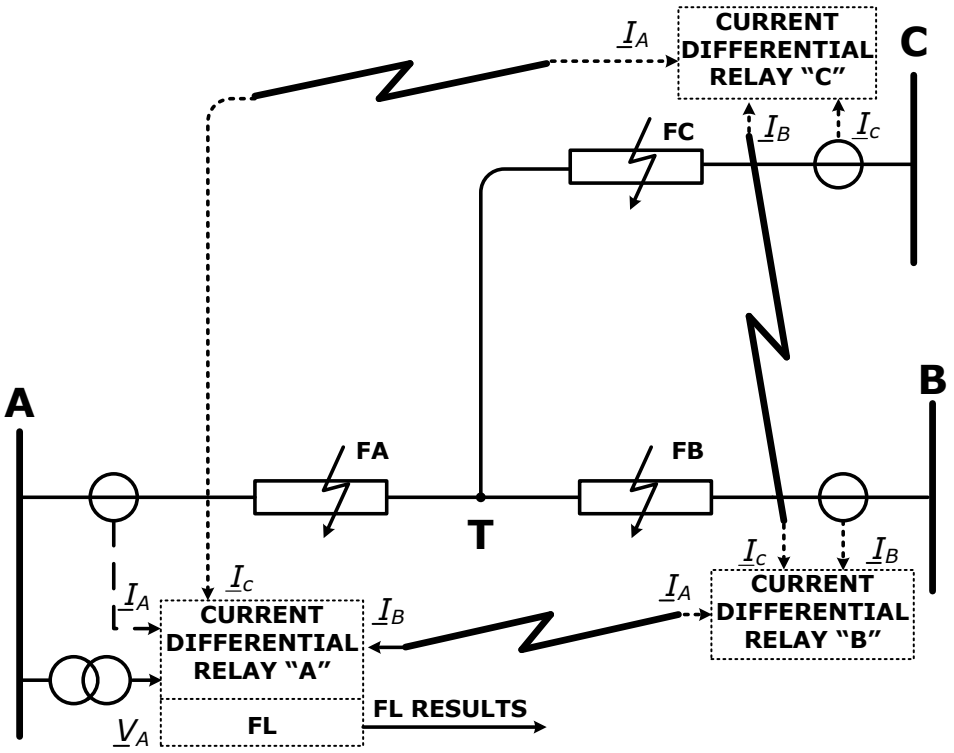

Fig. 1.7 Fault Locator using Current Differential Relays

In 2008, Silva et al. [14] presented a hybrid fault location method which is based on wavelet transform. The method uses either travelling wave theory or impedance calculation for locating the fault. A choice is made between the two depending on the signal noise level. In the case of higher noise level (less than 60 dB), impedance to fault method is activated to avoid errors with travelling wave approach. Otherwise, a two-ended travelling wave approach is activated. Fig.1.8 depicts the algorithm used by this hybrid method of fault location. Simulation results presented included the performance of the scheme with varying fault conditions and noise levels. A disadvantage of this method is less accuracy due to the application of SWT for phasor estimation.

In 2008, Bhalja and Maheshwari [15] developed a Current differential protection scheme by employing Wavelet transform. In this scheme, the operating and restraining quantities at each terminal are derived from the third level reconstructed signals using WT. The performance studies of the technique revealed the effectiveness in dealing with several difficult cases like out-feed condition, high resistance faults, weak in-feed. But, the method is not verified for variation in fault inception angle and double line to ground faults. As WTMM

(wavelet transform modulus maxima) is used for fault detection, the performance of the scheme is not guaranteed for all types of faults.

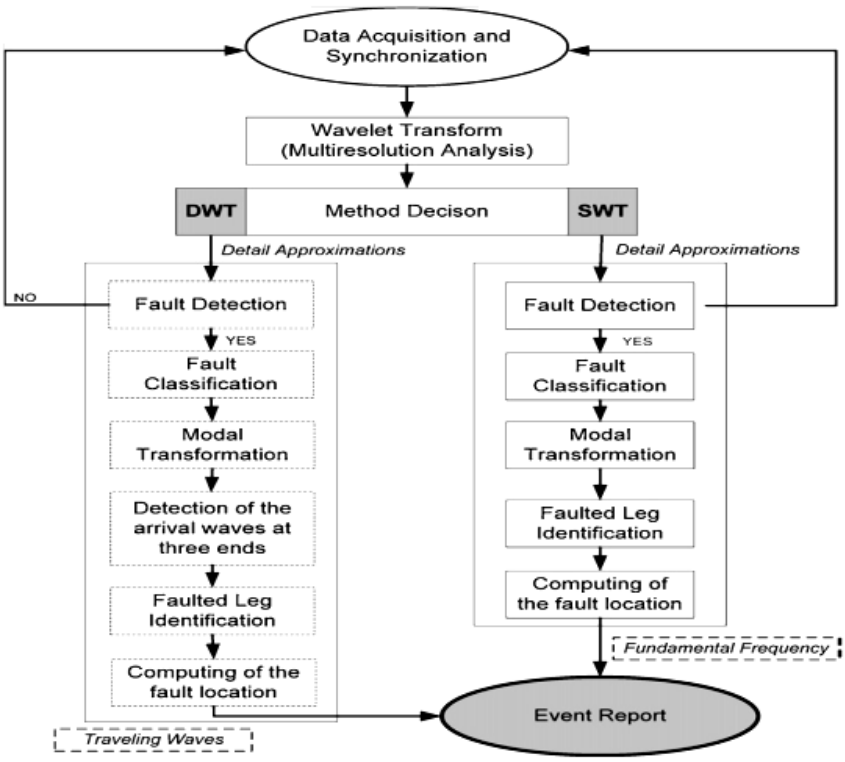

Fig. 1.8 Hybrid Fault Locator

In 2009, M.M. Eissa [16] presented a new scheme for tapped feeder based on directional relaying principle. Clear discrimination between forward and reverse faults is achieved in the case of weak sources, no feeding sources and feed around paths. The scheme uses pre-fault voltage & current signals and two directional quantities are formed at buses with two circuits.

In 2013, Jafarian and Sanaye Pasand [17] presented a protection scheme for the three-terminal line by using high-frequency transients. The measured current signals are decomposed into different frequency bands using wavelet transform. Based on the frequency spectrum, the SVM is used to classify internal and external faults. Performance studies show that the polynomial SVM classifier is most accurate and immune to noise. Line traps are installed at the transmission line ends to confine the high-frequency transients to the protected line as shown in Fig.1.9. The CT and fault arc models are used in evaluating the performance of the scheme. But, while training the SVM, fault inception angles in the range of 10-90 degrees only considered. This creates problems with a double line to ground faults. The scheme performance for internal faults with low inception angles is also not justified.

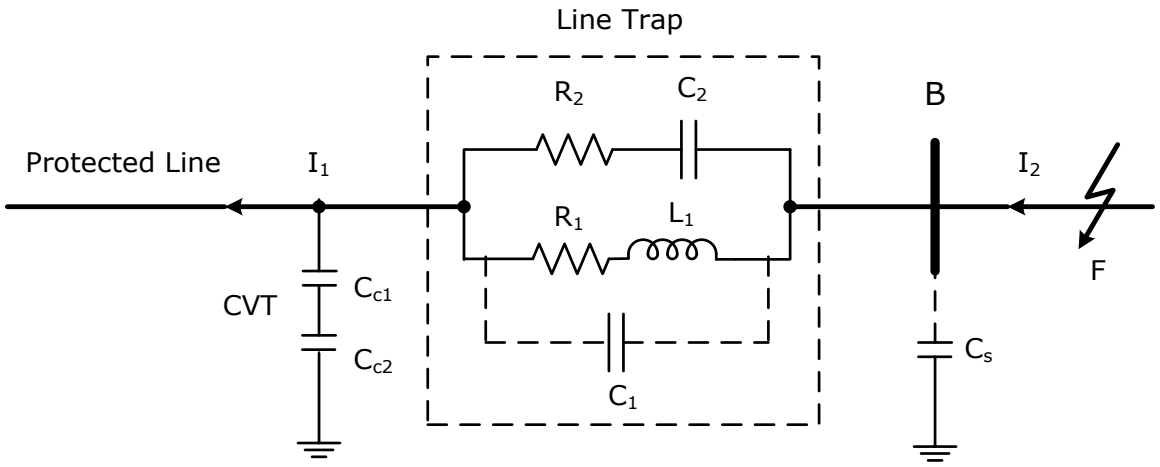

Fig. 1.9 Line Trap used in SVM-based scheme [17]

In 2013, Khodadadi and Shahrtash [18] proposed a non-communication protection scheme shown in Fig.1.10 for three-terminal lines by using Mathematical Morphology-based filters. The transient based technique is designed to discriminate the internal and external faults by using the high-stop filtering property of bus bars. The fault induced transients are successively processed by three MM-based filters and transients due to lightning or switching are prohibited from influencing the approach. The presented technique is applied to one of the three-terminal lines of Iran's transmission grid and the performance results claimed simultaneous operation of CBs at all terminals with high reliability. This method disadvantage is it requires the setting of four thresholds depending on the line under consideration and a sampling rate of 1 MHz.

In 2013, Hanif Livani and Cansin Yaman [19] presented a fault classification and location technique using Support Vector Machines (SVM). The DWT is applied to extract the features from voltage signals and these are given as input to SVM for classification and fault line/half identification. Then the fault is located by a travelling wave based approach. The performance of the technique is tested for different fault conditions by considering variation in fault resistance, FIA, fault location, loading levels, non-linear high impedance faults and non-typical faults.

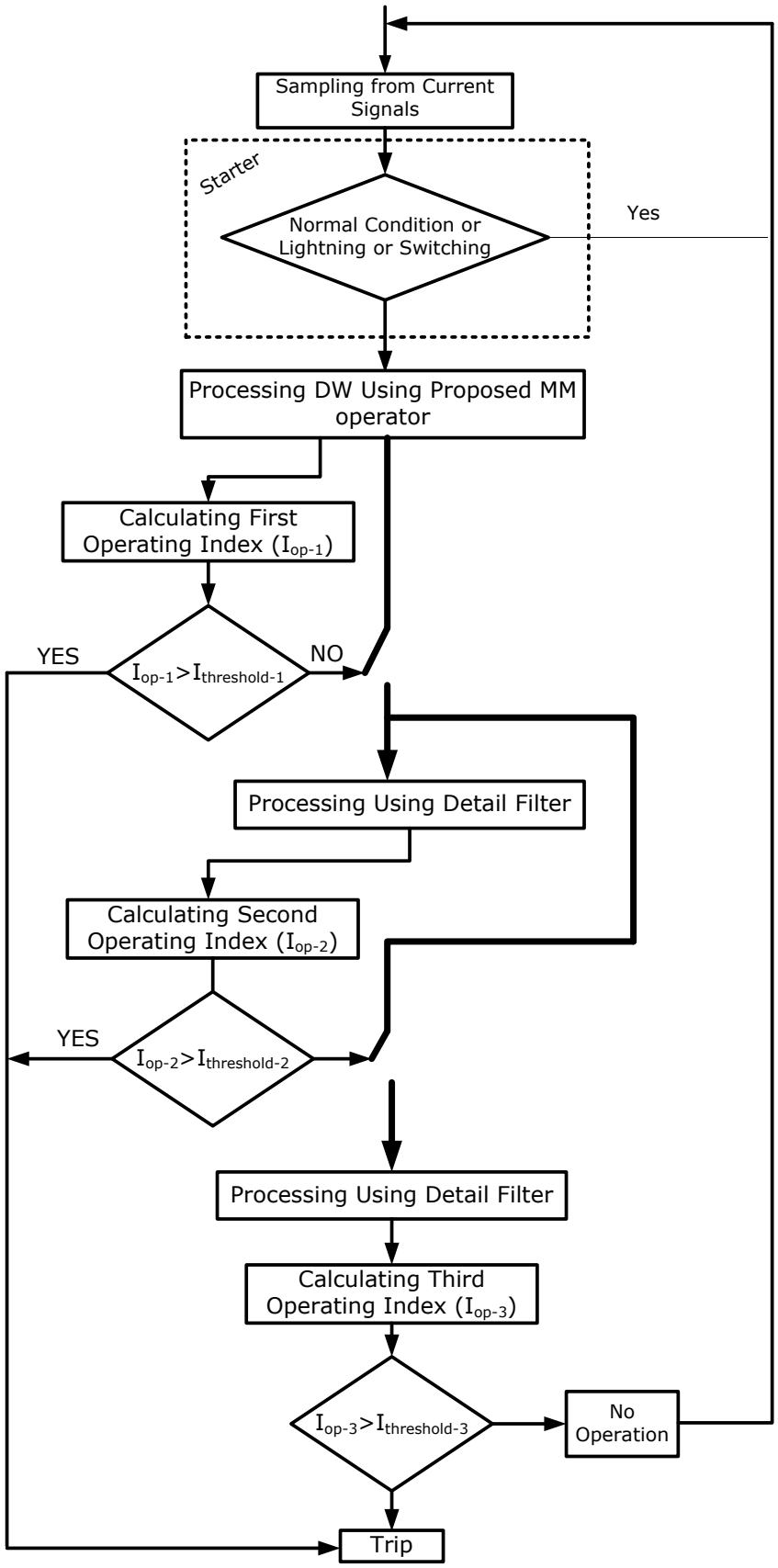

Fig. 1.10 A non-communication protection scheme using Morphology-based filters

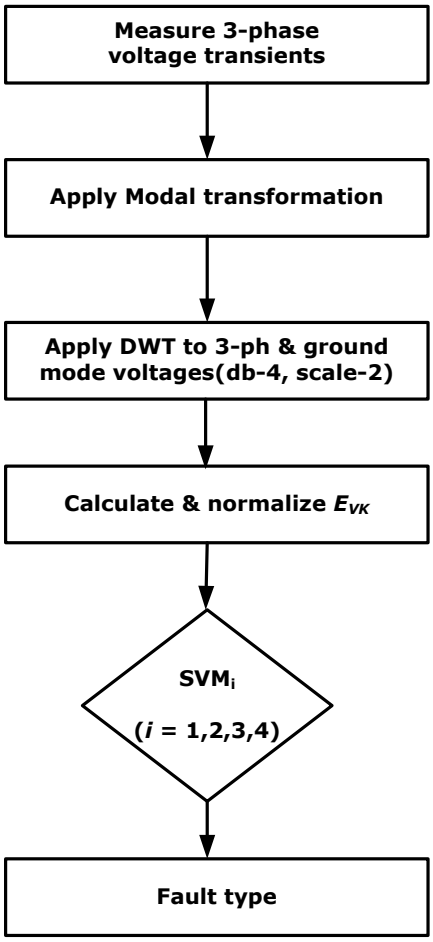

Fig. 1.11 SVM-based Classification algorithm

The discrete wavelet transform (DWT) is applied to transient voltage signals for extracting distinguishing features for fault classification. DWT processes a 40 ms fault voltage signal window for finding wavelet transform coefficients from which normalised wavelet energies are calculated. These features are then given to a set of four support vector machines (SVMs) for identifying fault type and faulted phase as shown in Fig.1.11. After determining the fault type, another set of SVMs is used for to determine the faulty line and the faulted half within that line. Finally, the fault is located by using arrival times of travelling waves with a single ended method. However, its poor performance with high resistance faults and overall accuracy of 90.3% in fault type classification and 95% accuracy in identifying faulty lines with grounded faults is not acceptable.

In all travelling wave based algorithms, extraction of wave arrival times plays a crucial role in location accuracy. Signal processing with wavelet transform is widely used for this purpose and recently Time-time transform & S-transform have been explored to find the arrival times accurately. A Time-time (TT) transform based algorithm is recently proposed by [20] to locate faults in single and double circuit three-terminal lines. The TT-transform is

claimed to be computationally efficient and capable of amplifying high-frequency components. Unlike wavelet transform, it requires no basis function or level setting. In this technique, the three-phase currents measured at the three ends are transformed by Clarke's transformation and then TT-transform is applied to detect the fault and find the wave arrival times.

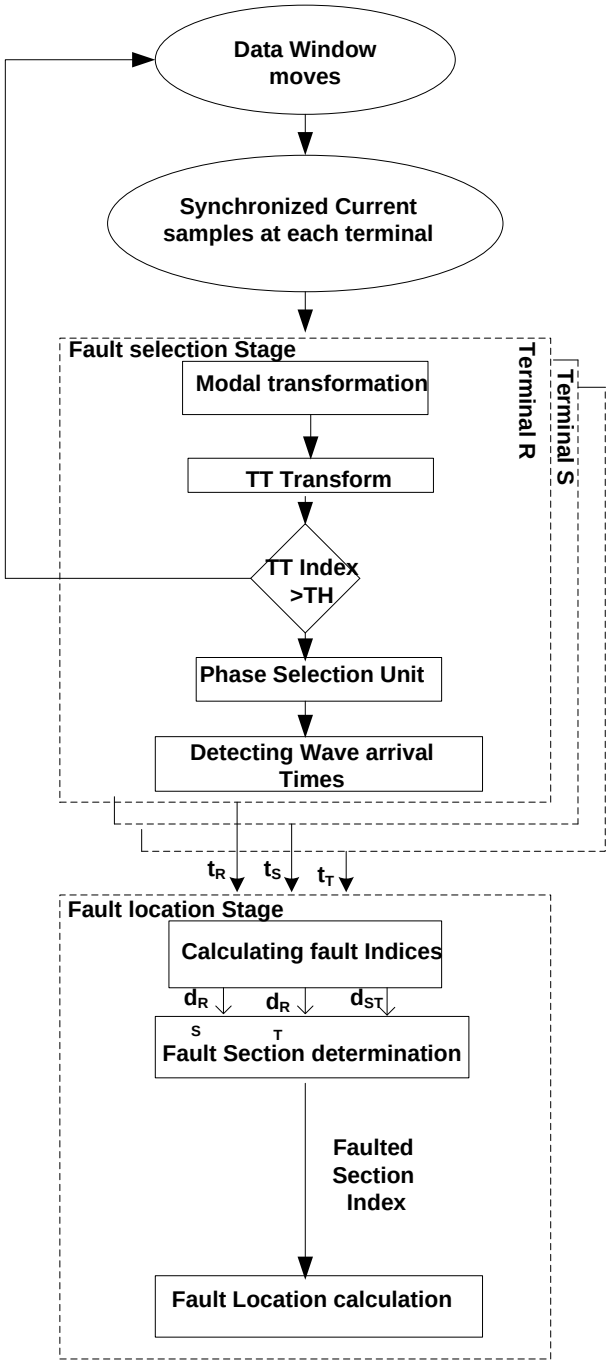

Fig. 1.12 Traveling wave based Fault locator using TT Transform

By using these arrival times, three indices are calculated by the equations as follows:

$$d_{R-S} = \frac{l_{RS} - v(t_S - t_R)}{2},$$
$$d_{R-T} = \frac{l_{RT} - v(t_T - t_R)}{2},$$
$$d_{S-T} = \frac{l_{ST} - v(t_T - t_S)}{2}.$$

In the above equations, R, S and T are the three line terminals. From these indices the faulted section and the exact location are identified. Fig.1.12 shows the overall flow chart of the technique. Results indicated the accuracy of the algorithm and its robustness, but the main drawback is that the fault inception angle variation not fully considered.

Different authors have proposed several fault classification algorithms for two-terminal lines which can be extended to three and multi-terminal lines. As fault classification in three-terminal lines is considered in this work, recent works on classification are elaborated in the following.

In 2014, a phasor based method using sequential reactive powers is proposed by Mahamedi and Zhu [21]. From the sampled three phase voltage & current signals of one cycle data window, negative & zero sequence reactive powers are calculated. The following flowchart shows (Fig.1.13) the algorithm used for classification.

Initially, the change in reactive power ΔQ12 is verified to identify line-to-line faults and the faulty phase. Later, the ratio of Q0/Q2 is examined to distinguish LLG and LG faults. If the value of the ratio is between 0 and 1, then the fault is LLG fault. If its value is greater than one, the fault is declared as LG fault. With these two faults, the faulted phase is found by checking Q20. The technique is not influenced by power swings and over-loading as only zero and negative sequence quantities are used. Despite its claim to be setting and synchronization-free, one cycle fault data requirement is a critical factor influencing the speed of response.

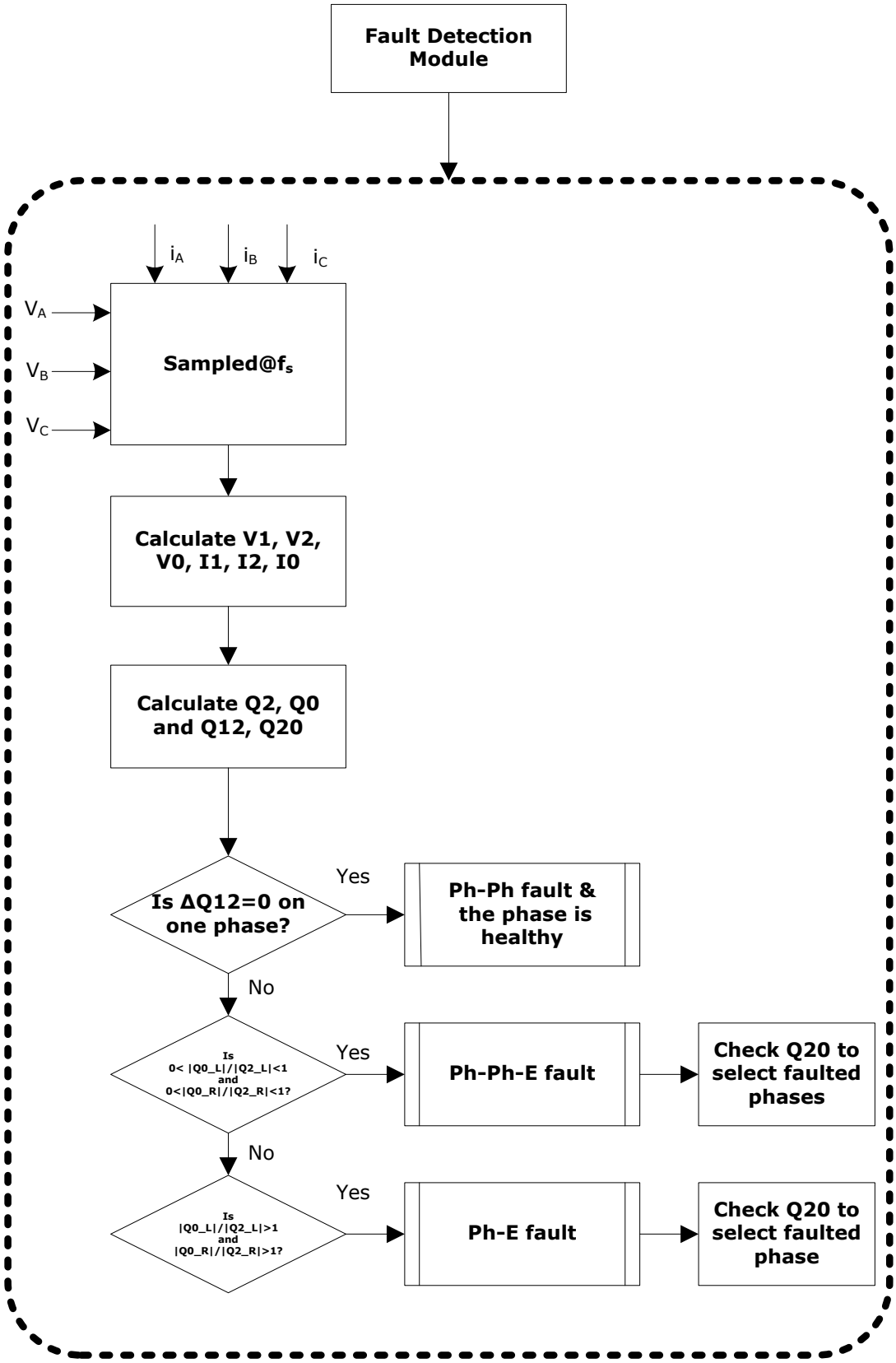

Fig. 1.13 Sequential Reactive power based Classification Algorithm

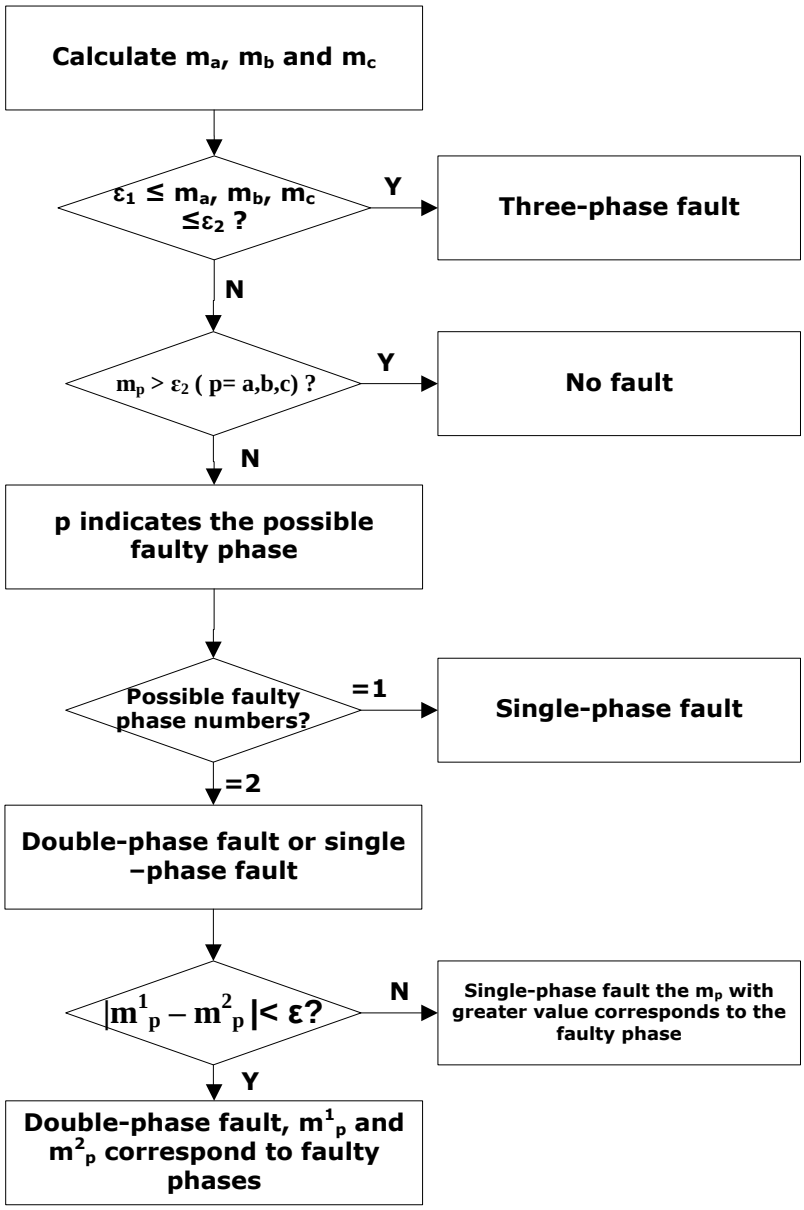

Fig. 1.14 Wavelet Singular Entropy-based Classification algorithm

Driven by the need for high speed relaying, with the availability of efficient signal processing techniques and high sampling rate hardware, a new class of classification algorithms based on the fault induced transients has evolved. These transient based algorithms process fault generated traveling waves or high-frequency components for feature extraction, mostly by using wavelet transform.

A wavelet singular entropy based technique is presented in [22] by using a half-cycle post fault voltage signals at 20 kHz sampling frequency. In this approach, the wavelet singular entropy (WSE) is calculated for each phase and three indices m_a, m_b *and* m_c are obtained using WSE ratios to deal with uncertainty and changing system conditions. From these

values, the faults are classified by the procedure shown in the flowchart below in Fig.1.14. The method is shown to be very effective and immune to noise compared to other methods. However, the problem with this method is it requires the setting of three thresholds according to system situation.

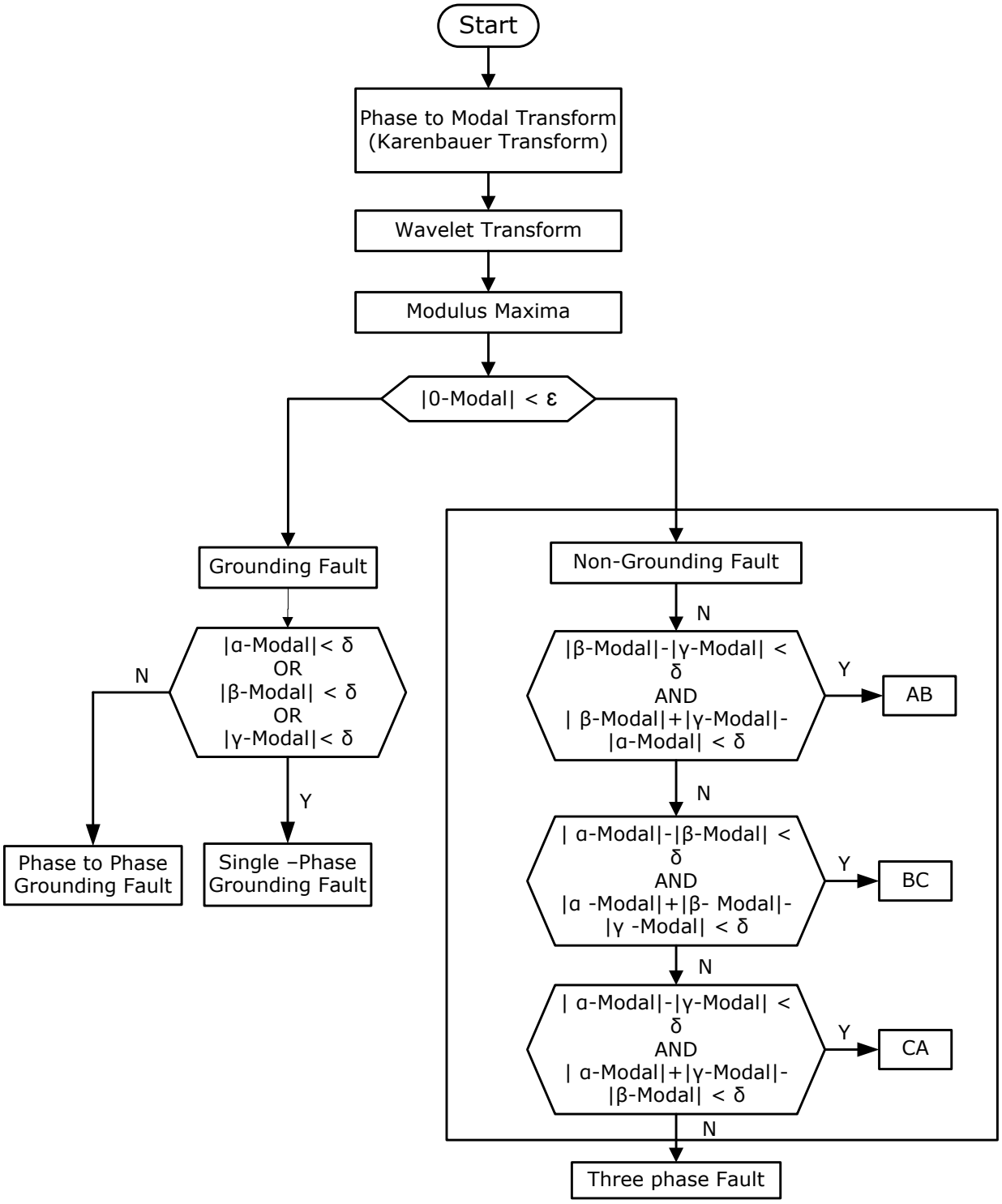

Fig. 1.15 Initial Travelling Wave based Classification algorithm

Another current transient based classification technique is proposed in [23] by processing three phase currents to extract high-frequency components. After applying Karenbauer transformation, single level wavelet decomposition is used in processing current signals. Though the technique is accurate for LG, LL and LLL faults, the accuracy with double-line to ground (LLG) faults is reported to be only around 90%.

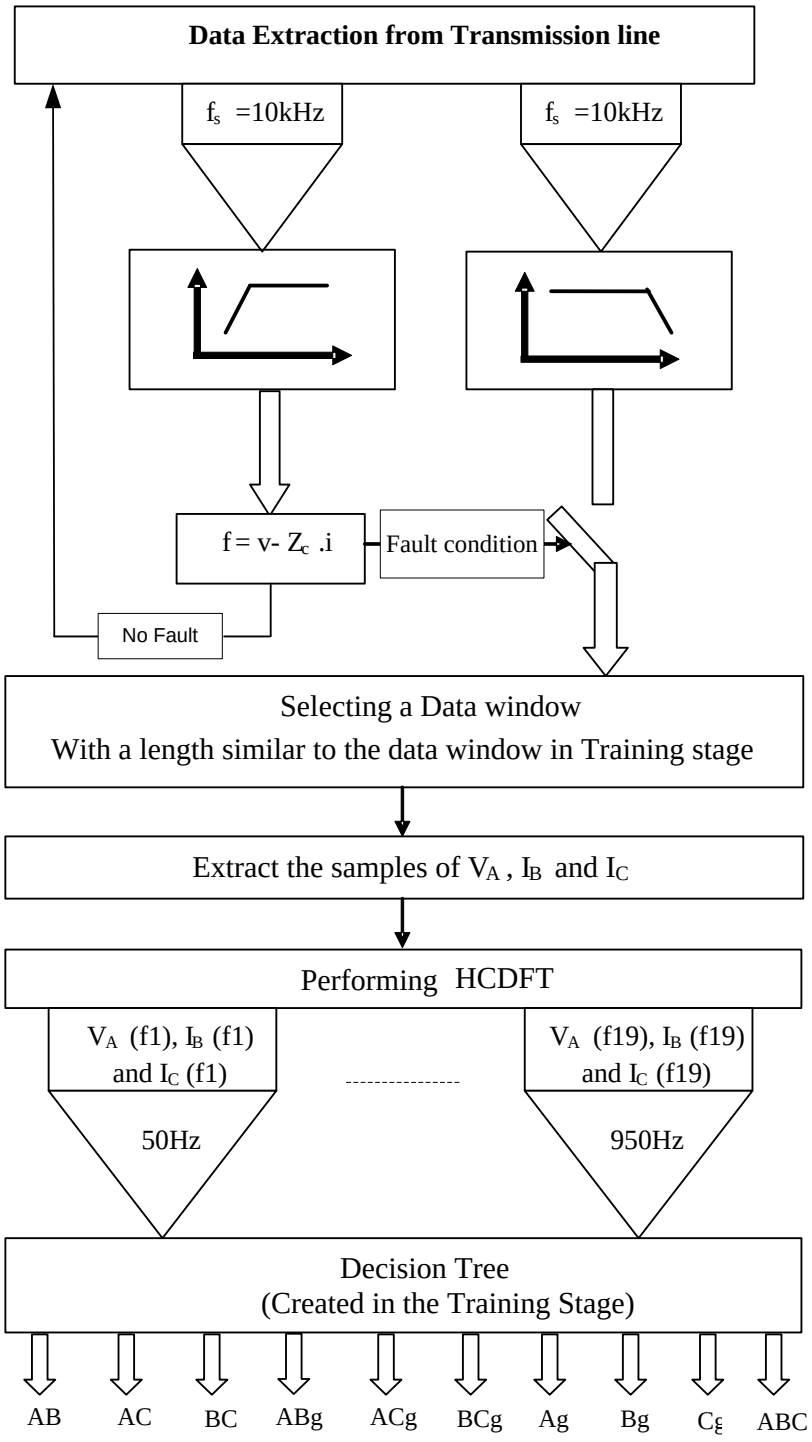

Fig. 1.16 Decision Tree based Classification algorithm

In [24], a method using initial current traveling wave is reported and the technique uses Karenbauer transform. The traveling waves are extracted from signals sampled at 450 kHz by using wavelet transform. By using modulus maxima from second to fourth scales of post-fault current, the traveling wave information is ascertained. As shown in Fig.1.15, the algorithm requires several thresholds for ε, δ *and* φ (required for the phase to phase grounding fault). This technique is shown to be performing well with faults other than LLL faults in simulation studies.

Despite their speed advantage, a major problem for all these deterministic transient based methods is the influence of fault inception angle (FIA) and fault resistance (R_f) on the fault transient magnitudes. Particularly, LLG fault classification poses a big challenge due to misleading transient patterns generated during the faults. In an effort to overcome the above problems due to system inconstancy and for better performance, several authors explored artificial intelligence (AI) applications with Fuzzy Logic [25,26], ANNs [27,28], SVMs [29,30] etc. to the fault classification problem. The inputs to these knowledge-based methods are mainly either steady-state or transient components of the fault voltage/current signals.

Recently, Jamehbozorg and Shahrtash [31] proposed a decision tree based method with HCDFT which requires computation of ten odd harmonic phasors. The decision tree is trained by odd harmonic components of voltage and current signals up to 19^{th} order. The method requires intensive computation for extracting harmonic phasors. Fig.1.16 shows the algorithm used.

A statistical DT based approach is presented in [32] that uses the 7^{th} level decomposition of three phase current signals from sending end. A classification and regression tree (CART) is used to classify faults accurately under different fault situations. The CART is trained with a huge number of samples to implement the above technique. In spite of the high accuracy reported, the technique is not suitable for high speed relaying as it takes two full cycles of post-fault current signals for transient extraction.

Another transient-ANN approach is developed with Rough Membership neural network (RMNN) in 2014 [33]. Ten time-frequency domain features and three time domain features are given as inputs to a set of ten RMNN classifiers as shown in Fig.1.17 below. The RMNN contains rough neurons in the input layer and fuzzy neurons in hidden & output layers. Though the above technique uses only a quarter cycle post-fault current signals for

high speed, its performance is not guaranteed as the simulation results presented include only a 90-degree variation of FIA.

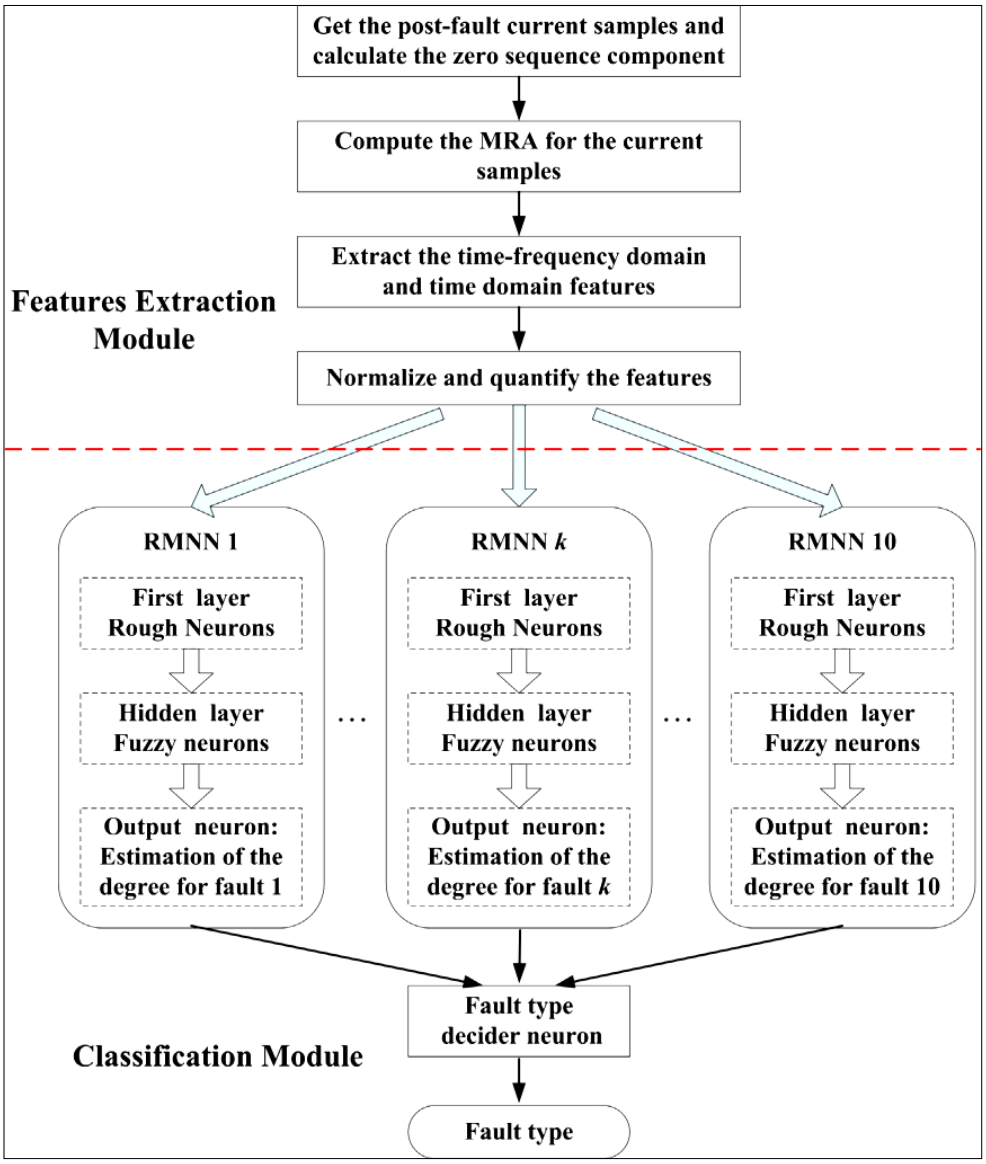

Fig. 1.17 RMNN based Classification algorithm

1.4.2 Multi-terminal Transmission Circuits

In 1992, Nagasawa et al. [34] presented a new fault location algorithm for multi-terminal two parallel transmission lines which is based on the magnitude of differential currents at each terminal. A three-terminal line procedure is extended after converting the n-terminal line to a three-terminal system. Multi-faults occurring simultaneously on both lines and single-fault on one line are located with reasonable accuracy. Masayuki and others [35] in 1995 developed a fault location system for the multi-terminal single transmission line. A synchronisation algorithm is used for synchronising samples. A reactive power based location

technique is extended to the multi-terminal system [36]. Results were verified numerically by EMTP simulation.

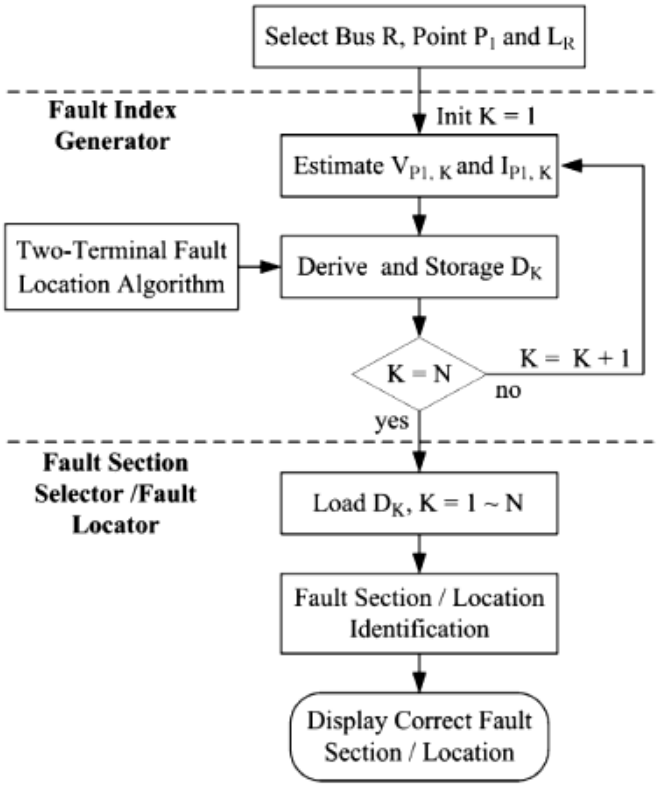

Fig. 1.18 Fault location scheme for N-terminal line with PMUs

In 2005, Brahma [37] proposed a scheme for multi-terminal line fault location using synchronised voltage measurements to avoid CT errors. The scheme works for both transposed and untransposed lines and independent of pre-fault conditions. Fault section is identified by using circuit principles and simulation results showed the reliable location unaffected by fault resistance. In 2006, Brahma [38] presented another method for fault location in a single multi-terminal transmission line by using synchronised voltage and current phasors. This iterative technique estimates the positive sequence source impedances and then Z-bus is formed. The location procedure is based on the properties of the Z-bus matrix. However, these methods require synchronised phasor measurements and exact source impedance must be known for accurate fault location. The techniques are developed for short lines and influence of shunt capacitance needs to be explored further.

In 2008, Liu et al. [39] presented a technique for fault location in N-terminal line by using synchronised phasor measurement units. A novel fault section selector and locator are developed from a two-terminal method as shown in Fig.1.18. Its computational burden is less and does not require the iterative procedure. Results of simulation indicated an error well

below one percent. Despite these advantages, the method needs synchronised phasor measurements and effect of FIA is not reported in the results presented.

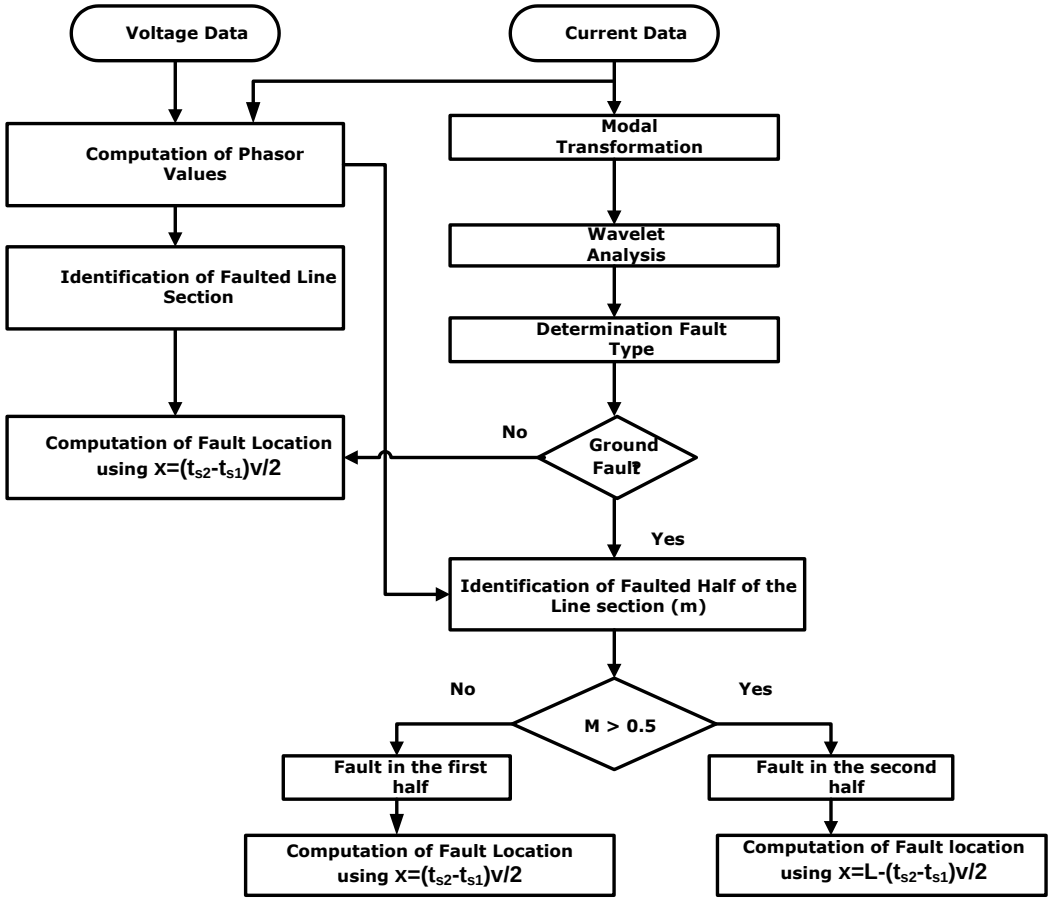

Fig. 1.19 Combined impedance & TW based fault location

In 2010, Manassero et al. [40] described an algorithm based on voltage and current phasors. The technique utilises the line parameters information, transformer loading information and their connection type. Development of phase component models for power system elements is also described. Higher fault resistances influenced the accuracy of the location in this approach.

In 2011, Ngu and Ramar [41] presented a method that uses both impedance and travelling wave principles. Impedance approach is used to identify the faulted line section as well as the faulted half of the line section. Arrival times of current travelling waves using aerial mode signals are used for fault location. The scheme shown in Fig.1.19 is tested with four and five terminal lines by considering different fault conditions. Influence of FIA, phasor accuracy and high sampling frequency are of concern in this method.

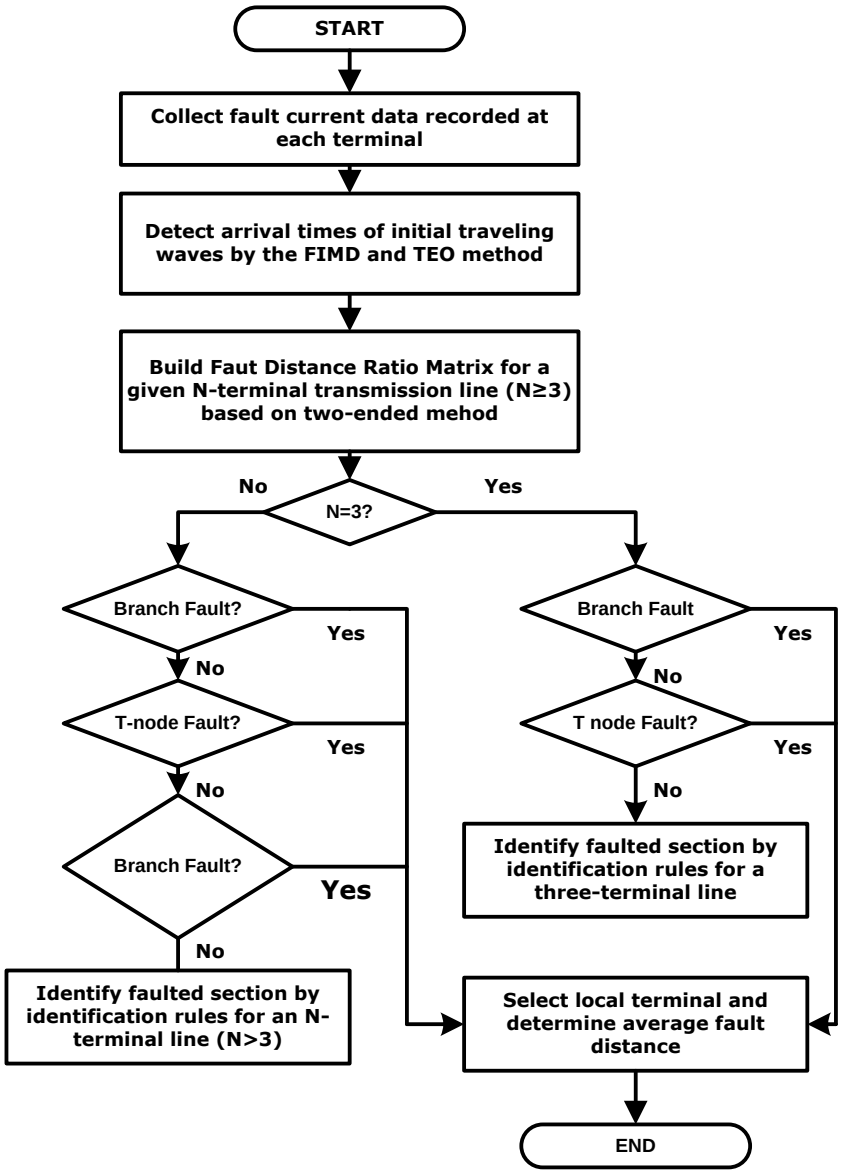

Fig. 1.20 Fault location using FIMD & TEO

A current traveling wave based fault location scheme is presented in [42]. A Fast Intrinsic Mode Decomposition (FIMD) and Teager Energy Operator (TEO) are combined to detect the arrival time of the traveling wave at each terminal. A Fault Distance Ratio Matrix (FDRM) is built to identiy the faulted section, whose elements are obtained by the ratio of the fault distance to the length of the branch from the terminal to the T node.

Using the Fault Distance Ratio Matrix (FDRM), rules are developed for identifying faulted sections of a multi-terminal transmission line. Fig.1.20 shows the flowchart of the overall scheme with this technique. Simulation results under various fault conditions are presented and a comparison is made with results obtained by using Hilbert–Huang Transform (HHT) for wave arrival time extraction. However, the influence of FIA is not reported and use of 2 MHz sampling frequency is of concern.

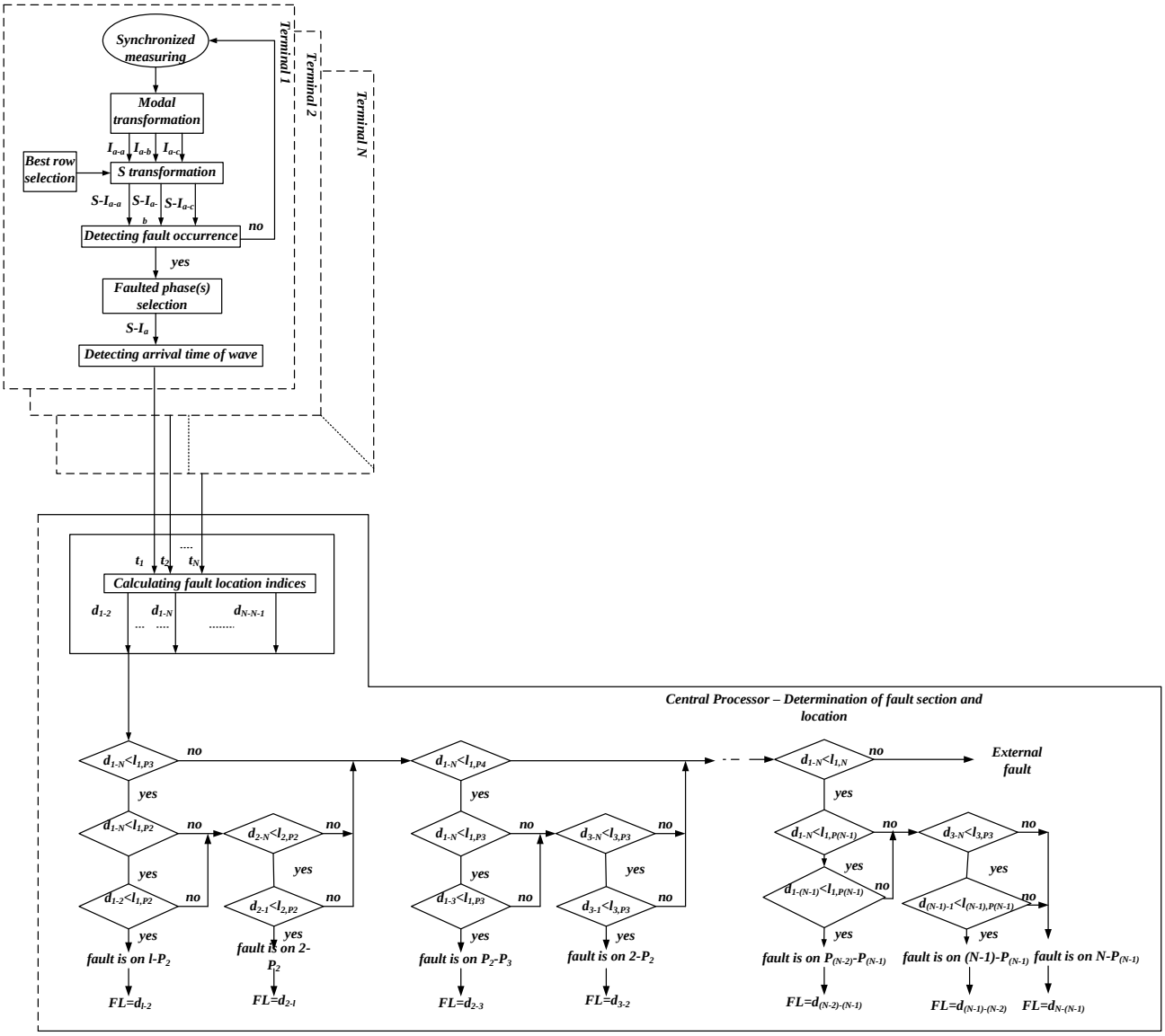

Fig. 1.21 Fault location using S-transform & travelling waves

Recently in 2013, Ahmadimanesh and Shahrtash [43] proposed a transient based technique by employing S-transform for locating faults in multi-terminal lines. S-transform is applied to aerial mode signals for finding the arrival times of current travelling waves. A procedure is described to select the best row of the S-transform matrix (frequency components). The flowchart in Fig.1.21 describes the scheme. Results presented indicated the accuracy of the technique for different fault situations. This approach needs synchronised measurements and shunt capacitance is not considered in simulation studies.

1.5 Motivation for Research and Main Objectives

From the above literature survey, the following observations may be inferred regarding the protection of teed and multi-terminal lines.

1. Protection systems of three-terminal lines are complex and need to be designed with care considering specific line configuration for reliable operation.

2. Many schemes presently in use are based on extensions of traditional distance relaying and differential relaying principles with communication assistance between terminals.

3. Digital protective relays implementing these phasor based techniques suffer from infeed/outfeed conditions, load encroachment, stable power swings.

4. Relay response time may not match modern power grid requirements as phasor estimation needs at least half-cycle time.

5. Transient based schemes use short post-fault data windows to enhance the speed of response.

6. Very few attempts have been made for fast detection and classification of internal faults in three-terminal lines.

7. Many recent works focused on the development of fault location techniques for three-terminal transmission circuits using phasor and travelling wave methods.

8. Fault location techniques for multi-terminal lines are only a few and mostly impedance based. A few attempts are made for transient based approaches.

9. Phasor based methods are sensitive to synchronisation errors, fault resistance and faults creating low transients lead to errors in transient based schemes.

10. Application of AI techniques for fault location in teed/multi-terminal lines is not investigated.

Other general issues of concern in protection schemes for transmission lines are use of voltage/current signals, pre-fault/post-fault signals, single-ended/multi-ended data, data synchronization, feature extraction tools using DFT/Wavelets/S-transform etc., post fault signal window size, sampling frequency, communication requirements, noise considerations etc.,

Based on the above study, the present work aimed to develop fast and accurate classification algorithms using transients and accurate fault location methods for teed and multi-terminal lines on the following lines.

- To develop an accurate transient based fault detection and classification technique
- Use wavelets for feature extraction
- To develop accurate fault location methods for EHV Teed and Multi-terminal circuits
- Use DFT for phasor estimation and wavelets and S-transform for detecting travelling waves
- Explore AI application to classification and location problems

1.6 Contributions and Thesis Overview

From the literature survey, it is observed that there is a need and scope for improvement in classification and location algorithms in terms of accuracy and speed unaffected by variation in FIA and fault resistance. Also, the accuracy of phasor estimation and synchronisation errors plays a significant role in the performance of the various algorithms.

Therefore, this thesis work aimed to contribute protection algorithms for teed and multi-terminal lines that overcome some of the above critical problems identified. Particularly, fast & accurate fault classification and accurate fault location are considered to be the requirements. The schemes are designed to be unaffected by fault conditions, particularly the fault inception angle. The errors in phasor estimation are overcome by incorporating a modified DFT technique and an analytical synchronisation procedure is applied to overcome the synchronisation errors. The main contributions are:

In this thesis work, the following protection algorithms are developed for teed and multi-terminal transmission circuits.

- Transient based Fault Classification in EHV Teed Circuits using Wavelet Transform
- Transient and Probabilistic Neural Network based Fault Classification in EHV Three-Terminal Lines
- Fault Location in Teed Circuits using Modified DFT Phasor Estimation
- Travelling Wave based Fault Location in Teed Circuits using S-Transform & Neural Networks

- A Hybrid Method for Fault Location in EHV Multi-Terminal Circuits
- A Non-iterative Fault Locator for Multi-Terminal Transmission Lines using Unsynchronized Phasors
- Two new simple algorithms proposed and used for fault detection

Thesis Organization

Chapter-1 begins with an introduction to transmission line protection in power systems and its significance. Specific problems with teed and multi-terminal lines are outlined. An exhaustive literature survey is presented to identify the state-of-the-art followed by the work proposal and thesis organisation.

Chapter-2 introduces the problem of fault classification and based on the literature survey, the problems to be addressed are identified. A transient based scheme is developed to classify faults in teed circuits. Subsequently, for improved accuracy, a transient and PNN based technique is described.

Chapter-3 begins with the elaboration of fault location problem. Both phasor based and travelling wave based approaches are discussed, followed by their application to teed circuits. Firstly, a transient and phasor based method using modified DFT is presented for fault location in teed circuits. Then, an AI solution with transient feature extraction using S-transform is developed for locating faults.

Chapter-4 describes the fault location in multi-terminal lines considering both synchronised and unsynchronized measurements. A hybrid method is presented to locate faults in multi-terminal circuits by utilising both transients and steady-state phasors. A non-iterative fault locator for a multi-terminal line with unsynchronized measurements is also described.

Chapter-5 presents the overall summary and conclusions followed by the possibilities for future work.

Chapter 2

Transient Based Fault Classification in Three-terminal Lines

2.1 Introduction to Fault Classification

Fault classification plays a critical role in the protection of transmission lines. In transmission line protection, after fault detection, the line relay invokes a fault classification function to identify the type of fault and the faulted phases for initiating possible single pole tripping and auto reclosing [2]. This information is also useful in distance relaying for activating proper distance element. Hence, the fault classifier must be very quick and accurate to maintain system stability and continuity of supply.

Two different principles are mainly used in fault classification techniques: Steady-state component based and Transient based approaches. The steady-state component based schemes use either fundamental phasors of voltages/currents or superimposed sequence components. These approaches cannot meet high speed requirements of modern grids and are highly influenced by factors like fault type and fault resistance. The second group of techniques is based on the use of fault generated transients like travelling waves. These techniques are immune to the dynamically changing system conditions, which is a definite advantage. Recent advances in digital signal processing made it possible to extract the transient features from wide band fault signals very effectively.

Despite many algorithms developed for fault classification using deterministic approaches, a need for knowledge based approaches is also identified. Several methods are proposed by using AI techniques such as ANNs and Fuzzy logic to improve the classification accuracy.

The classification module of the relay mainly processes the post fault voltage and/or current signals from one or more ends to extract discriminating features. Use of information from many ends improves the accuracy as well as the reliability of the schemes. In this work, transient based classification algorithms are developed for three terminal lines by using measurements from three ends. Fig.2.1 depicts different categories of classification and their attributes.

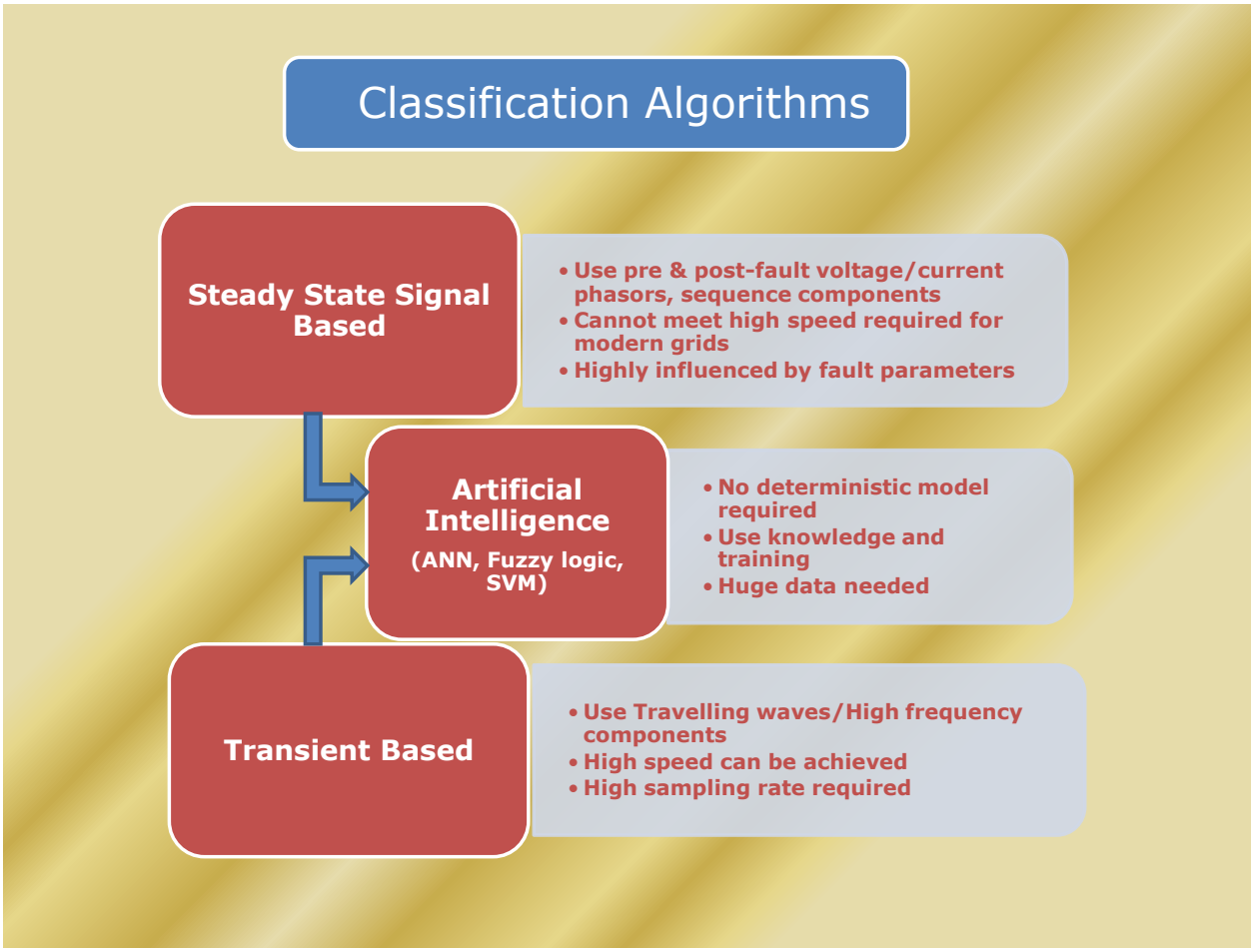

Fig. 2.1 Classification Algorithms

2.2 Fault Classification in Three-terminal Lines

From the literature survey in section 1.4, it is observed that EHV Teed circuits pose additional protection problems due to intermediate infeed or outfeed from the third terminal and superimposed reflections of the fault signal from T-point & the fault point. Other general factors that compound the problem further include asymmetrical nature of the teed circuit, fault resistance, variation in source impedances, fault inception angles, the presence of series capacitors, mutually coupled line sections, switching transients, CT saturation, line un-transposition and pre-fault loading conditions etc.

Regarding fault classification, many fault classification algorithms are traditionally phasor based where the estimation of post fault voltage/current phasors requires at least a half-cycle data. Most of these methods are affected by dynamically changing network configuration and fault conditions. Recently, a phasor based method using sequential reactive powers is proposed by Mahamedi and Zhu [21]. Despite its claim to be threshold setting and

synchronization free, one cycle fault data requirement is a critical factor influencing the speed of response.

Driven by the need for high speed relaying, with the availability of efficient signal processing techniques and high sampling rate hardware, a new class of classification algorithms based on the fault induced transients has evolved. These transient based algorithms process fault generated traveling waves or high frequency components for feature extraction, mostly by using wavelet transform. In [24], a method using initial current traveling wave is reported mentioning that it fails during certain three phase faults. A wavelet singular entropy based technique is presented in [22] by using a half-cycle post-fault voltage signals. The problem with this method is it requires the setting of three thresholds according to system situation. Another current transient based classification technique is proposed in [23] whose accuracy with double-line to ground (LLG) faults is reported to be only around 90%. Despite their speed advantage, a major problem for all these deterministic transient based methods is the influence of fault inception angle (FIA) and fault resistance (R_f) on the fault transient magnitudes. Particularly, LLG fault classification poses a big challenge due to misleading transient patterns generated during the faults.

To overcome the above problems due to system inconstancy and for better performance, several authors explored artificial intelligence (AI) applications with Fuzzy Logic [25,26], ANNs [27, 28], SVMs [29, 30] etc., to the fault classification problem. The inputs to these knowledge based methods are mainly either steady-state or transient components of the fault voltage/current signals. Recently, Jamehbozorg and Shahrtash proposed a decision tree (DT) based method with HCDFT [31] which requires computation of ten odd harmonic phasors. A statistical DT based approach [32] is shown to be accurate, but it takes two full cycles of current signals for transient extraction. Another transient-ANN approach is developed with Rough Membership neural network in [33], but the results presented include only a 90 degree variation of FIA. In addition to all the above methods primarily developed for two-terminal lines, a transient-SVM based classifier is designed for three terminal lines in [19]. However, its poor performance (95 % accuracy) in classifying grounded faults is not acceptable. Many of the methods mentioned above have not considered the influence of FIA on the accuracy of classification.

From the above discussion, it can be concluded that high speed classification is possible with transient based schemes, but their accuracy is influenced by fault inception angle & fault resistance. Many thresholds are used in different algorithms and their fixing is

another difficult task. Considering the speed requirements for fault classification and influence of fault conditions like FIA, fault resistance on the accuracy of classification in transient based methods, a thorough investigation into the transient patterns generated during faults is necessary for developing a useful classifier.

In the following sections, effective transient based schemes are developed for fault classification in three-terminal lines by addressing the problems with the influence of fault inception angle and fault resistance on fault transients. The threshold fixing problem is also considered in one of the proposed methods.

2.3 Transient Based Fault Classification

Unlike the phasor based methods, the transient based algorithms process short windows of fault signals due to wide band nature of transients generated during faults. Hence, transient based methods achieve high speed classification by extracting features like wavelet coefficient energy, travelling waves from the fault voltage and current signals. Transmission line faults induce high frequency transients in power systems and these transients appear on the post-fault voltage and current signals measured by the line relays. The transient based protection schemes process these transient components to extract the discriminating features for protective functions like detection, classification and location of faults. Generally, these transients need to be extracted by a signal processing tool that suits real time application, especially for detection and classification. The wavelet transform is proven to be such an effective tool for implementing transient based schemes because of its multi-resolution analysis feature. A fault classification scheme using transients is presented in the following section.

Conventional voltage and current transformers (wire wound and/or capacitor coupled instrument transformers) have shown excellent performance for traditional relaying applications in the power systems. These applications mostly use measurements of power frequency components that necessitate a lower sampling rate for voltage and current signals. However, the bandwidth of the conventional CTs and PTs is limited and they do not meet the requirements of relays based on high frequency components of fault current and voltage signals.

Many transient based protection schemes have been proposed over the years with sampling frequencies ranging from few KHz to 1MHz [18]. Optical CTs and PTs have a wide bandwidth which makes them suitable for real-time on-line measurement of transients as they

occur. Optical voltage and current sensors are linear devices with respect to signal frequency and magnitude. They are shown to be capable of measuring voltage and current signals in power systems at frequencies of the order of several MHz [97]. Therefore, in the proposed transient based schemes which use a sampling frequency of 200 KHZ, application of such optical devices is assumed.

2.4 Transient Based Fault Classification in EHV Teed Circuits using Wavelet Transform

The proposed scheme collects quarter-cycle sampled data moving windows of all measured synchronized phase voltages and currents from the three relaying ends-1, 2 and 3 of the teed circuit as shown in Fig.2.3. The synchronized voltage and current signals are obtained from the global positioning system (GPS) based communication systems installed at the three ends of the teed circuit. From the sampled phase voltages (V_a, V_b and V_c) and currents (I_a, I_b and I_c), the line voltages and ground currents at each end are obtained. These windows of voltage and current signals are used for processing in the proposed scheme. The algorithm used in the proposed scheme is elaborated in the following sections.

2.4.1 Wavelet Transform

Wavelet Transform (WT) [44,45] is a signal processing tool and is suitable for power system applications like power quality assessment, power system protection etc. which involve transient analysis. Unlike Fourier Transform (FT), which uses only sinusoid as a basis function, the WT uses several basis functions called 'mother wavelets' and variable sized windows for capturing both high frequency and low frequency components of the signal.

Introduction to Joint Time-Frequency & Time-Scale Analysis

The Fourier Transform operation, which is a one dimensional (1D) time- domain to one dimensional (1D) frequency-domain mapping, loses time information completely. It is suitable for analyzing signals whose frequency spectrum does not vary with time i.e. stationary signals.

The Joint time-frequency (JTF) representation fully describes the nature of non-stationary signals which is not possible in either time domain or frequency domain analysis. The well-known Fourier analysis decomposes a signal into its sinusoidal frequency components. Because of the eternal ($-\infty < t < \infty$) nature of $e^{j\omega t}$, this analysis provides a

perfect frequency resolution. However, it does not reveal anything about the time localization of each frequency component. When signals under study are non-stationary and have time-variant spectra, this approach fails to reveal the time information. Applications of joint time-frequency schemes include change detection, analysis of multi-component signals and de-noising.

The transient signal analysis for time localization is the area in which time-frequency analysis is most widely used. Transient signals are of short time duration and totally varying in nature (amplitude, frequency and phase). Transients are commonly found in condition monitoring applications, including disturbances in electric power networks and vibrations in mechanical systems.

Several methods for obtaining the energy density of a function, simultaneously in the time and frequency have been developed such as the Short Time Fourier Transform (STFT), Wavelet Transform (WT) and the *S*-transform. These transforms operate by mapping a 1D signal in the time domain, into a two dimensional representation of the signal in time-frequency or time scale. Scaling used in Wavelet transform and others can be shown to be related to frequency inversely and is closely linked with Multi Resolution Analysis (MRA) in signal processing. In MRA, a signal is divided into many successive approximations and details enabling local and global analysis. This MRA makes it possible to decompose signals at different levels or scales facilitating efficient processing for detection, estimation and decision making.

The Continuous Wavelet Transform (CWT)

The Continuous Wavelet Transform (CWT) of a finite energy signal $x(t)$ at scale *a* and delay *b* is given by (here *a* & *b* are continuous)

$$W(a,b) = \int_{-\infty}^{\infty} x(t)\psi_{a,b}^{*}(t)dt \tag{2.1}$$

Where ψ^{*} is the complex conjugate of the wavelet mother function ψ. The family of waveforms $\psi_{a,b}(t)$ is obtained by translating a single mother wavelet by *b* and scaling it with *a*.

$$\psi_{a,b}(t) = \frac{1}{\sqrt{a}}\psi\left(\frac{t-b}{a}\right). \tag{2.2}$$

Like in the wavelet packet case, several mother functions are also possible. The $1/\sqrt{|a|}$ factor in the above equation suggests, $\psi_{a,b}(t)$ is normalized so that it has the same energy at all scales. Also, the wavelet function must be of finite energy to have a compact support. For simplicity, the unity energy is taken, so that $\|\psi\|_2^2 = \|\psi_{a,b}\|_2^2 = 1$, where the *p*-norm of a function $h(x)$ is defined as

$$\|h(x)\|_p = \left(\int_{-\infty}^{\infty} |h(x)|^p \, dx \right)^{1/p}. \tag{2.3}$$

The inverse CWT or reconstruction formula of the wavelet transform is given by,

$$x_w(t) = \frac{1}{C_\psi} \int_{-\infty}^{\infty} \int_{-\infty}^{\infty} W(a,b) \frac{1}{\sqrt{|a|}} \psi\left(\frac{t-b}{a} \right) \frac{dadb}{a^2} \tag{2.4}$$

where

$$C_\psi = \int_{-\infty}^{\infty} \frac{|\hat{\psi}(\omega)|^2}{|\omega|} d\omega < \infty. \tag{2.5}$$

Apart from the normalization of $\psi_{a,b}(t)$, the wavelet mother function should also satisfy an admissibility condition: $C_\psi < \infty$, to provide the reconstruction of x without distortion. To satisfy (2.5), ψ must have a zero average, $\hat{\psi}(0) = 0$, where $\hat{\psi}$ is the Fourier transform of ψ, and $\hat{\psi}(\omega)$ be continuously differentiable. In addition, the above condition makes sure that the wavelet transform satisfies the energy conservation property:

$$\|x(t)\|^2 = \frac{1}{C_\psi} \int_{-\infty}^{\infty} \int_{-\infty}^{\infty} |W(a,b)|^2 \frac{dadb}{a^2} \tag{2.6}$$

This main property ensures that any variation of energy in the time or wavelet domain causes an equal variation in the other domain. Hence, the wavelet can be considered as an energy-conservative transform like the Fourier transform. The $1/a^2$ term appears because of the use of the scale notion instead of the frequency one.

Bi-orthogonal wavelets

With orthogonal wavelets, it is not possible to obtain symmetric FIR filters. Symmetric FIR filter gives linear phase characteristics for its frequency response-an important requirement in several applications. Using the MRA framework, perfect reconstruction linear-phase FIR filters can be designed if bi-orthogonality is applied instead of orthogonality. A bi-orthogonal wavelet is a wavelet where the associated wavelet transform is invertible but not necessarily orthogonal. The bi-orthogonal wavelets allow more degrees of freedom than orthogonal wavelets and an additional degree of freedom is the possibility of constructing symmetric wavelet functions. In the bi-orthogonal case, two scaling functions $\phi, \tilde{\phi}$, are used which may generate different multi-resolution analyses, and accordingly two different wavelet functions $\psi, \tilde{\psi}$.

Wavelet analysis of any signal begins with the selection of a suitable mother wavelet and analysis is performed using shifted and dilated versions of this wavelet. The discrete wavelet transform (DWT) of a digital signal is,

$$DWT(m,n) = \frac{1}{\sqrt{a_0^m}} \sum_k x(n) \psi \left(\frac{k - n b_0 a_0^m}{a_0^m} \right) \tag{2.7}$$

Where $\psi(t)$ is the mother wavelet and x(n) is the input signal, and the scaling and translation parameters ‘a’ and ‘b’ are functions of integer parameter *m*. The DWT implementation is carried out using a pair of finite impulse response filters called 'Quadrature Mirror Filters' (QMF) with impulse responses h(n) & l(n) respectively. Typically h(n) exhibits high-pass filter characteristics and l(n) exhibits low-pass filter characteristics. This implementation shown in Fig.2.2 is known as the three-level ‘Multi-Resolution Analysis’ (MRA). Here A3, D3, D2 and D1 are the approximation and detail coefficients of the input signal x(n). The original sampled signal x(n) is sent through a high pass filter, h(n) and a low pass filter l(n). The outputs from these filters are decimated by 2 to obtain the detail coefficients and the approximation coefficients at first level (D1 and A1). The approximation coefficients are then sent to the next stage to repeat the procedure. Thus, the signal is decomposed to the required level. If the sampling frequency of x(n) is F, then the signal information captured by D1 is between F/4 and F/2 of the frequency band. A1 retains the rest of the information of original

signal between 0 and F/4. With this process, it is possible to extract useful information from the original signal into several frequency bands without losing time information.

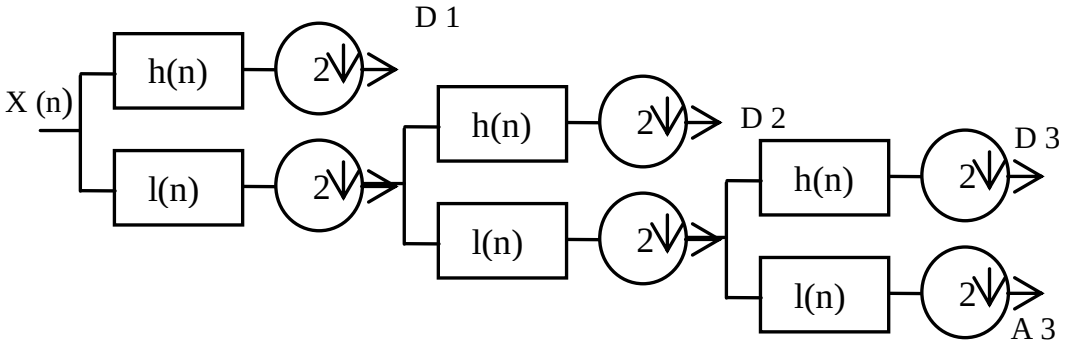

Fig. 2.2 Wavelet Multi-Resolution Analysis

In this work, a bi-orthogonal ‘bior2.2’ wavelet is selected as the mother wavelet as it is found to be very effective for power system fault transients [46].

2.4.2 Fault Detection

When a fault occurs within the teed circuit, the transient voltage and current signals in the faulted section contain predominant high frequency components. It is due to the superimposed reflections of the fault signals from the tee-point and the fault point. The energy of these high frequency signals is used as an indicator of the fault occurrence. In the proposed scheme, voltage signals at the relaying ends are used for detection. A modal voltage signal for each end is formed with the three phase voltages of the corresponding relay end. The modal voltage signal is formed by using transformation

$$V_m = V_a - 2V_b + 2V_c \tag{2.8}$$

The above modal signal covers all types of faults and eliminates the effects of mutual coupling with adjacent circuits. The modal voltage signals are then processed using DWT with ‘bior2.2’ as the mother wavelet to obtain the first level detail coefficients (D1). These D1 coefficients indicate the strength of the high frequency content. With these coefficients, a fault section energy index (FSEI) value is evaluated for each section from the signal energy using the Frobenius norm. The first and last five detail coefficients are truncated while computing the index to eliminate the edge effect. The Fault Section Energy Index is defined as

$$FSEI = \sqrt{\sum_{i=1}^{N}\left[D1(i)\right]^2} \tag{2.9}$$

Where N is the number of first level detail coefficients after truncation. A fault is detected whenever the FSEI value of any end exceeds a threshold. During normal operation, the FSEI values are very small and incase of any fault the FSEI values increase drastically. It clearly discriminates between fault and non-fault situations.

2.4.3 Fault Classification

In this work, a new classification procedure using transient voltage and ground current signals is developed to overcome the classification problems. The proposed method uses transient high frequency signal energy present in all the phase voltages, line voltages and ground currents of the three ends. Initially, the involvement of ground in the fault is checked by using the ground current (or zero sequence current). A line to ground fault creates high frequency components on all phase voltages making it difficult to identify the single faulted phase. Hence, the line to ground fault is identified using line voltages instead of phase voltages. The line voltage between the two un-faulted phases contains no transient energy whereas the remaining two line voltages contain appreciable transient energy. Thus the faulted phase can be clearly identified from the line voltages. In the case of line to line faults, the line voltage of the faulted phases contains more energy compared to the other line voltages but the phase voltage of the other phase and ground current contain no energy. If the phase voltage of the other phase also contains a significant amount of energy, it is a three phase fault. The double line to ground faults can be similarly identified by using line voltage and ground current information. The transient signal energy indices used as discriminating features are given by

$$\Psi_{ij} = \Psi_{ij1} + \Psi_{ij2} + \Psi_{ij3};\ i = a,b,c\ \&\ j = b,c,a \tag{2.10}$$

$$\Psi_{k} = \Psi_{k1} + \Psi_{k2} + \Psi_{k3};\ k = a,b,c \tag{2.11}$$

$$\Psi_{g} = \Psi_{g1} + \Psi_{g2} + \Psi_{g3} \tag{2.12}$$

where Ψ_{ij} is the Line Voltage Fault Index (LVFI) of line voltage between i^{th} & j^{th} phases;

$\Psi_{ij1}, \Psi_{ij2}, \Psi_{ij3}$ are the transient high frequency signal energies of line-voltages at ends 1,2 & 3.

Ψ_{k} is the Phase Voltage Fault Index (PVFI) of k^{th} phase voltage.

$\Psi_{k1}, \Psi_{k2}, \Psi_{k3}$ are the Transient high frequency signal energies of phase voltages at ends 1,2 & 3.

Ψ_g is the Ground Fault Index (GFI) of the ground current.

$\Psi_{g1}, \Psi_{g2}, \Psi_{g3}$ are the Transient high frequency signal energies of ground currents at ends 1,2 & 3.

All the above features are obtained by using the first level detail coefficients of the signals decomposed with DWT. The energies are calculated using the norm given in equation (2.9). The Transient signal energy indices (LVFI, PVFI and GFI) obtained by adding energies of the three ends are used to improve the sensitivity of the scheme with regard to the fault location. The classification algorithm is as follows.

Step-1: Start

Step-2: Obtain D1 coefficients for all phase voltage, line voltage and ground current data windows of all ends.

Step-3: Calculate fault indices as given by equations (2.9-2.12).

Step-4: Is any of $FSEI > FT$? If yes, go to next step. Otherwise, update data windows and go to step 2.

Step-5: If $\Psi_{ab} < FT,\ \Psi_{bc} > 10\Psi_{ab},\ \Psi_{ca} > 10\Psi_{ab}$ *and* $\Psi_g > GT$ then c-g fault. Similarly, check for a-g & b-g faults.

Step-6: If $\Psi_{ab} > \Psi_{bc},\ \Psi_{ab} > \Psi_{ca},\ \Psi_c < FT$ *and* $\Psi_g < GT$, then a-b fault. Similarly, check for other b-c & c-a faults.

Step-7: If $\Psi_{ab} > \Psi_{bc},\ \Psi_{ab} > \Psi_{ca}$ *and* $\Psi_g > GT$, then a-b-g fault. Similarly check for b-c-g & c-a-g faults

Step-8: Else, $\Psi_g < GT$ it is a three phase fault.

Step-9: End

In the above algorithm, FT (Fault Threshold) & GT (Ground Threshold) are thresholds whose values are fixed by extensive simulation studies.

2.4.4 Simulation Results

The above proposed algorithm is tested on the teed networks (both symmetrical and asymmetrical), shown in Fig.2.3, which are simulated using SimPowerSystems of MATLAB for various fault situations. The long line model considering distributed parameters is used in all algorithms. In MATLAB/SIMULINK simulations, the model is based on the Bergeron's

traveling wave method. The distributed parameter line represents the wave propagation phenomena and line end reflections with a better accuracy. The same model is used throughout for all the algorithms in this work. The line parameters of 500 kV, 50Hz teed transmission systems are R_0 = 0.1888 Ω/km, R_1=0.02 Ω/km, L_0 = 3.5 mH/km, L_1 = 0.94 mH/km, C_0 =0.0083 µF/km & C_1 = 0.012 µF/km.

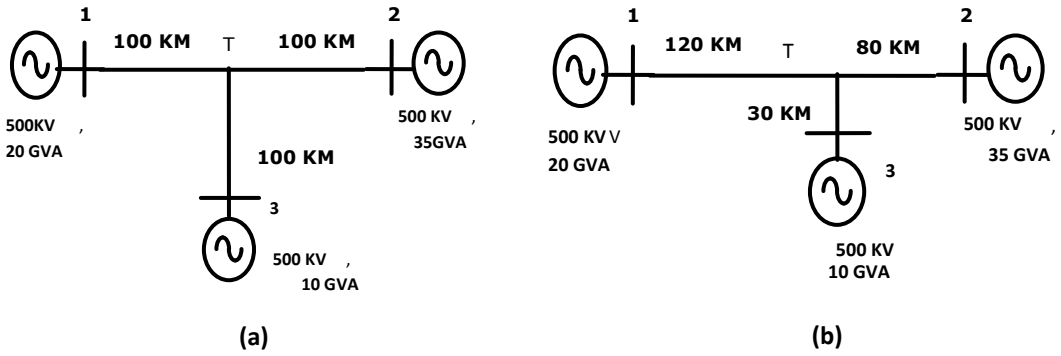

Fig. 2.3 EHV Teed circuits a) Symmetrical b) Asymmetrical

The 'Transient Based Fault Classification in EHV Teed Circuits Using Wavelet Transform' algorithm uses two thresholds namely Fault Threshold (FT) and Ground Threshold (GT).

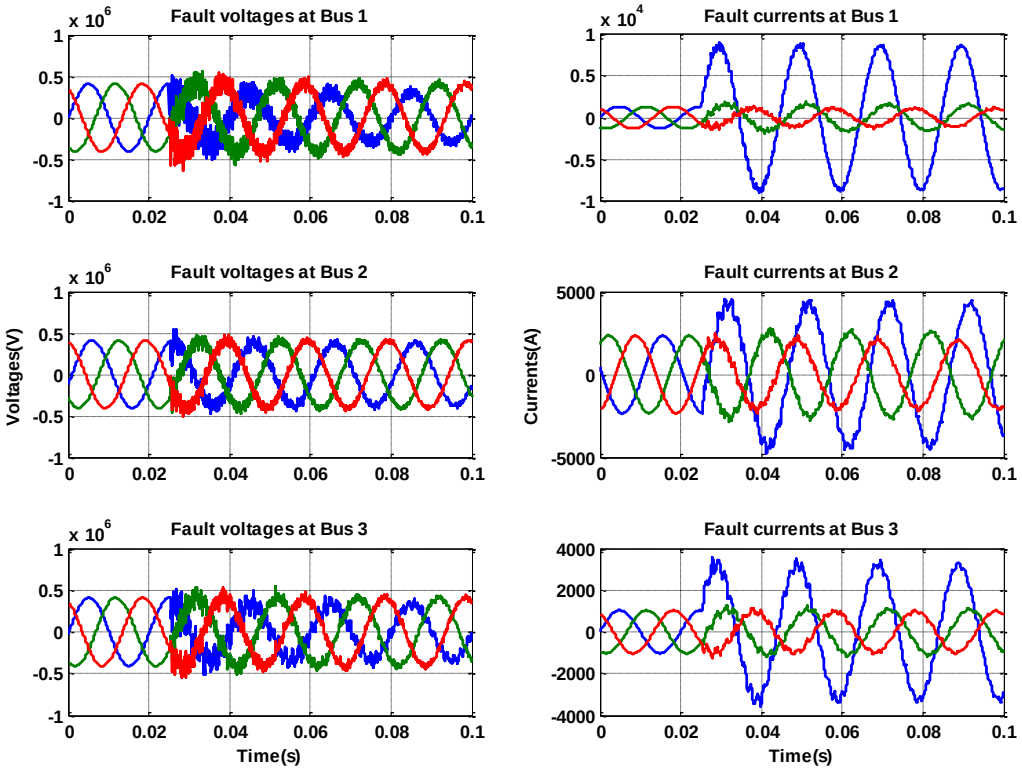

Fig. 2.4 Fault voltage & current signals for an a-g fault in symmetrical teed circuit. (R_f = 0Ω & Inception angle, θ=90^0)

The first threshold is for the purpose of detecting a fault based on the transient energy of modal voltage signal (equation 2.8) and the second threshold GT is to find whether the ground is involved in the fault or not.

The two thresholds are set after exhaustive computer simulations of the power system under consideration. Particularly, the fault inception angle plays a critical role in deciding the magnitudes of FSEI and GFI. The two thresholds FT and GT are set to be equal to 300 and 0.1 respectively for both symmetrical and asymmetrical teed circuits.

A sampling frequency of 200 kHz is chosen to capture the high frequency content of voltage and current signals around the centre frequency of 75 kHz [47]. Adoption of such high sampling frequency avoids the use of anti-aliasing filter thus reducing some delay [48]. At this sampling frequency, each quarter-cycle data window contains 1000 samples. Fig.2.4 shows typical voltage and current waveforms at all the ends during a line to ground fault in section-1 of the symmetrical teed circuit at 60 km from the source end.

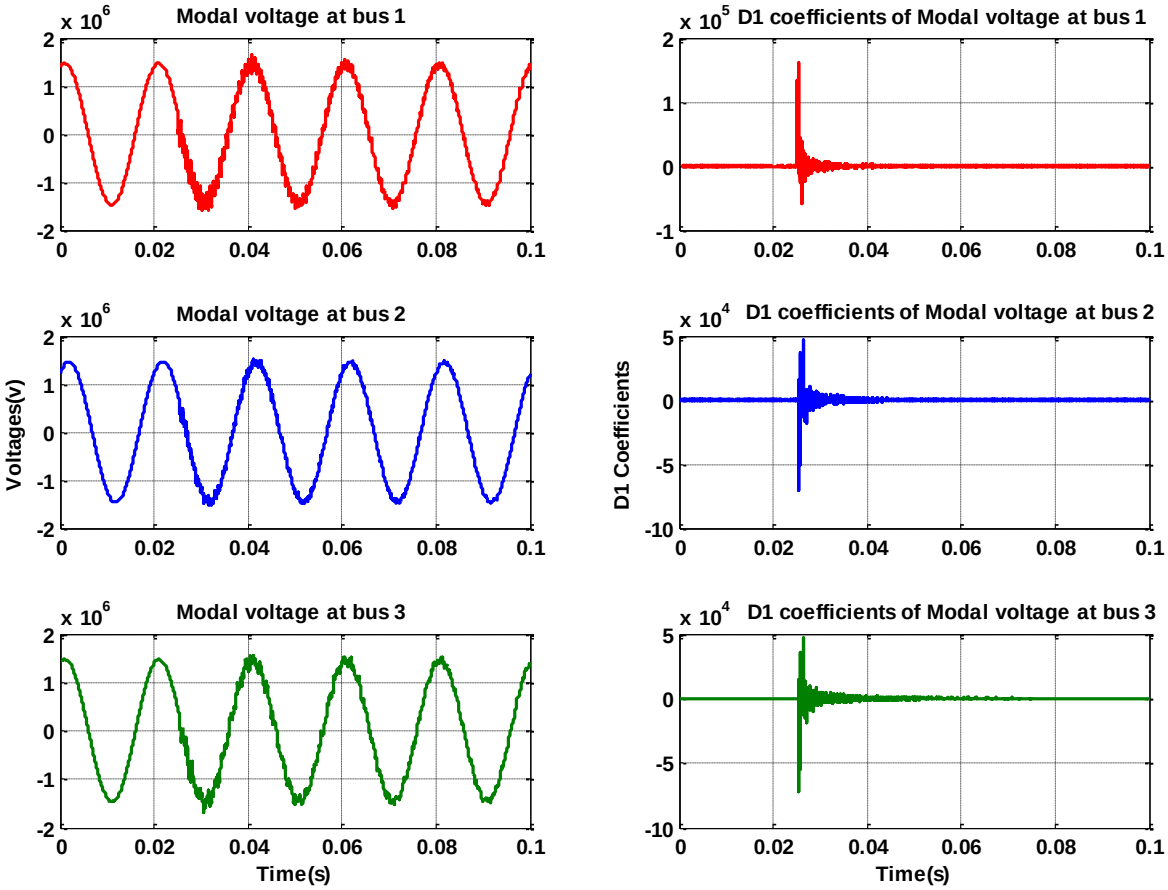

Fig. 2.5 Modal voltage signals for a-g fault section-1at 60 km from the source end (Fault resistance, $R_f = 0\Omega$ & Inception angle, $\theta = 90^0$)

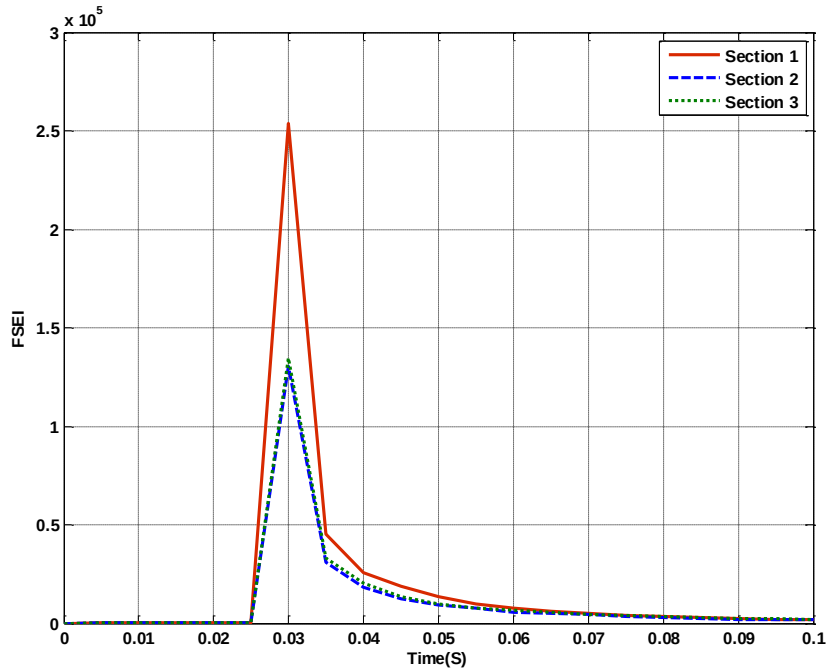

Fig. 2.6 FSEI variation for a-g fault in section-1 at 60 km from the source end ($R_f = 0\Omega$ & $\theta = 90^0$)

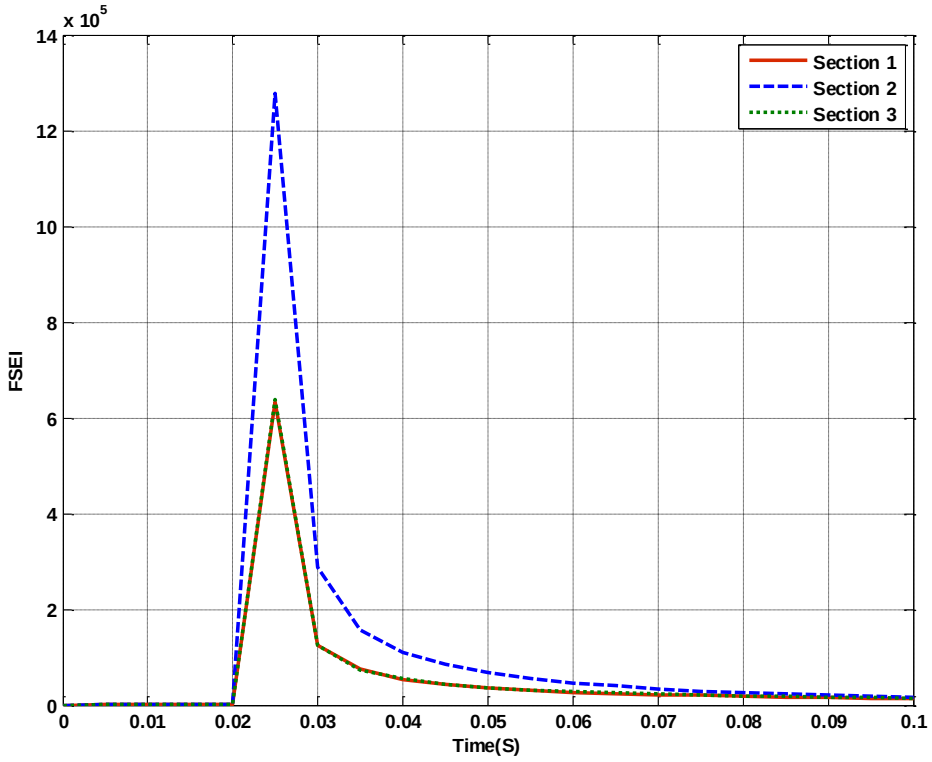

Fig. 2.7 FSEI variation for b-c fault in section-2 at 90 km from the source end ($R_f = 50\Omega$ & $\theta = 0^0$)

Exhaustive simulations are carried out for different types of faults occurring in different sections at various locations within the teed circuit. For each type of fault at a particular location, the fault inception angle is widely varied (0^0-180^0) to evaluate the performance of the proposed scheme. Influence of fault resistance is also evaluated by considering fault resistance values of 0 ohms and 50 ohms. All the phase voltages and currents of the three ends are fed as inputs to the proposed protection algorithm.

The performance of the scheme in detecting faults in symmetrical teed circuits for various types of faults i.e. line-to-ground, line-to-line, double line-to-ground, three phase faults is evaluated by considering 2160 cases in all. In all these cases studied, the scheme can correctly detect the fault. Fig.2.5 shows the waveforms of modal voltage signals of three ends and corresponding detail coefficients respectively for an a-g fault in section-1 at 60 km from the source end of the symmetrical teed circuit. Figs.2.6 and 2.7 show the variation of FSEI for two different faults in symmetrical teed circuit clearly discriminating between fault and non-fault situations.

Once the fault is detected, in all types of faults, the scheme could correctly verify whether the ground is involved in the fault or not. Fig.2.8 shows the phase and line voltages for an a-g fault in section-1 at 60 km from the source end and corresponding variations in PVFI. The variation in LVFI and GFI for the same fault is shown in Fig.2.9.

In all the simulation studies made, the performance of the proposed classification procedure is found to be highly accurate for all types of faults except double line to ground faults. The irregular transient energy patterns during LLG faults lead to less classification accuracy with such faults which is around 80%. Thus, the procedure based on direct comparison of transient high frequency signal energy is found to be effective only for faults other than LLG faults.

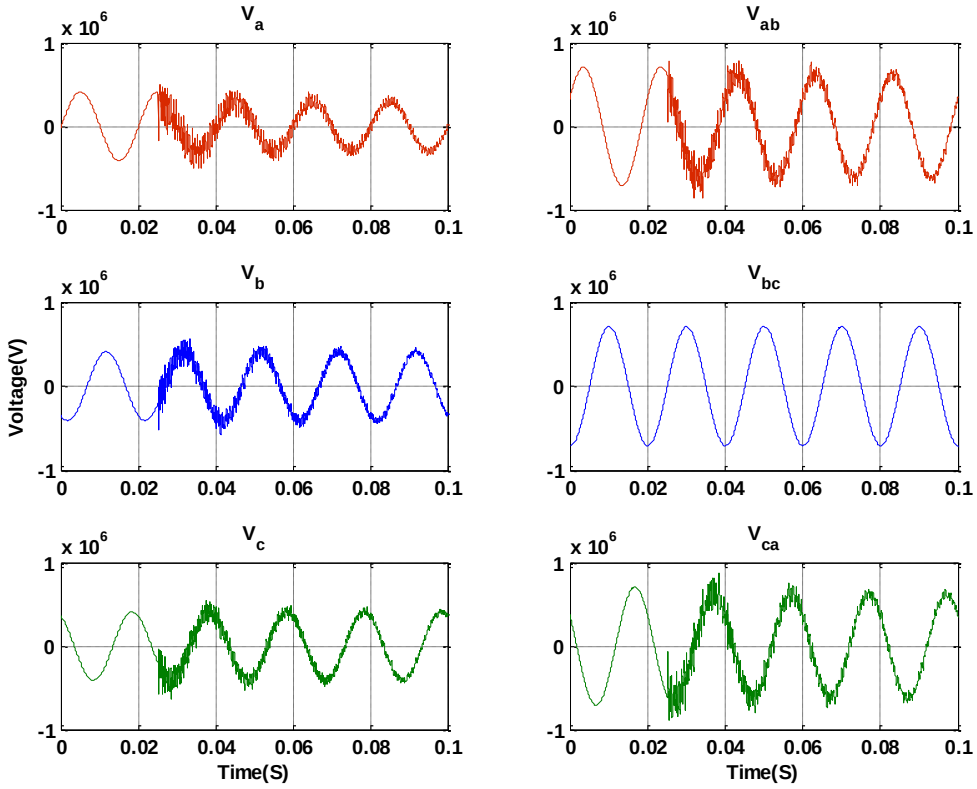

(a)

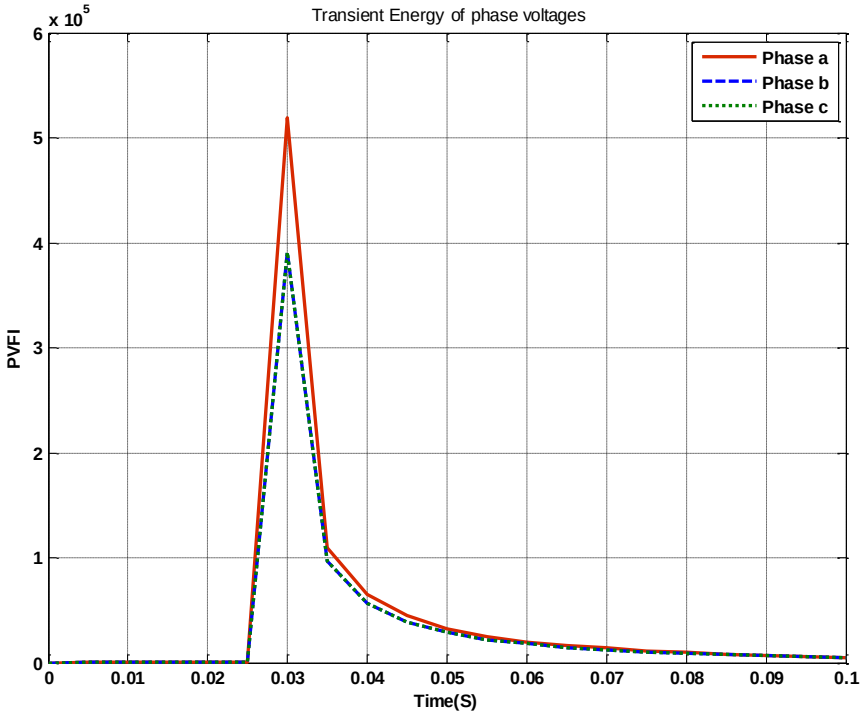

(b)

Fig. 2.8 Variation of Indices for an a-g fault in section-1 (a) Phase & line voltages (b) PVFI ($R_f = 0\Omega$ & Inception angle, $\theta = 90^0$)

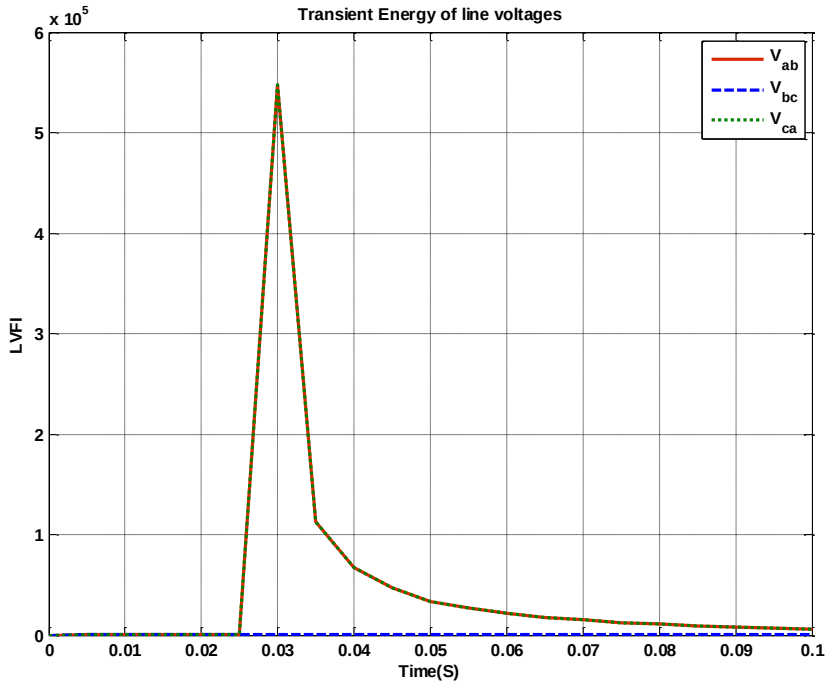

(a)

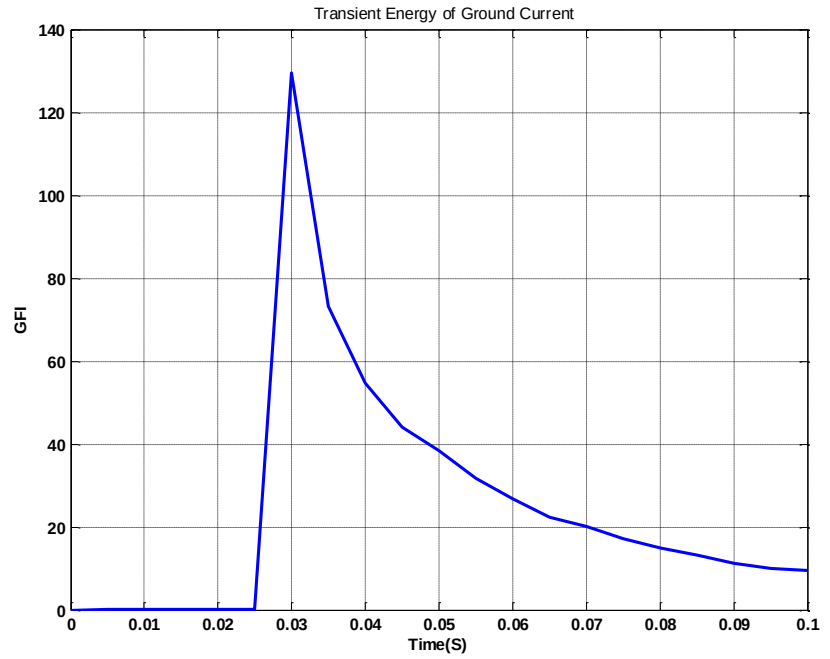

(b)

Fig. 2.9 Variation of Indices for an a-g fault in section-1
(a) LVFI (b) GFI ($R_f = 0\Omega$ & Inception angle, $\theta = 90^0$)

Table 2.1 shows the classification results for a few representative faults in symmetrical teed circuit. Tables 2.2 and 2.3 depict the overall accuracy of the scheme for symmetrical and asymmetrical teed circuits respectively. The overall accuracy is more than 94% though the scheme is less accurate with LLG faults.

Table 2.1: Classification Results

Sl. No	Fault section	Actual fault type	Fault Location (km)	Fault inception angle(θ^0)	R_f (Ω)	Detected fault type
1	1	AG	20	0	0	AG
2		BC	40	22.5	50	BC
3		CAG	60	45	0	CAG
4		ABC	80	135	50	ABC
5	2	BG	20	0	0	BG
6		CA	40	67.5	50	CA
7		ABG	60	157.5	0	CAG
8		ABC	80	112.5	50	ABC
9	3	CG	20	45	0	CG
10		AB	40	0	50	AB
11		BCG	60	90	50	BCG
12		ABC	80	157.5	50	ABC

Table 2.2: Classification Accuracy with Symmetrical Teed Circuit

Sl. No	Actual fault type	No. of cases	No. of cases Correctly classified	% Accuracy
1	AG	216	216	100
2	BG	216	216	100
3	CG	216	216	100
4	AB	216	216	100
5	BC	216	216	100
6	CA	216	216	100
7	ABG	216	180	83.33
8	BCG	216	175	81.02
9	CAG	216	174	80.55
10	ABC	216	216	100
TOTAL		2160	2041	94.49

Table 2.3: Classification Accuracy with Asymmetrical Teed Circuit

Sl. No	Actual fault type	No. of cases	No. of cases Correctly classified	% Accuracy
1	AG	180	180	100
2	BG	180	180	100
3	CG	180	180	100
4	AB	180	180	100
5	BC	180	180	100
6	CA	180	180	100
7	ABG	180	149	82.78
8	BCG	180	144	80.00
9	CAG	180	145	80.56
10	ABC	180	180	100
TOTAL		1800	1698	94.33

However, the scheme will not classify such faults as LG faults. In view of the poor classification accuracy with LLG faults, a thorough investigation into the transient patterns becomes necessary and is carried out in the following section.

2.5 Analysis of Transient Patterns in Fault Signals

The transient energy present on any signal depends on several factors based on the system configuration and fault conditions. These factors include the source strength, line loading, fault resistance, fault location, fault inception angle. Mainly, the fault inception angle (FIA) plays a very influencing role in deciding the transient magnitudes which is evident from the results presented by several authors. The studies reveal the effects of fault inception angle (FIA) on the transient patterns generated during different types of faults. The variation of transient energy (Ψ) with FIA is shown to be a square sinusoidal function given by [49],

$$\Psi(\theta_f) = E_0 + E_1 \sin^2(\theta_f + \delta_E) \tag{2.13}$$

Where θ_f is the fault inception angle, δ_E is a constant decided by the type of fault, E_0 and E_1 are constants decided by the system and fault parameters. The above expression is obtained by curve fitting with regression analysis considering only FIA variation while keeping fault resistance and location unchanged. Based on the patterns revealed, an accurate fault classification algorithm is developed by considering the influence of fault resistance and

location on transient variations also. The transient energy feature is extracted from the fault signals by wavelet transform as described below.

In order to identify the transient patterns, the transient energy present on fault voltage signals measured at the relay end of section-1 shown in Fig.2.10 is analyzed for different types of faults in the following. The first level wavelet decomposition is used to obtain high frequency content of voltage signals.

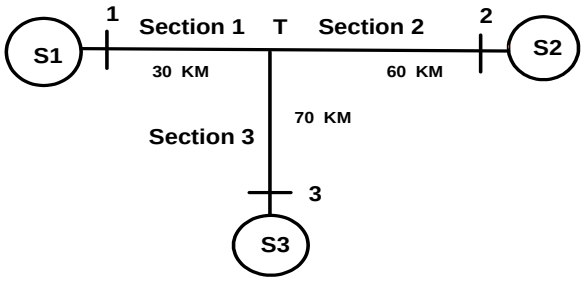

Fig. 2.10 A 400 KV Three-terminal Transmission Circuit

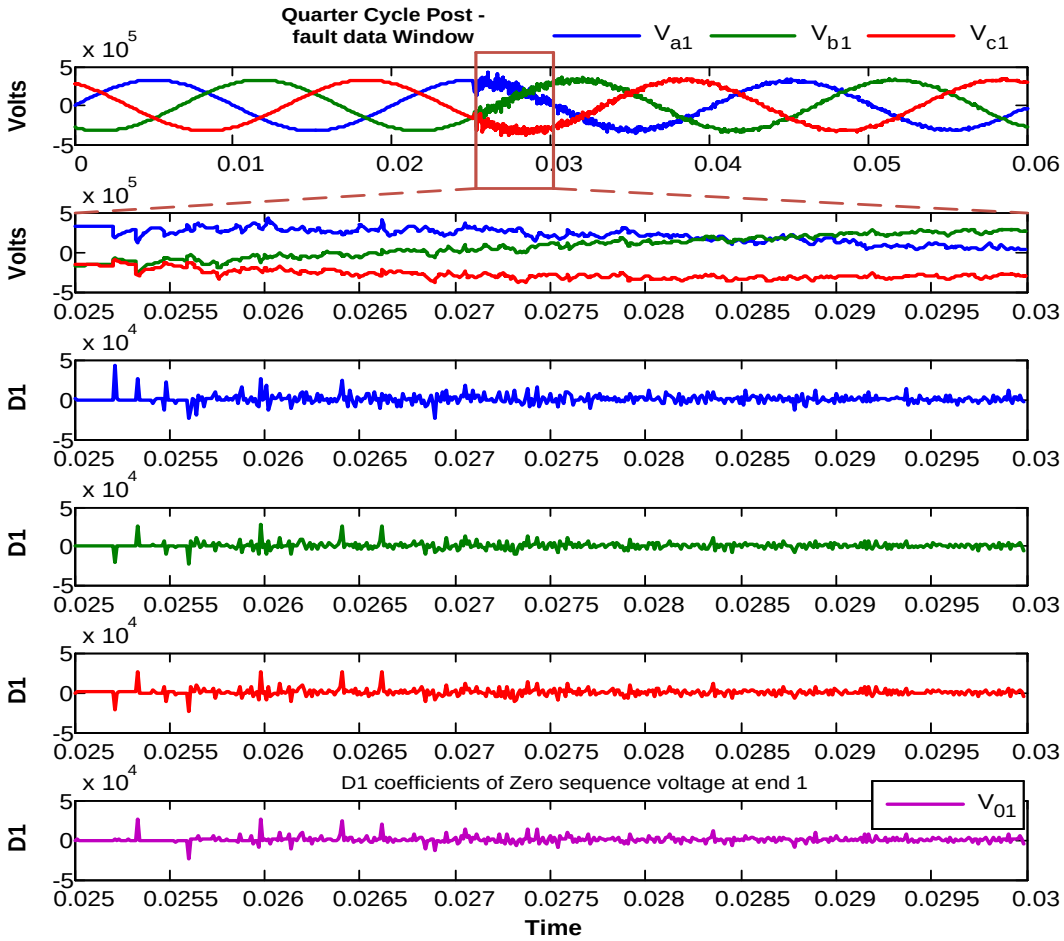

Fig. 2.11 Phase Voltages at end 1 and the D1 coefficients with an AG fault in section-3

The transient energy of any voltage signal is obtained from the detail coefficients (D1) using the Frobenius norm as,

$$\text{Transient Energy, } \psi = \sqrt{\sum_{i=1}^{N} [D1(i)]^2} \quad , \tag{2.14}$$

Where N is the number of first level detail coefficients after truncation, applied to eliminate the edge effect. Fig.2.11 shows typical waveforms of measured Phase Voltages at end-1 and the D1 coefficients for an AG fault in section-3.

2.5.1 Transient Energy during Grounded Faults

Single Line-to-Ground Faults (LG): LG faults constitute nearly 85% of total faults that occur on transmission lines and identifying such faults quickly allows single-pole tripping. With these faults, the un-faulted phases also exhibit transient energy that is comparable to that of the faulted phase. Fig.2.12 (a) shows the variation of transient energy on different voltage signals (Ψ_a, Ψ_b, Ψ_c and Ψ_g for three phases and zero sequence respectively) with FIA for an AG fault in the section- 1 of the three-terminal circuit.

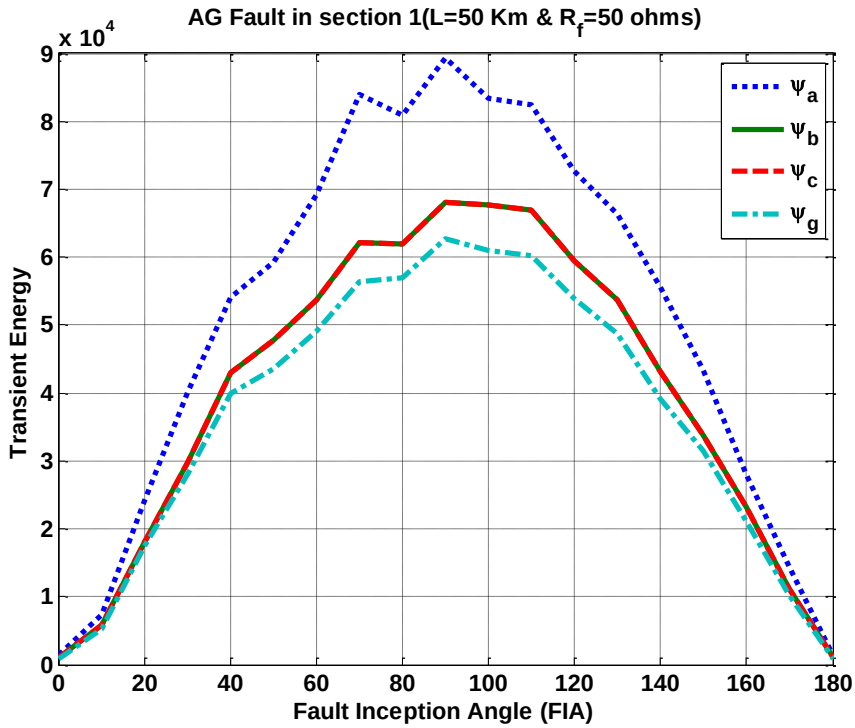

(a)

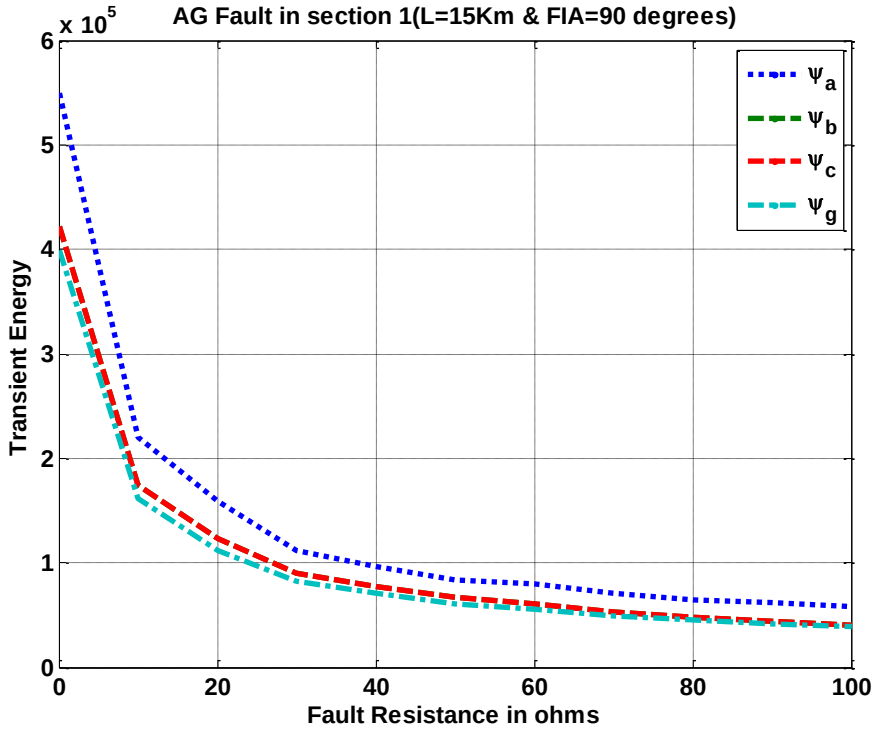

(b)

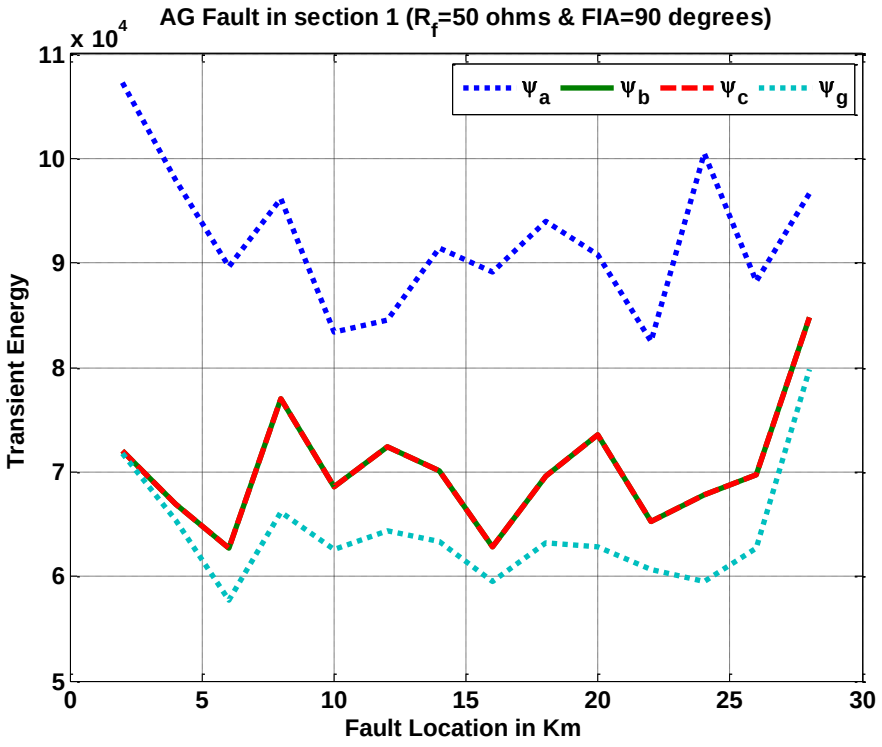

(c)

Fig. 2.12 Variation of Transient Energy with AG fault w.r.t
a) FIA b) Fault Resistance c) Fault Location

A maximum energy transient is created in the faulted phase when the FIA is 90^0 and a minimum appears with an FIA of 0 or 180 degrees. It is observed that the faulted phase always contains more energy compared to the un-faulted phases which carry identical energies as shown. Fig.2.12(b) and Fig.2.12(c) show the variation of energy with fault resistance and fault location respectively from which it can be observed that energy decreases with increase in fault resistance and remains fairly constant with change in location. In view of the similar behavior observed with BG and CG faults also, LG faults can be classified directly based on the magnitudes of the energy.

Double Line-to-Ground (LLG) Faults: Fig.2.13(a) shows the variation of transient energy on different voltage signals with respect to the FIA for an ABG fault in section-1. In contrast to the conclusion made by the reference [49], for a range of inception angles, the un-faulted phase is found to be having more energy than the faulted phases. Similar misleading patterns appear with BCG and CAG faults also and such transient patterns lead to poor accuracy with LLG fault classification based on transient magnitudes. An FIA of 60^0 leads to very small energy on the un-faulted phase.

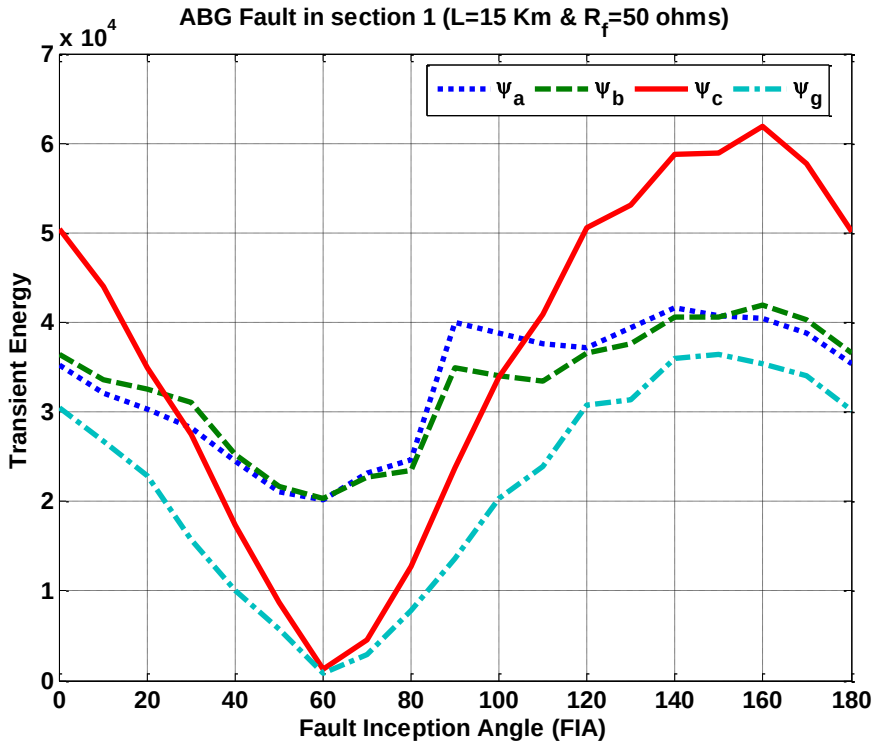

(a)

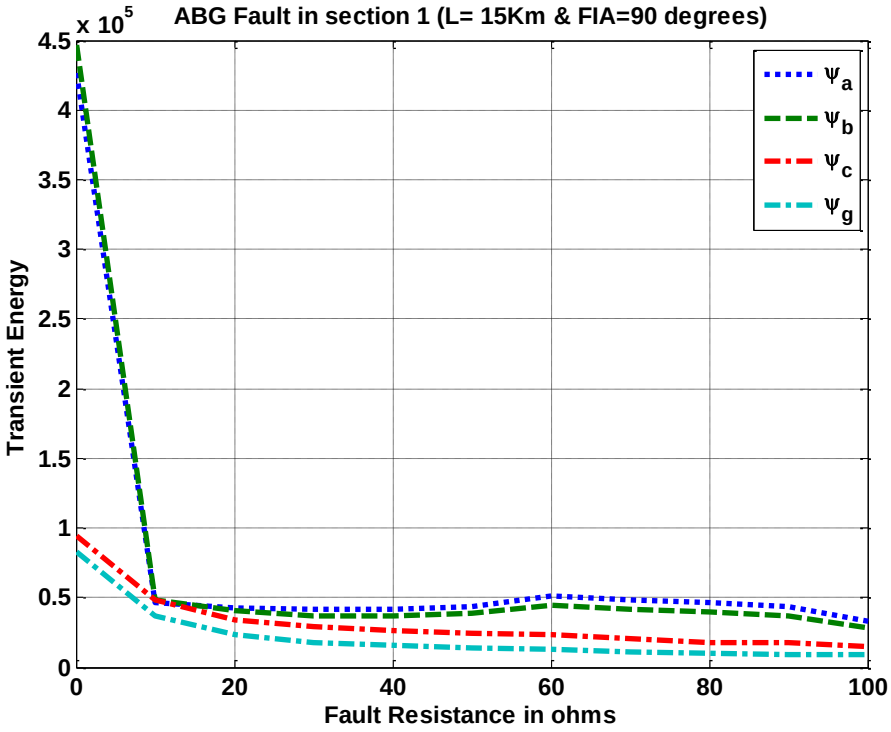

(b)

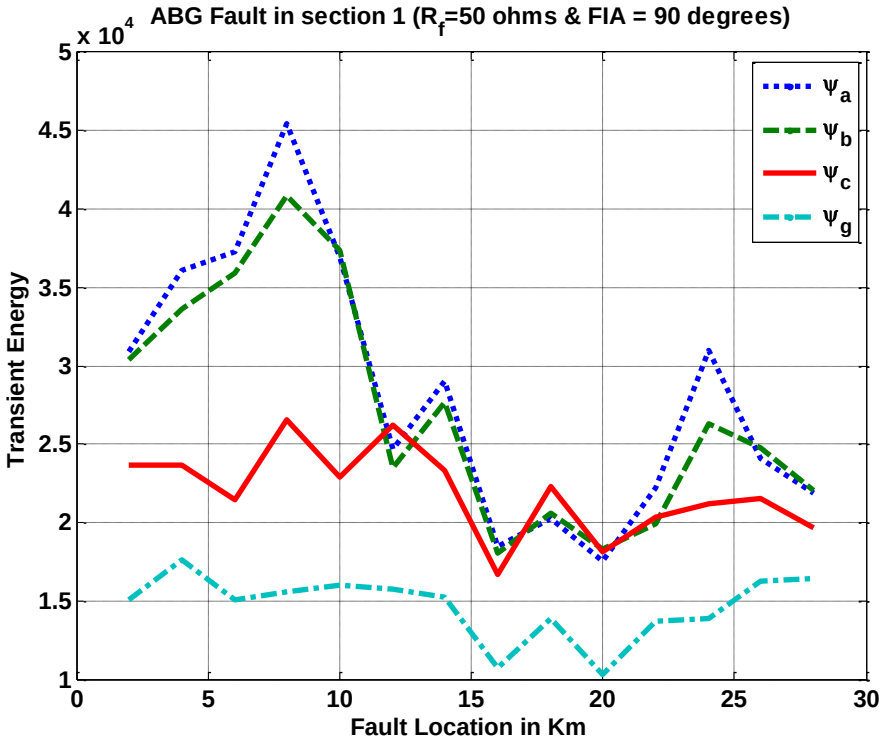

(c)

Fig. 2.13 Variation of Transient Energy with ABG fault w.r.t

a) FIA b) Fault Resistance c) Fault Location

Fig.2.13(b) and Fig.2.13(c) show the variation of energy with fault resistance and fault location respectively for an ABG fault. For a given fault resistance and inception angle, the location also plays a role in generating misleading transient patterns as shown.

2.5.2 Transient Energy during Ungrounded Faults

Line-to-Line (LL) faults: In the case of Line-to-Line (LL) faults, the two faulted phases contain equal values of transient energy in their phase voltages and the another phase contains no transient energy. Fig.2.14(a) shows that the two faulted phases in AB fault containing equal energies ($\Psi_a = \Psi_b$) and the unfaulted phase having zero energy along with the zero sequence voltage ($\Psi_c = 0$ and $\Psi_g = 0$). Fig.2.14(b) and Fig.2.14(c) show the influence of fault resistance and fault location on the transient energy during AB fault. Similar patterns are observed with BC and CA faults also.

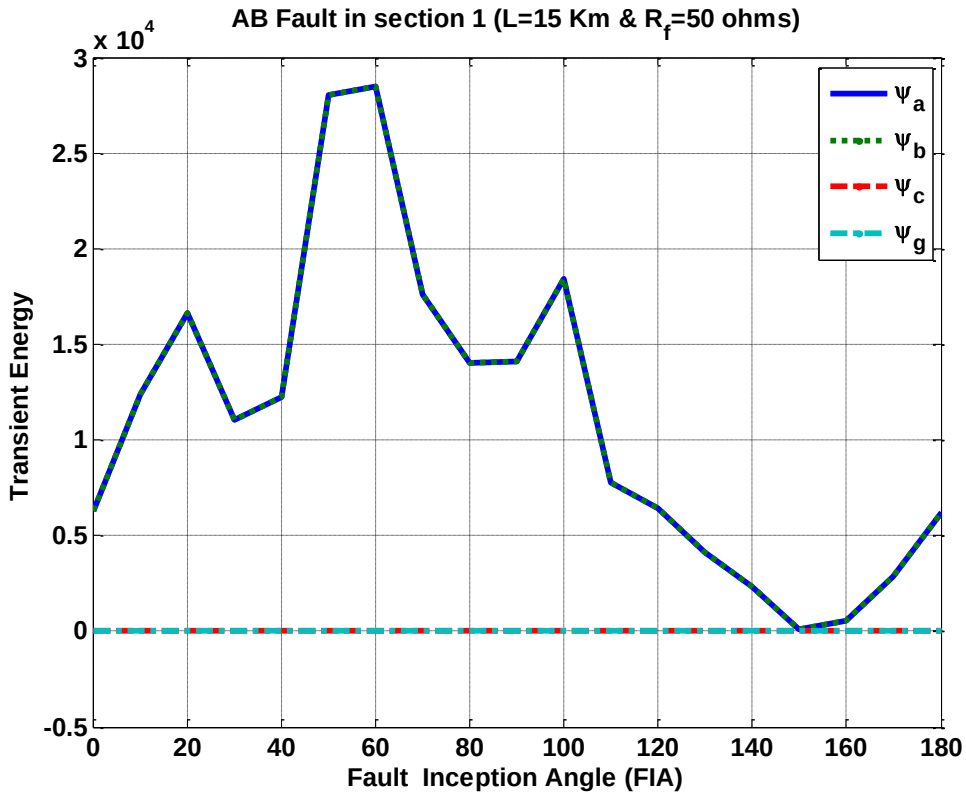

(a)

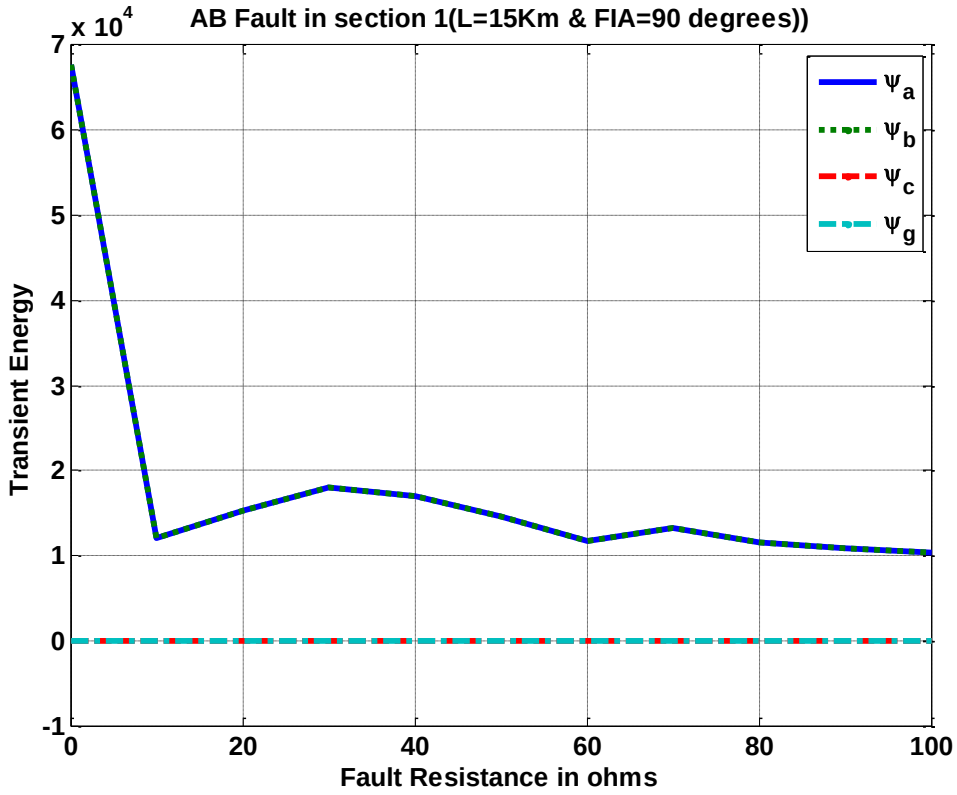

(b)

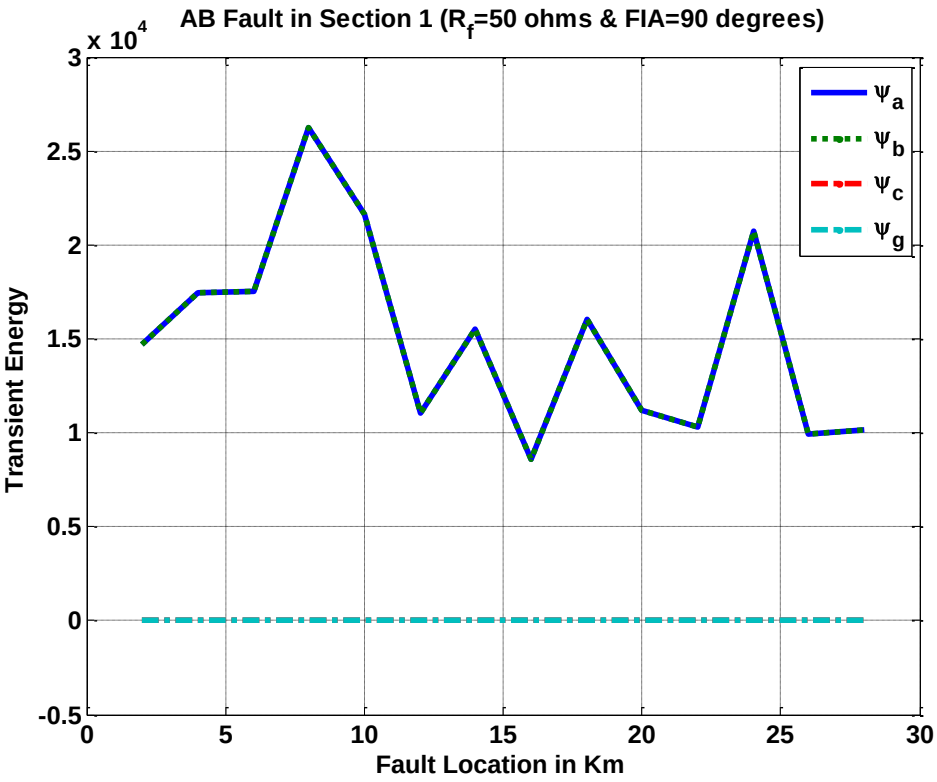

(c)

Fig. 2.14 Variation of Transient Energy with AB fault w.r.t
a) FIA b) Fault Resistance c) Fault Location

Three phase faults (LLL): The three phase faults (LLL) generate transient energy on all phases whose magnitudes depend on the FIA as shown in Fig.2.15(a).

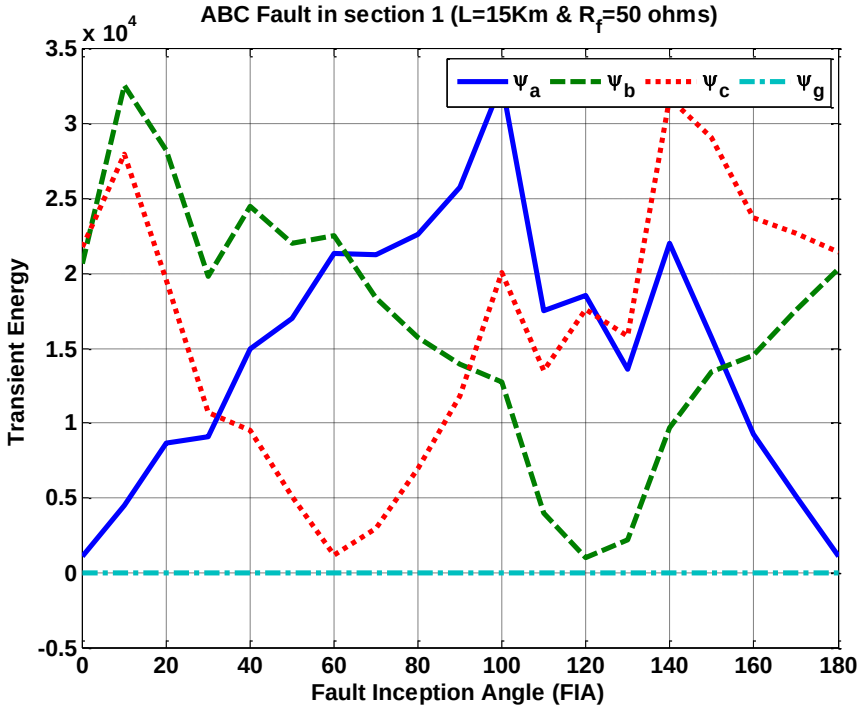

(a)

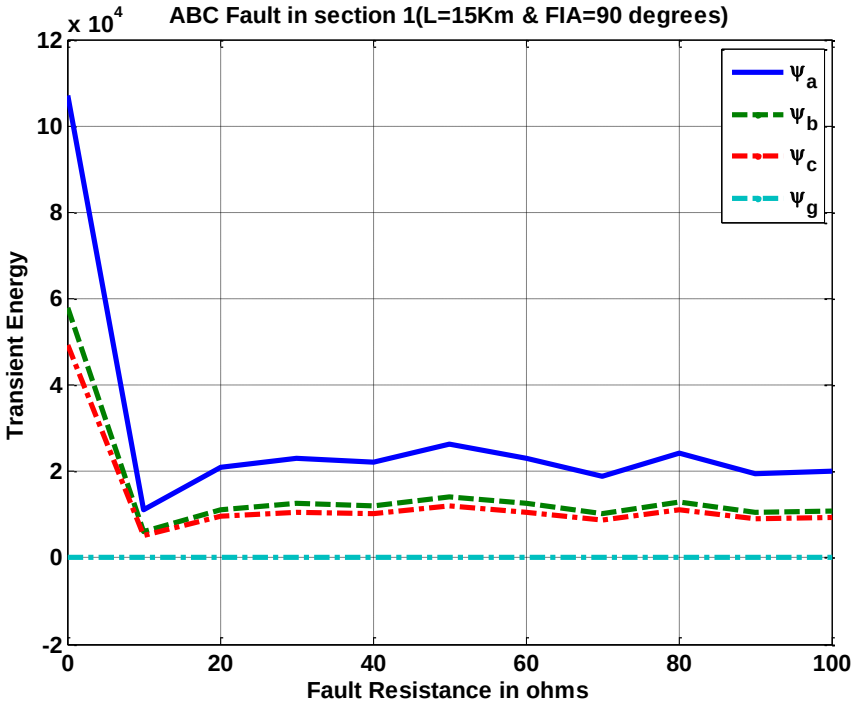

(b)

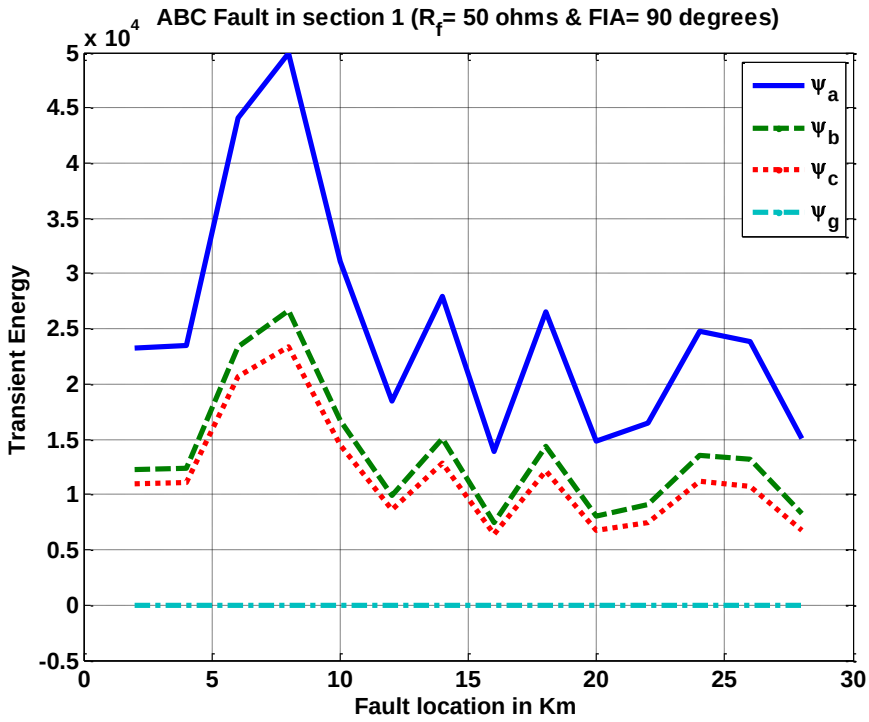

(c)

Fig. 2.15 Variation of Transient Energy with ABC fault w.r.t
a) FIA b) Fault Resistance c) Fault Location

Particularly, when FIA is 0 or 60 or 120 degrees, one of the phase voltages will contain very small transient energy. In such cases, the transient patterns appear to be similar to that of LL faults. Fig.2.15(b) and Fig.2.15(c) show the influence of fault resistance and location on transient energy during three phase faults.

Based on the analysis of above transient patterns, a new classification algorithm is developed in the following section to classify faults in three terminal circuits with high speed and accuracy.

2.6 Transient and Probabilistic Neural Network Based Fault Classification in EHV Three-Terminal Lines

Many transient based classification techniques depend on a comparison of the fault transient energy magnitudes of different phase voltages or currents and these magnitudes widely vary depending on the type of fault and fault parameters. Therefore, direct energy threshold based methods fail to give accuracy and, normalization becomes a necessity to fix

the thresholds. Despite the normalization, threshold fixing is difficult and many a time leads to inaccurate classification.

The proposed algorithm extracts the distinguishing features from the three phase voltage signals by using wavelet transform and a probabilistic neural network (PNN) is included to improve the accuracy of the classifier with LLG faults. Unlike many other techniques, the scheme is simple, requires single threshold setting and its speed & accuracy are significantly high. The performance of the method is verified by simulation of a three terminal line shown in Fig.2.16 using MATLAB/SIMULINK environment.

In this method, only post-fault voltage signals of a quarter cycle duration from all the three ends are taken as inputs and the choice is based on the fact that voltage transients are more than current transients during faults in power systems. The statement "Voltage transients are more than current transients in power systems" is based on the changes in magnitudes of voltage and current signals during the transient period. During faults, in any typical system, the voltage magnitude change will be much higher in value than the value of current magnitude change in a sample time. When the transient energy of fault signal is extracted by wavelet analysis, it is observed that voltage signal exhibits more energy than the current signal. For example, the voltage may change from 400 KV to 20KV where as current change will be from few hundred amperes to a maximum of 50 KA. Simulation waveforms for fault voltage and current signals also indicate the same behavior as revealed in Fig.2.4. Further, it has been mentioned in [46] that voltage transients are more than current transients.

A sampling frequency of 200 kHZ is used as the faulted lines contain high frequency components in the range of 10–100 kHZ [51]. Such a sampling rate is common with currently available hardware and in addition avoids the use of an anti-aliasing filter in digital relays [48]. The high frequency components present in voltage signals are extracted by using discrete wavelet transform (DWT) which is proven to be an effective signal processing tool for power systems [52]. Though many earlier techniques used higher-level decomposition, in this work only first level is preferred due to computational simplicity and accuracy of transient energy calculation. To avoid the effect of noise, transient based methods need de-noising of input signals before their processing and an assumption is made to that effect.

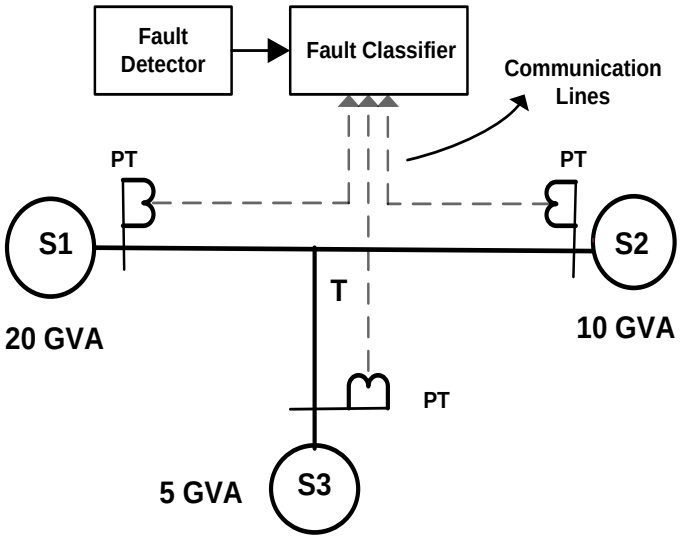

Fig. 2.16 Signal Communication for the proposed Fault Classifier

Now the Effective Transient Energy for each voltage signal is obtained by adding the signal energies of the three ends-1, 2 and 3. The effective transient energies for phase and line voltage signals $\Psi_a, \Psi_b, \Psi_c, \Psi_{ab}, \Psi_{bc}, \Psi_{ca}$ are calculated by using equations (2.10) & (2.11) and effective transient energy, Ψ_0 for zero sequence voltage is obtained using (2.12).

The above set of energies is normalized to form a feature array, called Normalized Effective Transient Energy (NETE) Array as shown in Fig.2.17. The NETE array describing the high frequency transient content on voltage signals is used as input for classifying faults in the present technique. In the above procedure, the addition of three end energies is done to improve the sensitivity of the scheme with respect to the fault location and fault resistance.

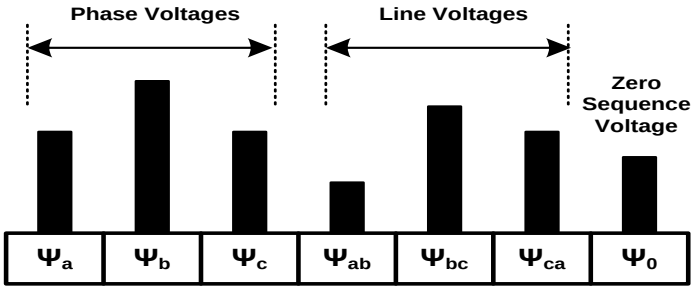

Fig. 2.17 NETE array input to the Classifier

The NETE feature array formed from the fault voltage signals will provide necessary information for classifying the fault without using any thresholds. Initially, the ground involvement in the fault can be checked by verifying the energy on zero sequence voltages i.e. Ψ_0. For ungrounded faults, its value will be zero.

Based on the transient analysis carried out in earlier sections, a hybrid algorithm is developed to classify all types of faults very accurately. In this algorithm, determination of ground involvement and classification of LG, LL & LLL faults will be carried out by a deterministic procedure as explained earlier. For LLG faults, in view of the misleading transient patterns, a neural network is incorporated thus making the algorithm a hybrid one. The algorithm takes the NETE array as input and initially checks whether the fault is grounded or not. If the fault does not involve ground, then it checks for LL or LLL fault. In the case of grounded fault, the algorithm first checks for different LG fault and if not concluded, the only remaining possibility is an LLG fault. Then, a trained PNN with seven inputs and a single output is activated for LLG fault to identify the faulted phases as shown in Fig.2.18. A PNN application only for LLG faults gives better overall accuracy and makes the algorithm suitable for real time implementation. A brief description of PNNs followed by the overall flow-chart is given below.

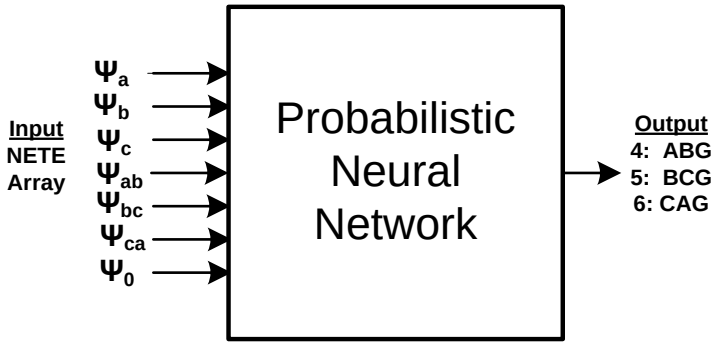

Fig. 2.18 PNN for LLG fault classification

2.6.1 Probabilistic Neural Networks

A Probabilistic Neural Network is a supervised learning network that belongs to the general category of 'Radial basis networks'. The PNN model has features that are different from other networks in the learning process. There is no need to set the initial weights of the neural network. In these networks, there is no relationship between learning and recalling processes and the difference between the inference and the target vectors will not be used to change the network weights. Many classification problems utilize pattern recognition techniques that are based on the theory of Bayesian classification [53]. These techniques realized by probabilistic model networks require estimation of probability density function (pdf) and for an input *X* belonging to a category A, the pdf is given by

$$f_A(X) = \frac{1}{(2\pi)^{p/2}\sigma^p}\frac{1}{m}\sum_{1}^{m}\exp\left[-\frac{(X - X_{Ai})^T(X - X_{Ai})}{2\sigma^2}\right] \tag{2.15}$$

Where i is the pattern number, m is the total number of training patterns, X_{Ai} is i^{th} pattern from category A, σ is the smoothing parameter and p is the dimensionality of measurement space. The architecture of a PNN is shown in Fig.2.19 below.

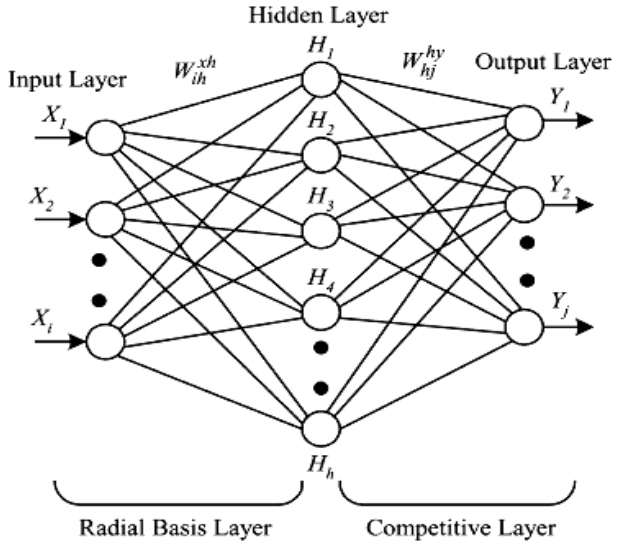

Fig. 2.19 Probabilistic Neural Networks (PNN) Architecture

Modifying and applying the above equation to the output vector H of the hidden layer in the PNN,

$$H_h = \exp\left(\frac{-\sum_i (Xi - W_{ih}^{xh})^2}{2\sigma^2}\right)$$

$$net_J = \frac{1}{N_j}\sum_h W_{hj}^{hy} H_h \text{ and } N_j = \sum_h W_{hj}^{hy} \tag{2.16}$$

$$net_j = \max_k(net_k) \text{ then } y_j = 1, \text{ else } y_j = 0$$

where

i is number of input layers;

h is number of hidden layers;

j is number of output layers;

k is number of training examples;

N is number of classifications (clusters);

σ is smoothing parameter (standard deviation);

X is input vector;

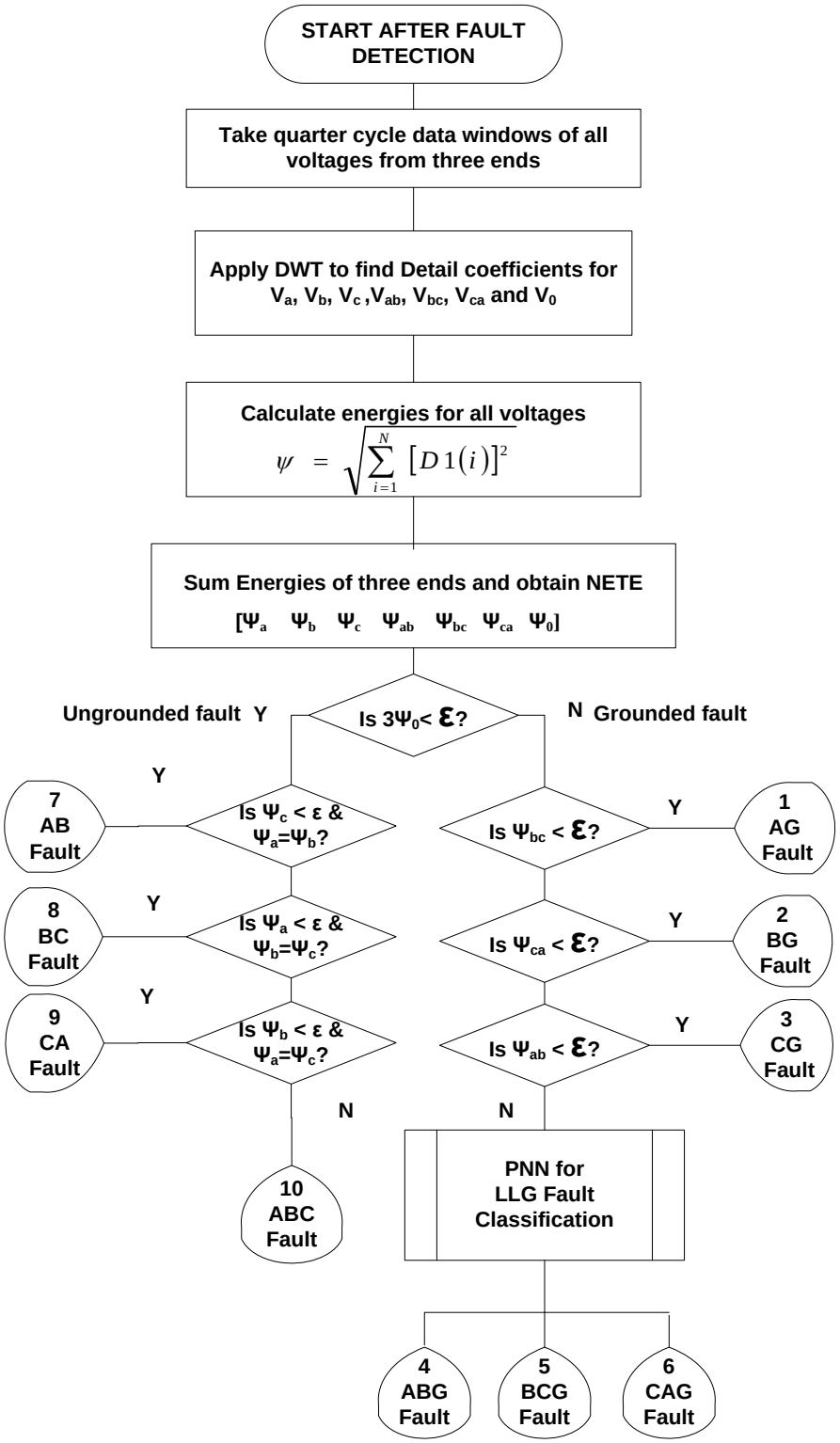

Fig. 2.20 Overall flowchart for the proposed algorithm

and where $\| X - X_{kj} \|$ is the Euclidean distance between the vectors X and X_{kj} , i.e., $\| X - X_{kj} \| = \sum_i (X - X_{kj})^2$; W_{ih}^{xh} is the connection weight between the input and the hidden layers X and H; and W_{hj}^{hy} is the connection weight between the hidden layer H and the output layer Y.

Given an input pattern, its probability of belonging to a particular category is determined from the pdfs. Then, the input pattern is decided to be in the group with which it has the highest probability. With enough training data, a PNN is guaranteed to converge and its fast learning makes it suitable for real time applications also [54]. In the present application, the PNN is initially trained with several NETE patterns obtained from the simulation for different LLG faults. Patterns are generated by considering wide variations in FIA, R_f and fault location.

The overall flowchart for the proposed scheme is shown in the Fig.2.20. The value of ε is set to be very small and should be ideally zero.

2.6.2 Simulation Results

The classification procedure developed above is now verified by simulation using a 400 KV line shown in Fig. 2.16 and the line parameters are R_0 = 0.16192 Ω/km, R_1=0.029792 Ω/km, L_0 = 3.947042 mH/km, L_1 = 1.05678 mH/km, C_0 = 7.130141 nF/km & C_1=11.04137 nF/km. The long line model considering distributed parameters is used in simulations.

The system is simulated in MATLAB/SIMULINK environment [55] with distributed parameter model for the transmission lines so that the fault signals exhibit the high frequency transient components generated. Wavelet decomposition is done using bior2.2 as mother wavelet because of its effectiveness in processing power system transients. A total number of 14040 different fault cases are considered for simulation by varying fault type, fault location, fault inception angle and fault resistance as shown in Table 2.4 to verify the performance of the proposed algorithm. A practical value of 0.02 is chosen for the single threshold ε in simulations. The transient energy patterns obtained for different faults are shown in polar scatter plots to justify the validity of the proposed algorithm.

Table 2.4: Fault Conditions Considered

Condition	Range
Fault type	AG, BG, CG, AB, BC, CA, ABG, BCG, CAG, ABC
Fault Resistance	0Ω, 50Ω, 100Ω
Fault Inception Angle	0^0 to 350^0 in steps of 10^0
Fault Location	Every 10 KM in each section
Total number of Cases	14040 (1404 for each fault type)

The performance of the proposed technique for line-to-ground (LG) faults is assessed by simulating 4212 faults at different locations. Fig.2.21(a) & (b) show the variation of transient energy with FIA on phase & line voltages respectively for AG faults (1404 cases). Note that Ψ_b and Ψ_{ab} patterns are not visible in these plots as they lie beneath Ψ_c and Ψ_{ca} respectively. Though the energy values of phase voltages for both faulted (Ψ_a) and unfaulted (Ψ_b & Ψ_c) lines are nearly overlapping, the values of line voltages clearly discriminate the faulted phase i.e. for all AG faults the value of Ψ_{bc} approaches zero. An accuracy of 100% is achieved for classifying LG faults by the developed procedure and Table 2.5 presents NETE values for a few LG faults simulated.

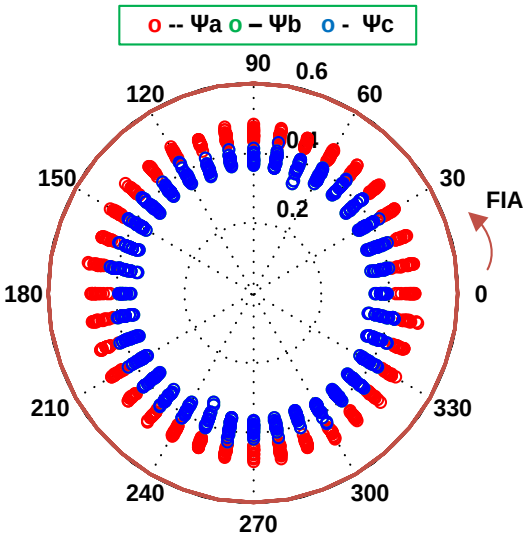

(a)

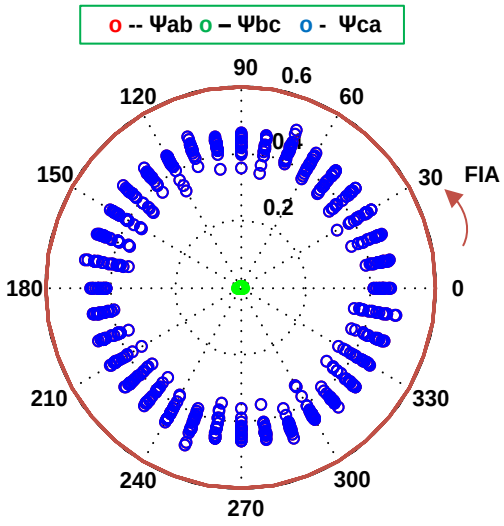

(b)

Fig. 2.21 Energy patterns for AG faults a) Phase voltages b) Line voltages

Table 2.5: NETE Values for LG Faults

Fault Type*	ɵ	Ψ_a	Ψ_b	Ψ_c	Ψ_{ab}	Ψ_{bc}	Ψ_{ca}	Ψ_0
AG R_f = 0 S =1:L = 20	0^0	0.4528	0.3706	0.3706	0.4503	0.0005	0.4503	0.3388
	90^0	0.4487	0.3698	0.3698	0.4544	0.0000	0.4544	0.3351
BG R_f = 0 S = 2:L = 40	0^0	0.3719	0.4470	0.3719	0.4530	0.4530	0.0001	0.3365
	90^0	0.3635	0.4499	0.3635	0.4610	0.4610	0.0001	0.3292
CG R_f=100 S = 3:L = 60	0^0	0.3865	0.3865	0.4664	0.0001	0.4186	0.4186	0.3650
	90^0	0.4086	0.4086	0.4729	0.0003	0.3800	0.3800	0.3919

*S: Section L: Location in KM R_f: Fault Resistance in Ω ɵ: Fault Inception Angle

In LLG faults, the transients generated clearly brought out the typical patterns that make classification difficult. Fig.2.22(a) and (b) show the variation of energy on phase voltages for ABG faults with two different fault resistances (0Ω and 100Ω). The un-faulted phase energy (Ψ_c) is observed to be more than the faulted phase energy for a range of inception angles and this range is found to be large with an increase in fault resistance. Similar patterns are obtained for BCG and CAG faults as well. The symmetry of patterns in the polar plots shows that consideration of FIA variation from 0 to 180 degrees is very much necessary while developing transient based classification algorithms. Table-2.6 gives the NETE values for a representative set of LLG faults simulated.

Regarding the performance levels, the PNN is activated for all LLG faults without fail and the classification accuracy with the trained PNN is found to be very high (99.59%). The results of 4212 cases simulated validate the application of PNN for classifying only double line to ground faults.

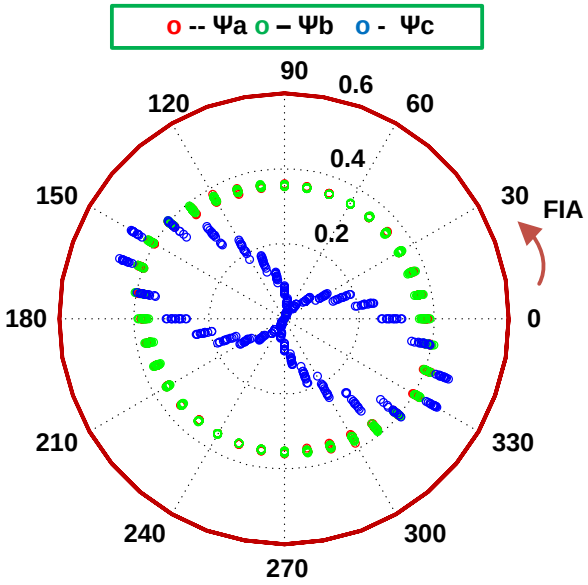

(a)

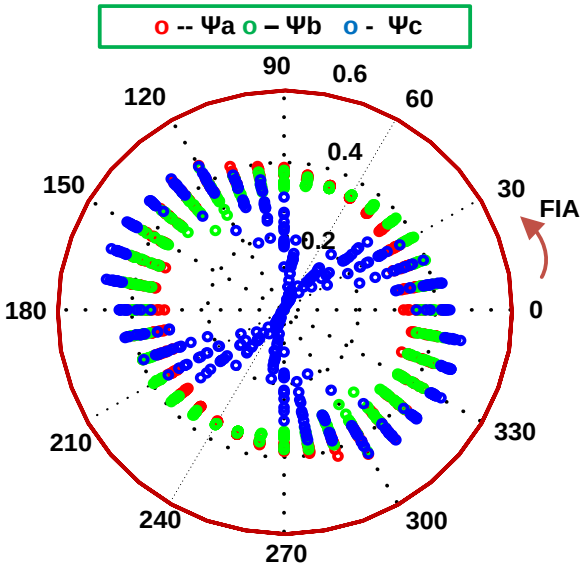

(b)

Fig. 2.22 Energy patterns on phase voltages for ABG faults

a) $R_f = 0\Omega$ b) $R_f = 100\Omega$

Table 2.6: NETE Values for LLG Faults

Fault Type*	θ	Ψ_a	Ψ_b	Ψ_c	Ψ_{ab}	Ψ_{bc}	Ψ_{ca}	Ψ_0
ABG R_f =100 S =1:L = 10	0^0	0.3585	0.3957	0.3864	0.3860	0.4619	0.3335	0.3033
	90^0	0.3707	0.3451	0.1707	0.6562	0.3118	0.4106	0.1338
BCG R_f =100 S = 2:L = 30	0^0	0.0296	0.3507	0.3561	0.3473	0.7050	0.3623	0.0191
	90^0	0.4507	0.3608	0.3574	0.4692	0.0534	0.4612	0.3213
CAG R_f=100 S = 3:L = 50	0^0	0.4061	0.4057	0.4050	0.3059	0.4004	0.3190	0.3482
	90^0	0.3853	0.2826	0.3836	0.3910	0.3282	0.5495	0.2490

In the case of line-to-line (LL) faults, the present technique classified all faults except 2 (out of 4212 cases) correctly by using the energy values of the phase voltages. Fig.2.23 shows the variation of energy of phase voltages for all phase- A to phase-B (AB) faults simulated (Ψ_a patterns not visible). Clearly, the un-faulted phase always exhibited a value of energy (Ψ_c) close to zero. The normalized energy on faulted phase voltage signals (Ψ_a and Ψ_b) remains fairly constant at 0.353. A similar pattern is obtained for BC and CA faults as well. As can be seen in Table-2.7, the energy on unfaulted phase is very close to zero in all LL faults.

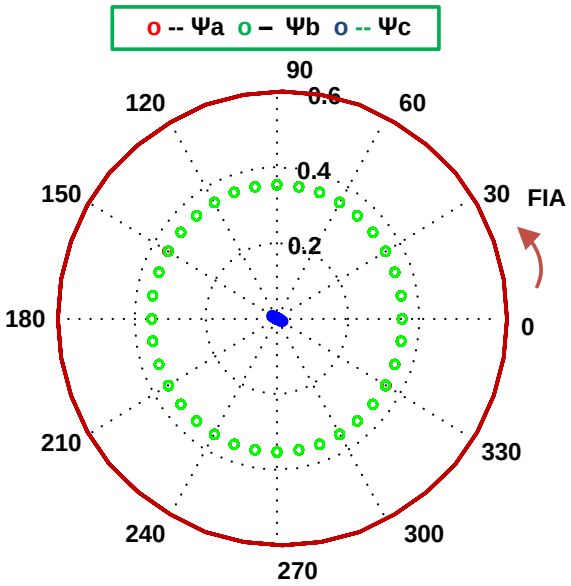

Fig. 2.23 Energy patterns on Phase Voltages with AB Faults

Table 2.7: NETE Values for LL Faults

Fault Type*	θ	Ψ_a	Ψ_b	Ψ_c	Ψ_{ab}	Ψ_{bc}	Ψ_{ca}	Ψ_0
AB R_f =0 S =1:L = 20	0^0	0.3536	0.3535	0.0001	0.7071	0.3535	0.3536	0.0000
	90^0	0.3536	0.3536	0.0000	0.7071	0.3536	0.3536	0.0000
BC R_f =50 S = 2:L = 40	0^0	0.0001	0.3536	0.3536	0.3535	0.7071	0.3536	0.0000
	90^0	0.0052	0.3537	0.3534	0.3540	0.7070	0.3532	0.0018
CA R_f=100 S = 3:L = 60	0^0	0.3535	0.0007	0.3536	0.3534	0.3537	0.7071	0.0003
	90^0	0.3536	0.0005	0.3535	0.3536	0.3535	0.7071	0.0002

All the symmetrical three phase faults (ABC faults) simulated have been classified by the present method with 100% accuracy. Fig.2.24 shows the typical transient patterns developed on phase voltages for three phase faults. The NETE magnitudes of different voltage signals varied widely with respect to FIA and in no case, the NETE meets the pattern of any LL fault. A set of NETE values obtained with LLL faults is shown in Table-2.8.

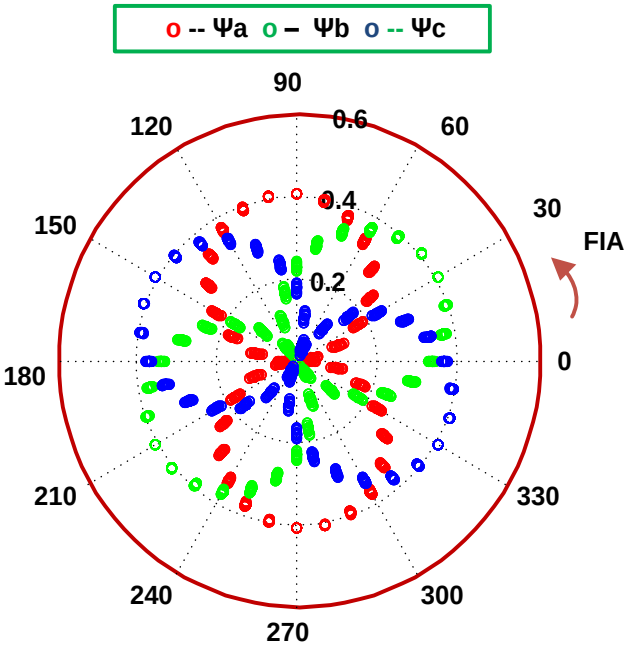

Fig. 2.24 Energy patterns on Phase Voltages with ABC Faults

Table 2.8: NETE Values for LLL Faults

Fault Type*	θ	Ψ_a	Ψ_b	Ψ_c	Ψ_{ab}	Ψ_{bc}	Ψ_{ca}	Ψ_0
ABC R_f = 50 S =2:L = 30	0^0	0.0386	0.3327	0.3713	0.2941	0.7039	0.4098	0.0000
	90^0	0.4064	0.2367	0.1698	0.6431	0.0669	0.5762	0.0000
ABC R_f =100 S = 3:L = 60	0^0	0.0265	0.3396	0.3661	0.3131	0.7056	0.3926	0.0000
	90^0	0.4074	0.2267	0.1807	0.6341	0.0460	0.5881	0.0000

The overall accuracy of performance with the proposed hybrid classifier is found to be very high. Particularly, its ability to classify more frequent single-line-to-ground (LG) faults with 100% accuracy is an attractive feature. The results of simulation show that the technique is quiet insensitive to fault location, fault resistance and FIA which is a definite advantage over conventional phasor based methods. Also, the classification of LLG faults by using a PNN overcomes the major drawback of many existing methods in classifying LLG faults. Table-2.9 gives the complete simulation results for all 14040 faults considered with only 19 misclassifications in total.

Table 2.9: Overall Classification Results

Given Fault Type (Each 1404 cases)	Fault Classification Result									
	1 AG	2 BG	3 CG	4 ABG	5 BCG	6 CAG	7 AB	8 BC	9 CA	10 ABC
AG	1404	0	0	0	0	0	0	0	0	0
BG	0	1404	0	0	0	0	0	0	0	0
CG	0	0	1404	0	0	0	0	0	0	0
ABG	0	0	0	1400	0	2	2	0	0	0
BCG	0	0	0	1	1397	4	0	2	0	0
CAG	0	0	0	2	2	1398	0	0	2	0
AB	0	0	0	0	0	0	1404	0	0	0
BC	0	0	0	0	0	2	0	1402	0	0
CA	0	0	0	0	0	0	0	0	1404	0
ABC	0	0	0	0	0	0	0	0	0	1404

A performance comparison with a recently reported method [19] in Table-2.10 reveals the improvement in accuracy achieved by the proposed technique. Other preliminary studies have shown that the scheme performs well with close-up faults and tolerates synchronization errors with measured signals.

Table 2.10: Accuracy of Classification

Sl. No	Fault Type	Number of Cases	Accuracy %	% Accuracy reported by [19]
1	LG	4212	100	95.3
2	LL	4212	99.95	99.3
3	LLL	1404	100	99.7
4	LLG	4212	99.59	96.8
	Overall	14040	99.88	97.77

2.7 Fault Classifier-Reliability Enhancement

Reliability of digital relays can be enhanced by introducing a degree of redundancy in to the software/hardware and using different principles within the same relay [56]. Redundancy is defined as 'the existence of more than one means for performing a given function' and the two important aspects of reliability are dependability and security.

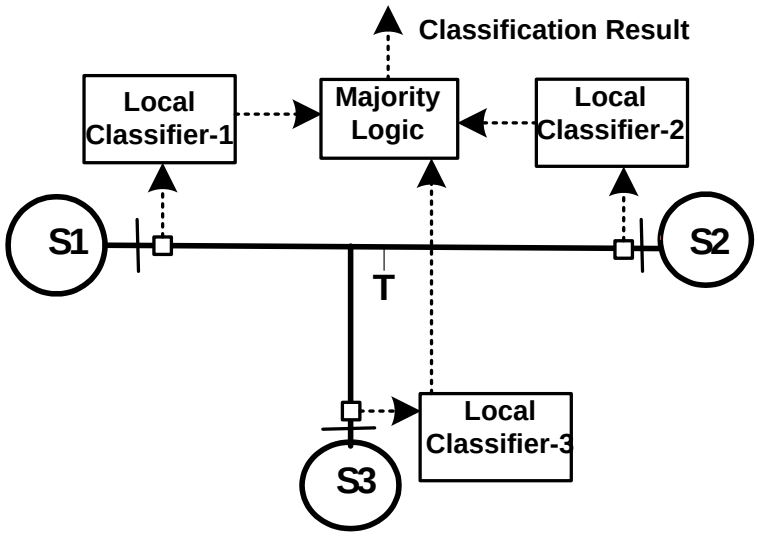

Fig. 2.25 Fault Classifier with reliability enhancement

Dependability is a measure of the degree of certainty that a protective system will operate correctly when required and security is a measure of the degree of certainty that a protection system will not operate incorrectly. These measures are mutually conflicting and generally a balance is maintained between dependability and security.

Extending these principles to the proposed fault classification system, an improvement in accuracy and dependability is achieved by providing three identical local classifiers at the three ends of the three-terminal line as shown in Fig.2.25. The fault classification decisions of the classifiers at three ends are given as input to a ‘majority block’ whose output is always equal to the input with the highest majority as shown in Fig.2.26. The final classification decision is given by the ‘majority block’ if at least two inputs are equal otherwise the output will be zero to indicate a failure to classify. For example, if decision is ‘AG fault’ from end1 and end2, and ‘BG fault’ from end3, then the final decision is AG fault. A simple communication channel is required to implement this classification methodology.

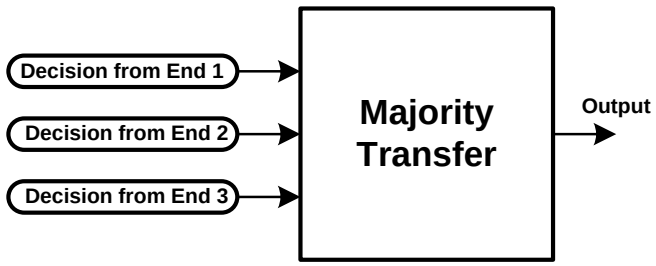

Fig. 2.26 Reliability Enhancement with Majority logic

With this additional set-up, even when a classifier fails at a particular end, the fault type is identified. Thus, it improves the dependability of the scheme. Also, if there is any misclassification at one end due to low transients, the overall result is not affected and an improvement in accuracy is attained.

2.7.1 Simulation Results

The results of the classifier with only local end information are obtained for all the faults simulated earlier. Table-2.11 shows the accuracy of classification at different ends. The total number of misclassifications at each end is 116, 157 and 111 respectively. Table-2.12 shows the overall accuracy averaged over all types of faults at each end.

By making use of the classification decisions made at different ends, the final reliability of classification is enhanced further by taking majority logic decision as depicted in Table-2.13. In this case, the total number of misclassifications is reduced to 73 thus improving the dependability of the scheme. This scheme also reduces the communication burden as only decision indicator needs to be conveyed to the main classifier. Table-2.14 reports the accuracy of classification with reliability enhancement as compared to a recent SVM based approach [19].

Table.2.11: Fault Classification Results with Single End Information

Given Fault Type (Each 1404 cases)	Fault Classification Result									
	1 AG	2 BG	3 CG	4 ABG	5 BCG	6 CAG	7 AB	8 BC	9 CA	10 ABC
End-1 Classifier										
AG	1404	0	0	0	0	0	0	0	0	0
BG	0	1404	0	0	0	0	0	0	0	0
CG	0	0	1404	0	0	0	0	0	0	0
ABG	0	0	24	1380	0	0	0	0	0	0
BCG	17	0	0	0	1387	0	0	0	0	0
CAG	0	22	0	0	1	1381	0	0	0	0
AB	0	0	0	8	0	0	1396	0	0	0
BC	0	0	0	0	6	0	0	1398	0	0
CA	0	0	0	0	0	3	0	0	1401	0
ABC	0	0	0	0	0	0	11	12	12	1369
End-2 Classifier										
AG	1404	0	0	0	0	0	0	0	0	0
BG	0	1404	0	0	0	0	0	0	0	0
CG	0	0	1404	0	0	0	0	0	0	0
ABG	0	0	29	1373	0	2	0	0	0	0
BCG	26	0	0	2	1375	1	0	0	0	0
CAG	0	30	0	1	0	1373	0	0	0	0
AB	0	0	0	13	0	0	1391	0	0	0
BC	0	0	0	0	12	0	0	1392	0	0
CA	0	0	0	0	0	12	0	0	1392	0
ABC	0	0	0	0	0	0	9	11	12	1372
End-3 Classifier										
AG	1404	0	0	0	0	0	0	0	0	0
BG	0	1404	0	0	0	0	0	0	0	0
CG	0	0	1404	0	0	0	0	0	0	0
ABG	0	0	20	1384	0	0	0	0	0	0
BCG	9	0	0	0	1395	0	0	0	0	0
CAG	0	23	0	0	0	1381	0	0	0	0
AB	0	0	0	14	0	0	1390	0	0	0
BC	0	0	0	0	17	0	0	1387	0	0
CA	0	0	0	0	0	18	0	0	1386	0
ABC	0	0	0	0	0	0	4	2	4	1394

Table.2.12 Overall Accuracy of Classification

Sl. No	Fault Type	Number of Cases	% Accuracy of Classification with single ended information		
			End-1	*End-2*	*End-3*
1	LG	4212	100	100	100
2	LLG	4212	98.48	97.84	98.76
3	LL	4212	99.59	99.12	98.83
4	LLL	1404	97.50	99.72	99.28
Overall		14040	99.17	98.86	99.20

Table 2.13: Classification Results with Reliability Enhancement

Given Fault Type (Each 1404 cases)	Fault Classification Result									
	1 AG	2 BG	3 CG	4 ABG	5 BCG	6 CAG	7 AB	8 BC	9 CA	10 ABC
AG	1404	0	0	0	0	0	0	0	0	0
BG	0	1404	0	0	0	0	0	0	0	0
CG	0	0	1404	0	0	0	0	0	0	0
ABG	0	0	11	1393	0	0	0	0	0	0
BCG	7	0	0	0	1397	0	0	0	0	0
CAG	0	16	0	0	0	1388	0	0	0	0
AB	0	0	0	12	0	0	1392	0	0	0
BC	0	0	0	0	9	0	0	1395	0	0
CA	0	0	0	0	0	12	0	0	1392	0
ABC	0	0	0	0	0	0	1	3	2	1398

Table 2.14: Accuracy of Classification

Sl. No	Fault Type	Number of Cases	Accuracy %	% Accuracy reported by [19]
1	LG	4212	100	95.3
2	LL	4212	99.19	99.3
3	LLL	1404	99.21	99.7
4	LLG	4212	99.57	96.8
Overall		14040	99.48	97.76

2.8 Conclusions

In this chapter, firstly, a transient based classification is developed for the three terminal lines whose performance is found to be poor with double-line to ground faults. In order to overcome this problem, an exhaustive fault transient analysis is carried out to develop improved classification algorithms. Based on the analysis, another transient-PNN based algorithm is presented. The following conclusions can be drawn from the observations made through digital simulation.

The first method 'Transient Based Fault Classification in EHV Teed Circuits using Wavelet Transform' is found to be offering many advantages. The salient features are

- The fault detection technique using modal signal is found to be accurate and capable of detecting any type of fault occurring on any section of the teed circuit.
- Fault classification procedure using phase voltage, line voltage and ground current signals is highly accurate for all types of faults except double-line-ground faults
- The technique is insensitive to fault location, fault inception angle and fault resistance.
- Less accurate in double-line-ground faults
- Results indicate that the overall scheme is fast & accurate and applicable for both symmetrical and asymmetrical teed circuits.

In view of the less accuracy with double-line-ground faults in the first method because of irregular transient patterns, the second method 'Transient and Probabilistic Neural Network Based Fault Classification in EHV Three-Terminal Lines' uses an ANN based solution. The main observations are

- Fault classification procedure using phase voltage, line voltage and ground current signals is highly accurate for all types of faults
- Improvement in accuracy with double-line-ground faults classification by the use of PNN is significant.
- The method copes well with the adverse influence of fault inception angle and fault resistance.
- The method is simple, requires one threshold and insensitive to fault conditions
- Exhaustive simulation results presented indicate the accuracy of the scheme with all types of faults

- Dependability of the classification scheme is enhanced by the use of single ended data with good accuracy.

The two classification algorithms proposed make use of information from all ends. If a communication link from an end to the central station fails, the classification result can be still obtained as the algorithm uses the sum of transient energies from all ends. It is evident from the results shown in Table 2.12 that even with single ended information the classification accuracy is satisfactorily high. In addition, when reliability enhancement is introduced, the majority concept will still retain the high accuracy (99.48%). Further, communication burden is also less as only decision indicator needs to be communicated from each end to the central station. Therefore, it can be concluded that the proposed classification algorithms fail gracefully whenever communication link fails from one or two ends. The overall conclusions are presented in chapter-5.

Chapter 3

Fault Location in Three-Terminal Transmission Lines

3.1 Introduction to Fault Location in Transmission Lines

Reliable operation of power transmission lines is essential for modern power grids to minimize grid disturbances and consequential customer service interruptions. Despite many advances in power transmission technologies, permanent faults do occur on long overhead lines due to several reasons like natural disasters leading to unavoidable line outages. In order to restore power supply, Power utilities include fault locator features in the line protection equipment installed in substations. A fault locator must be accurate so that the repair crew can quickly reach the location and restore service. Such a fault locating feature can also facilitate fault analysis to identify weak spots in the system. The objective of any fault locator is to find the fault distance 'x' accurately as shown in Fig.3.1 by using measurements at the line ends.

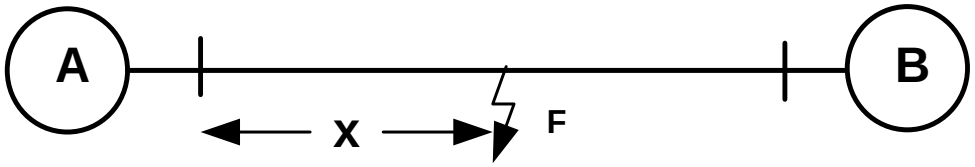

Fig. 3.1 Two-terminal Transmission Line

Methods available for fault location on transmission lines can be grouped into two main categories as Fundamental phasor based approaches and Travelling wave based approaches. In the phasor based techniques, the fundamental frequency components of post-fault voltage/current signals measured at the relay points are used as input discriminating features for the locator. These techniques involve calculation of fault loop impedance from circuit principles by using the estimated fault voltage and current phasors. However, phasor based methods using only single-ended data suffer from many limitations due to the effects of fault resistance, line loading and source impedances. With the availability of communication channels, techniques that use phasor information from two ends have been developed to overcome the drawbacks of the single-ended method.

The travelling wave approaches utilize the high frequency transients generated by the fault in the form of traveling waves. By finding the arrival times of waves at the relay end, the fault location can be estimated. These techniques are insensitive to fault resistance, fault type, source impedance and are proved to be immune to power swings and CT saturation. Despite many advantages, these methods require high sampling rate and noise rejection abilities. Several improvements have also been made to travelling wave techniques by processing information from two ends using communication facilities. In such schemes, the accuracy of fault location is influenced by the synchronization errors and reliability of communication channels becomes an issue.

Lack of information about network parameters and availability of limited measurements created an opportunity for applying artificial intelligence techniques to solve fault location problems. Particularly, ANNs are found to be useful to locate faults accurately. Fig.3.2 shows a broad classification of available fault location algorithms. Most of these algorithms currently available are applicable to two-terminal transmission lines only.

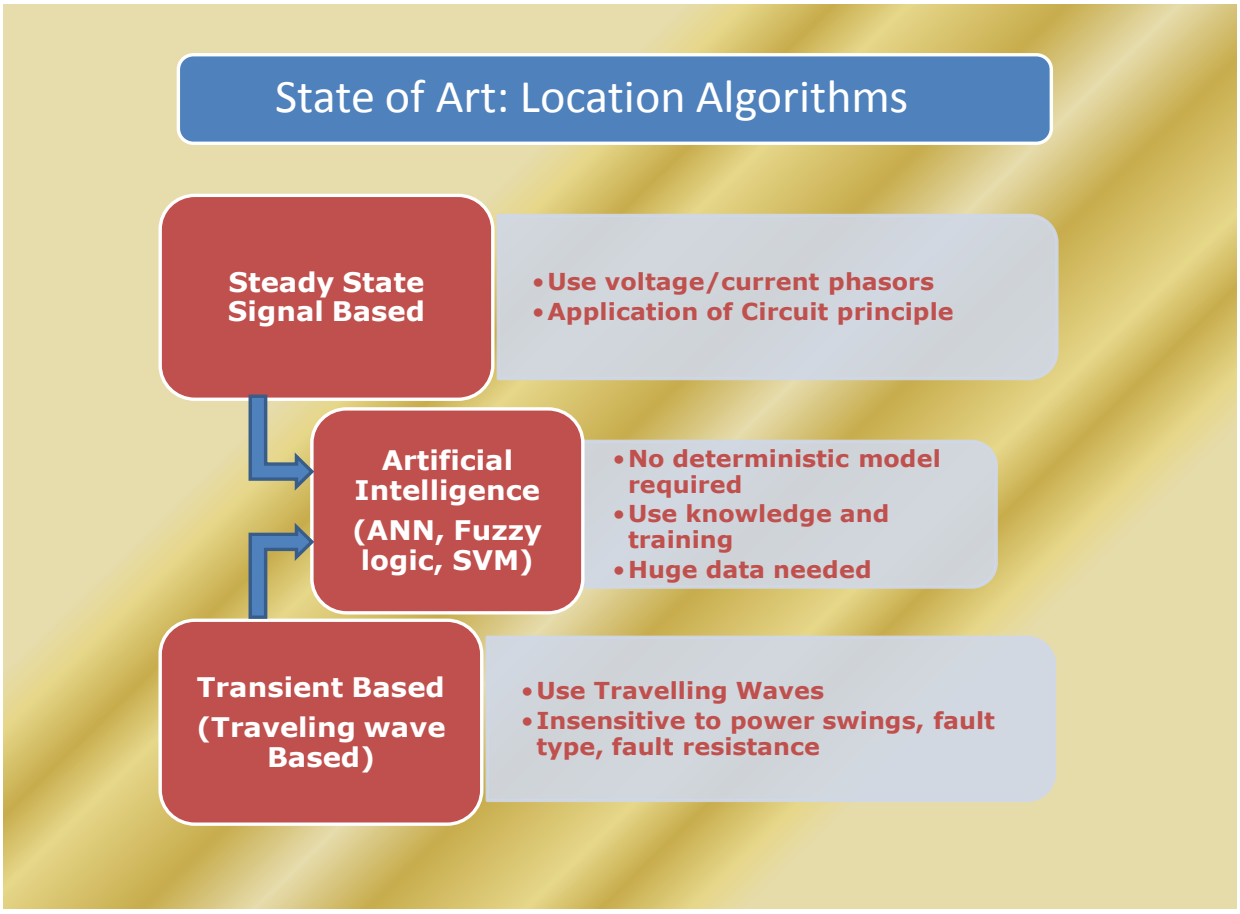

Fig. 3.2 Classification of Fault Location Algorithms

3.2 Fault Location in Three-terminal Transmission Lines

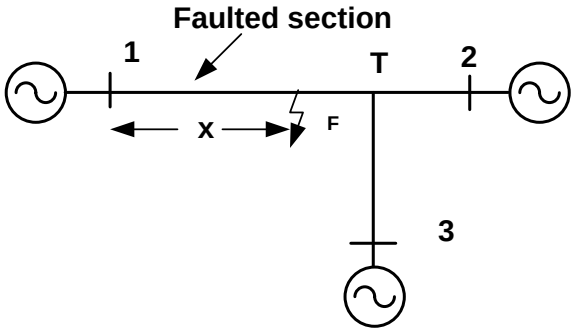

Fig. 3.3 Fault Location in Three-terminal Line

Non-availability of measurements at the tap point makes the process of locating faults difficult in three-terminal lines as shown in Fig.3.3. The intermediate infeed or outfeed from the third terminal mainly causes errors in impedance based methods due an under or over distance calculation. And these errors are further aggravated by unequal line lengths from the tap point and different source capacities. In addition, the distortion in voltage and current signals measured at the line ends due to multiple reflections of fault generated travelling waves is another issue of concern.

Based on the literature survey presented in section 1.4, the following observations may be inferred regarding fault location in three-terminal lines.

1. Fault location techniques for three-terminal transmission circuits mostly use data from all the three ends and they are either phasor based or travelling wave based.
2. Phasor based methods are sensitive to phasor estimation accuracy, synchronization errors, fault resistance and source capacities. Therefore, correct synchronized voltage and current phasor estimation is necessary for accurately locating faults.
3. Travelling wave based schemes need to find wave arrival times accurately by processing the measured voltage/current signals. Particularly, faults creating low transients lead to errors while detecting travelling waves.
4. Identification of the faulted section is also very crucial to correctly locate faults in three-terminal lines. Asymmetrical nature of the teed circuit may lead to other problems.
5. Application of AI techniques for fault location in teed circuits is not investigated.

In the light of the above observations, an attempt is made to develop fault location algorithms for teed circuits to achieve better accuracy. Fault location using ANNs is also explored to resolve the problems with deterministic approaches. In the following sections, two fault location techniques for teed circuits are presented along with their performance results. Firstly, for accurate fault location in teed circuits, an algorithm using both transients and steady state phasors is developed with improved phasor estimation accuracy. Later, an ANN based fault locator is also developed by using travelling wave arrival times that exhibit uncertainties.

3.3 Fault Location in Teed Circuits Using Modified DFT Phasor Estimation

In this section, a new fault location scheme for teed circuits is presented which is based on the transient fault voltage and current signals from all the three ends. The multi-resolution analysis using wavelet transform is applied to obtain the fault induced high frequency components of the measured voltage and current signals. A modal voltage signal is used to detect the fault as described earlier in chapter-2. Once a fault is detected, the faulted section is first identified by using the transients measured at the three ends of the teed circuit. Then, the location of the fault within the faulted section is estimated by an accurate fault locator method given by [57] which makes use of the fundamental voltage and current phasors. These phasors are estimated using a Discrete Fourier Transform (DFT) based modified algorithm [58] which mitigates the effects of exponentially decaying DC offsets. The scheme is tested for different types of faults with varying fault incidence angles and fault resistances on typical symmetrical and asymmetrical teed circuits shown in Fig.2.9. The algorithm used in the proposed scheme is elaborated in the following sections.

3.3.1 Faulted Section Identification & Location of Fault

Once a fault is detected on the line, the fault section needs to be identified first. For identifying the faulted section the FSEI values given by eqn. (2.9) will be processed from the three ends. The faulted section is identified by comparing the FSEI values of the three sections. The FSEI value of the faulted section end will always be higher than the other two because fault induced transients have to propagate through a junction to reach the other two ends. Therefore, the section with highest measured transient energy at its terminal is decided to be the faulted one.

Once the section is identified, the scheme collects a full cycle of post-fault voltage and current signals of all phases from the relay ends of the three sections to locate the fault. The fault location procedure based on the technique proposed in [57], which uses the theory of natural modes (modal transformation), is applied for locating the fault within the faulted section. In this procedure, the voltage & current phasors at the tee-point and relay end of the faulted section are required for locating the fault in the faulted section. The tee-point phasors are obtained by utilizing the phasor information of any un-faulted section relay end. With voltage and current phasors at the T point known, the following procedure can be applied to locate the fault within the faulted section treating it as a two-terminal line shown in Fig.3.4.

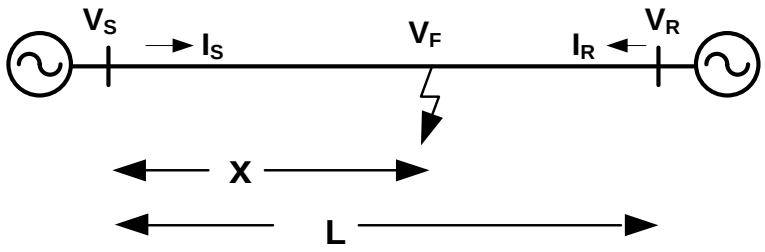

Fig. 3.4 Fault section of a teed circuit treated as a two-terminal line.

In a single phase line, the voltage at the fault point can be expressed by using long line equations from both sending and receiving ends

$$V_F(S) = V_S \cosh(\gamma x) - Z_0 I_S \sinh(\gamma x) \tag{3.1}$$

$$V_F(R) = V_R \cosh(\gamma(L-x)) - Z_0 I_R \sinh(\gamma(L-x)) \tag{3.2}$$

Expanding equation (3.2),

$$\begin{aligned} V_F(R) &= V_R\left(\cosh(\gamma L)\cosh(\gamma x) - \sinh(\gamma L)\sinh(\gamma x)\right) \\ &-Z_0 I_R\left(\sinh(\gamma L)\cosh(\gamma x) - \sinh(\gamma x)\cosh(\gamma L)\right) \end{aligned} \tag{3.3}$$

$$\begin{aligned} V_F(R) &= V_R\left(\cosh(\gamma L)\cosh(\gamma x)\right) - V_R\left(\sinh(\gamma L)\sinh(\gamma x)\right) \\ &-Z_0 I_R\left(\sinh(\gamma L)\cosh(\gamma x)\right) + Z_0 I_R \sinh(\gamma x)\cosh(\gamma L) \end{aligned} \tag{3.4}$$

Equating (3.1) and (3.2),

$$V_F(S) = V_F(R)$$

$$\begin{aligned} &V_S \cosh(\gamma x) - V_R\left(\cosh(\gamma L)\cosh(\gamma x)\right) + Z_0 I_R\left(\sinh(\gamma L)\cosh(\gamma x)\right) = \\ &Z_0 I_S \sinh(\gamma x) - V_R\left(\sinh(\gamma L)\sinh(\gamma x)\right) + Z_0 I_R \sinh(\gamma x)\cosh(\gamma L)) \end{aligned} \tag{3.5}$$

$$\cosh(\gamma x)(V_S - V_R(\cosh(\gamma L)) + Z_0 I_R(\sinh(\gamma L))$$
$$= \sinh(\gamma x)(Z_0 I_S - V_R(\sinh(\gamma L)) + Z_0 I_R \cosh(\gamma L)) \quad (3.6)$$

From the above,

$$\tanh \gamma x = \frac{-(V_R(\cosh(\gamma L)) - Z_0 I_R(\sinh(\gamma L) - V_S)}{(Z_0 I_S - V_R(\sinh(\gamma L)) + Z_0 I_R \cosh(\gamma L))}$$

$$B = -(V_R(\cosh(\gamma L)) - Z_0 I_R(\sinh(\gamma L) - V_S)$$
$$A = (Z_0 I_S - V_R(\sinh(\gamma L)) + Z_0 I_R \cosh(\gamma L))$$

$$\tanh \gamma x = \frac{-B}{A} \; or \; x = \frac{\tanh^{-1}\left(\frac{-B}{A}\right)}{\gamma} \quad (3.7)$$

The above equation cannot be directly applied to three phase lines. Therefore, modal transformation using the theory of natural modes is applied to the three-phase signals to decouple the equations into three single phase equations. These three equations are called modal equations namely earth mode, aerial mode-1 and aerial mode-2. The above equation (3.7) is applicable for any mode signals with appropriate modal surge impedance and propagation constant included.

The distance *x* from the source end of the faulted section can be obtained by using the following equation in which k=1 for earth mode, and k=2 or 3 for aerial modes.

$$x = \left[\tan h^{-1}\left(-\frac{B_k}{A_k}\right)\right] / \gamma_k \quad (3.8)$$

where $A_k = Z_{ok} cosh(\gamma_k L) I_{Tk} - sinh(\gamma_k L) V_{Tk} + Z_{ok} I_{Sk}$,
$B_k = cosh(\gamma_k L) V_{Tk} - Z_{ok} sinh(\gamma_k L) I_{Tk} - V_{Sk}$,
$\gamma_k = Modal\ \ propagation\ constant$, $Z_{ok} = Modal\ surge\ impedance$,
$L = Length\ of\ \ the\ \ faulted\ section.$

The quantities V_s & I_s and V_T & I_T are voltage and current phasors of the relay end of the faulted section and tee-point respectively. Depending on the type of fault, a suitable mode is selected for locating the fault.

The modal surge impedance (Z_{0k}) and the modal propagation constant (γ_k) are calculated from the line impedances and shunt admittances matrices of the transmission line. With perfect line transposition, the simplified expressions for the modal surge impedance and modal propagation constant are given by $Z_{0k} = \sqrt{\frac{Z}{Y}}$ and $\gamma_k = \sqrt{ZY}$. In these expressions, k=1 is for earth mode (mode 1) and k=2 or 3 for aerial modes (modes 2 & 3). For earth mode, $Z=Z_0$ & $Y=Y_0$ and for aerial modes, $Z=Z_1$ and $Y=Y_1$.

The accuracy of the estimated phasors plays a significant role in this method to correctly locate the fault. Using the modified DFT based phasor estimation algorithm, the fundamental voltage and current phasors are estimated to calculate the distance of the fault from the relay end. This algorithm can remove the decaying DC component from the fault signal waveforms and estimate the phasors with a high degree of accuracy. The method is briefly presented below.

3.3.2 Modified DFT Phasor Estimation

Many techniques have been developed over the years for finding the phasors from samples of voltages and currents measured by the transducers. The accuracy of the estimated phasors and the speed are very important in applications like protective relaying. The following methods are available.

- Discrete Fourier Transform (DFT)
- Cosine Algorithm
- Least Error Squares algorithm
- Kalman Filtering
- Wavelet Transform

Out of these algorithms, the DFT, Cosine Filter and LES methods or their combinations are incorporated in commercial relays currently being used.

Discrete Fourier Transform:

The DFT is applied to signals in time domain which are represented by a sequence of numbers where as Fourier Transform is applied to continuous time signals. It is a variation of Fourier analysis in which the signal is considered to be having fundamental frequency

components and harmonics of that frequency. In DFT the signal exists for a small duration of time called window. The DFT of a signal is implemented by,

$$V_h = \tfrac{2}{N}\sum_{n=0}^{N-1} v_n e^{-j2\pi nh/N} \quad , \tag{3.9}$$

where,

v = instantaneous value of voltage,

n = nth sample in the data window,

V = phasor of voltage,

h = order of harmonic,

N = number of samples in the data window.

For h=1, the above equation evaluates the fundamental phasor and if h=0, it finds the DC component. Using Euler's identity, the above equation can be written as,

$$V_h = \tfrac{2}{N}\sum_{n=0}^{N-1} v_n \left[\cos\left(\frac{2\pi nh}{N}\right) - j\sin\left(\frac{2\pi nh}{N}\right)\right]. \tag{3.10}$$

The real and imaginary components of the phasor are,

$$V_h \cos\theta = \tfrac{2}{N}\sum_{n=0}^{N-1} v_n \cos\left(\frac{2\pi nh}{N}\right) \tag{3.11}$$

$$V_h \sin\theta = \tfrac{2}{N}\sum_{n=0}^{N-1} v_n \sin\left(\frac{2\pi nh}{N}\right). \tag{3.12}$$

The angle θ represents the angle of the measured signal. In DFT technique, a window size of one time-period of the fundamental component must be used. Also, it is important to use proper sampling frequency to avoid aliasing effect otherwise there is a need for pre-filtering for removing energies of frequency components above the Nyquist frequency.

In many electrical engineering applications the DFT approach is used to get the estimates of fundamental phasors. The advantages of DFT is the fundamental frequency phasors of voltage and current can be obtained and a relay can be made to operate based on these phasors ignoring other frequency components. In the case of differential protection of transformer, the DFT can be used to obtain fundamental frequency phasors as well as second and fifth harmonics. These harmonics can be used to avoid in-rush effect and restrain during over excitation.

Cosine Filter:

This approach is suitable especially when the signals contain more decaying DC components. However, the estimation of phasors is delayed by a quarter cycles when compared to DFT. In this approach, the imaginary part of the phasor will be obtained from the sample occurring one fourth cycles later than the real part of the output samples. Cosine filter is faster in finding satisfactory estimates in some cases compared to DFT.

Least Error Squares Method:

LES method is based on minimizing the mean square error between actual and assumed waveform. The waveform is modelled as a sum of an exponentially decaying dc component, fundamental frequency component and harmonics of specified orders

$$V(t) = V_0 e^{-t/\tau} + \sum_{n=1}^{N-1} V_n \sin(n\omega_0 t + \theta_n), \tag{3.13}$$

where

V(t) = instantaneous value of voltage at time t,

τ = time constant of decaying dc component,

N = highest order of harmonic component present in the signal,

ω_0 = fundamental freq of the system,

V_0 = magnitude of dc offset at t=0,

V_n = peak value of nth harmonic component,

θ_n = phase angle of nth harmonic component.

Modified Discrete Fourier Transform:

In this work, a modified DFT algorithm [58] is used for phasor estimation to reduce the effects of decaying DC. Given a discrete current signal i(n),

$$i(n) = A_0 e^{-n\Delta t/\tau} + \sum_{k=1}^{N/2-1} A_k \cos\left(\frac{2\pi k}{N} n + \varphi_k\right) \tag{3.14}$$

Where τ and A_0 are the primary time constant and the magnitude of an exponential component A_k and φ_k are the amplitude and the phase angle of the K^{th} harmonic component,

Δt is the sampling interval, and N is the number of samples per cycle. The phasor of the fundamental frequency component is calculated by DFT as follows:

$$I_{DFT} = \frac{2}{N}\sum_{n=0}^{N-1} i(n).e^{-j\frac{2\pi}{N}n} = I_{DFT}^{funda} + I_{DFT}^{dc}, \tag{3.15}$$

where

$$\begin{aligned} I_{DFT}^{funda} &= A_1 e^{j\phi_1}, \\ I_{DFT}^{dc} &= \frac{2}{N} A_0 (1-E^N)/(1-Ee^{-j\frac{2\pi}{N}}), \\ E &= e^{-\Delta t/\tau}. \end{aligned} \tag{3.16}$$

The I_{DFT} contains an error, I_{DFT}^{dc} due to the exponentially decaying dc offset. The I_{DFT} can be decomposed into the even-sample-set DFT and the odd-sample-set DFT as follows.

$$\begin{aligned} I_{DFT} &= \frac{2}{N}\sum_{n=0}^{N-1} i(n).e^{-j\frac{2\pi}{N}n} \\ &= \frac{2}{N}\sum_{n=0}^{N/2-1} i(2n).e^{-j\frac{2\pi}{N}2n} + \frac{2}{N}\sum_{n=0}^{N/2-1} i(2n+1).e^{-j\frac{2\pi}{N}(2n+1)} \\ &= I_{DFT}^{even} + I_{DFT}^{odd} \end{aligned} \tag{3.17}$$

The even-sample-set DFT can be rearranged as follows:

$$\begin{aligned} I_{DFT}^{even} &= \frac{2}{N}\sum_{n=0}^{N/2-1} i(2n).e^{-j\frac{2\pi}{N}2n} \\ &= \frac{2}{N}\sum_{n=0}^{N/2-1}\left(A_0 E^{2n} + A_1\cos\left(\frac{2\pi}{N}2n+\varphi_1\right)\right)e^{-j\frac{2\pi}{N}2n} \\ &= \frac{1}{2}A_1 e^{j\phi_1} + \frac{2}{N}A_0\sum_{n=0}^{N/2-1} E^{2n}e^{-j\frac{2\pi}{N}2n} \\ &= \frac{1}{2}A_1 e^{j\phi_1} + \frac{2}{N}A_0\frac{1-E^N}{1-\left(Ee^{-j\frac{2\pi}{N}}\right)^2} \end{aligned} \tag{3.18}$$

Similarly, the odd-sample-set DFT can be rearranged as follows:

$$
\begin{aligned}
I_{DFT}^{odd} &= \frac{2}{N}\sum_{n=0}^{N/2-1} i(2n+1).e^{-j\frac{2\pi}{N}(2n+1)} \\
&= \frac{2}{N}\sum_{n=0}^{N/2-1}\left(A_0E^{(2n+1)} + A_1\cos\left(\frac{2\pi}{N}(2n+1)+\varphi_1\right)\right)e^{-j\frac{2\pi}{N}(2n+1)} \\
&= \frac{1}{2}A_1e^{j\phi_1} + \frac{2}{N}A_0\sum_{n=0}^{N/2-1}E^{2n+1}e^{-j\frac{2\pi}{N}(2n+1)} \\
&= \frac{1}{2}A_1e^{j\phi_1} + \frac{2}{N}Ee^{-j\frac{2\pi}{N}}A_0\frac{1-E^N}{1-\left(Ee^{-j\frac{2\pi}{N}}\right)^2}
\end{aligned}
\tag{3.19}
$$

As shown in (3.18) and (3.19), the even-sample-set DFT and the odd-sample-set DFT have the same fundamental frequency component, $\frac{1}{2}A_1e^{j\phi_1}$. The fundamental frequency component can be eliminated by subtracting (3.19) from (3.18).

$$
I_{DFT}^{even} - I_{DFT}^{odd} = \frac{2}{N}A_0(1-E^N)/(1+Ee^{-j\frac{2\pi}{N}}) \tag{3.20}
$$

Decomposing (3.20) into the real and imaginary parts, (3.21) is obtained as follows:

$$
\begin{aligned}
A &= \mathrm{Re}(I_{DFT}^{even} - I_{DFT}^{odd}) = \frac{2}{N}A_0\frac{1-E^N}{1+E^2+2E\cos(2\pi/N)}\times(1+E\cos(2\pi/N)) \\
B &= \mathrm{Im}(I_{DFT}^{even} - I_{DFT}^{odd}) = \frac{2}{N}A_0\frac{1-E^N}{1+E^2+2E\cos(2\pi/N)}\times E\sin(2\pi/N)
\end{aligned}
\tag{3.21}
$$

From the above E can be obtained as,

$$
E = B/(A.Sin\left(\frac{2\pi}{N}\right) - B.Cos\left(\frac{2\pi}{N}\right) \tag{3.22}
$$

The DFT output of the fundamental frequency component due to the decaying dc component, in (3.15) can be rewritten by using (3.20) as follows:

$$
I_{DFT}^{DC} = (I_{DFT}^{even} - I_{DFT}^{odd}).(1+Ee^{-j\frac{2\pi}{N}})/(1-Ee^{-j\frac{2\pi}{N}}) \tag{3.23}
$$

Substituting (3.22) for E in (3.23), the DFT output of the fundamental frequency component due to the decaying dc offset can be determined with the even-sample-set DFT and the odd sample-set DFT. Therefore, the accurate fundamental frequency component phasor of the input signal can be obtained as.

$$I_{DFT}^{funda} = I_{DFT} - I_{DFT}^{dc} \tag{3.24}$$

In the present technique, the required voltage and current phasors are estimated by using the above algorithm. The overall protection scheme is shown in the flowchart of Fig.3.5.

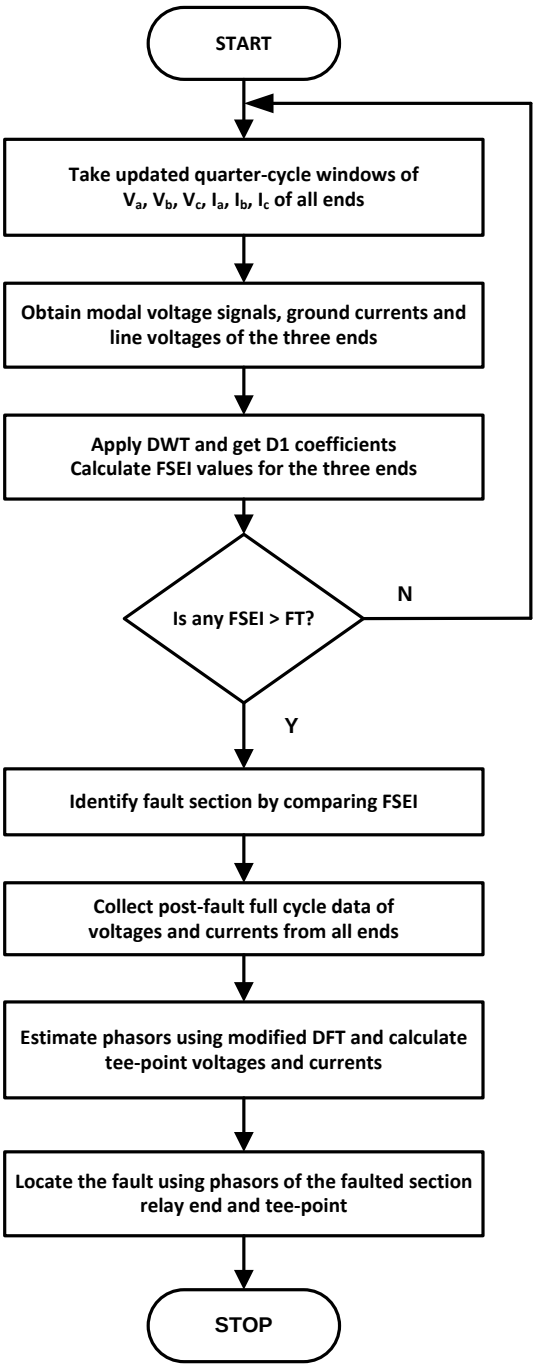

Fig. 3.5 Flow Chart for the Proposed Method

3.3.3 Simulation Results

The teed networks (both symmetrical and asymmetrical), shown in Fig.2.3, are simulated using MATLAB SimPowerSystems [55] for various fault situations. The long line model with distributed parameters is used, and in MATLAB/SIMULINK simulations, the model is based on the Bergeron's traveling wave method. The distributed parameter line represents the wave propagation phenomena and line end reflections with a better accuracy.

Fig.3.6 shows typical voltage and current waveforms at all the ends during a double line to ground fault in section-1 of the symmetrical teed circuit at 100 km from the source end.

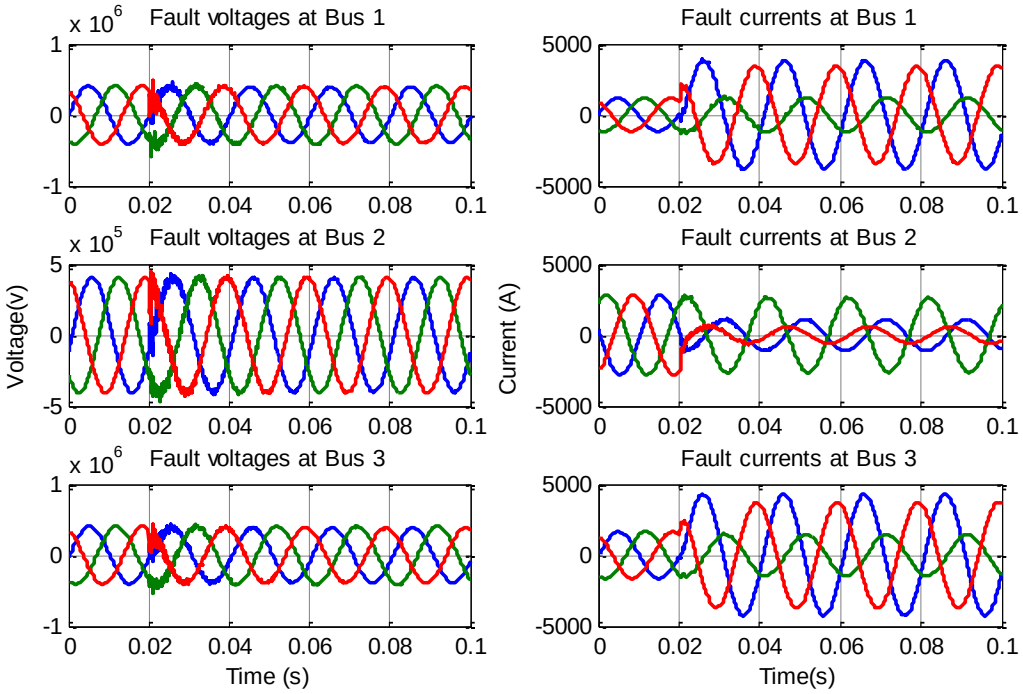

Fig. 3.6 Fault voltage & current signals for a c-a-g fault in asymmetrical teed circuit. (Section-1at 100 km from the source end: $R_f = 0\Omega$ & Inception angle, $\theta=0^0$)

Exhaustive simulations are carried out for different types of faults occurring in different sections at various locations within the teed circuit. For each type of fault at a particular location, the fault inception angle is widely varied (0^0-180^0) to evaluate the performance of the proposed scheme. Influence of fault resistance is also evaluated by considering fault resistance values of 0 ohms and 50 ohms. All the phase voltages and currents of the three ends are fed as inputs to the proposed protection algorithm.

The performance of the scheme in detecting faults and faulted sections in symmetrical teed circuits for various types of faults i.e. line-to-ground, line-to-line, double line-to-ground, three phase faults is evaluated by considering 2160 cases in all. In all these cases studied, the scheme is able to detect the fault and identify the faulted section correctly. Fig.3.7 shows the waveforms of modal voltage signals of three ends and the corresponding detail coefficients respectively for a c-a-g fault in section-1 at 100 km from the source end of the asymmetrical teed circuit.

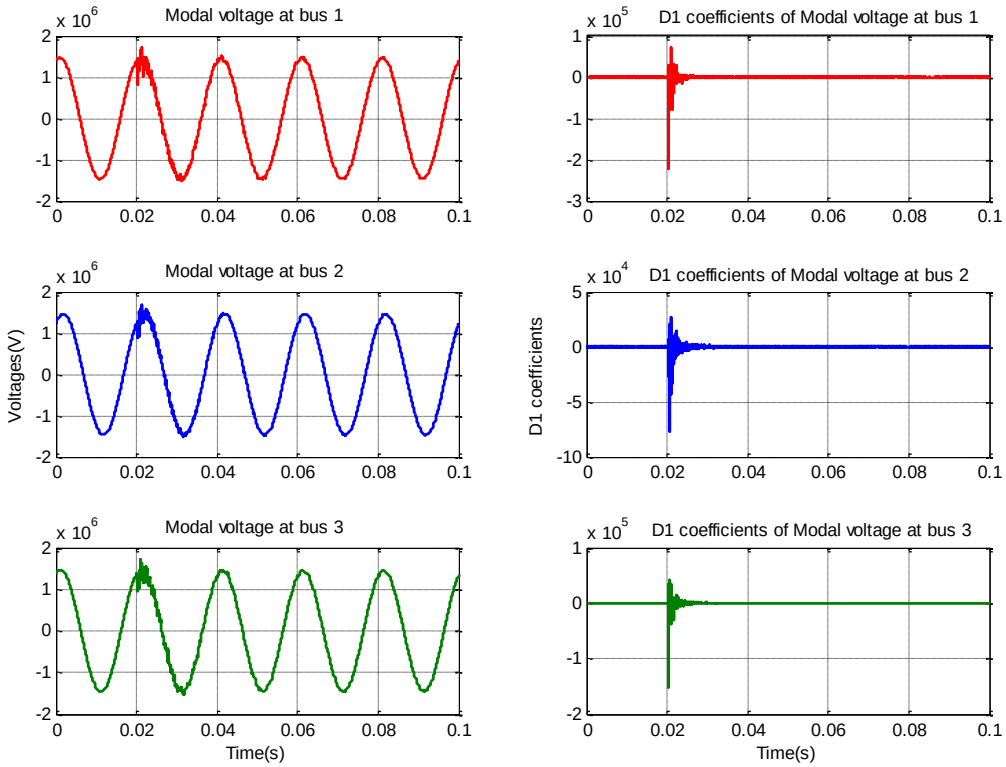

Fig. 3.7 Modal voltage signals for c-a-g fault in section-1 at 100 km from the source end & their Detail coefficients (Fault resistance, $R_f = 0\Omega$ & Inception angle, $\theta = 0^0$)

Fig.3.8 shows the variation of FSEI for a b-c-g fault in section-1 at 100 km and a-b-c fault in section-3 at 20 km from the source end of the asymmetrical teed circuit. It can be observed from Fig.3.8 (a) that, though the fault in section-1 is nearer to the end-3(50 km), the FSEI value of end-1 is much higher than the remaining two FSEI values. It is observed that the faulted section FSEI values are always higher than the values of the remaining sections. This feature is used to identify the faulted section. In the case of a fault very near to the T-point, the FSEI values of three ends are nearly equal and the scheme could clearly detect and segregate such a fault.

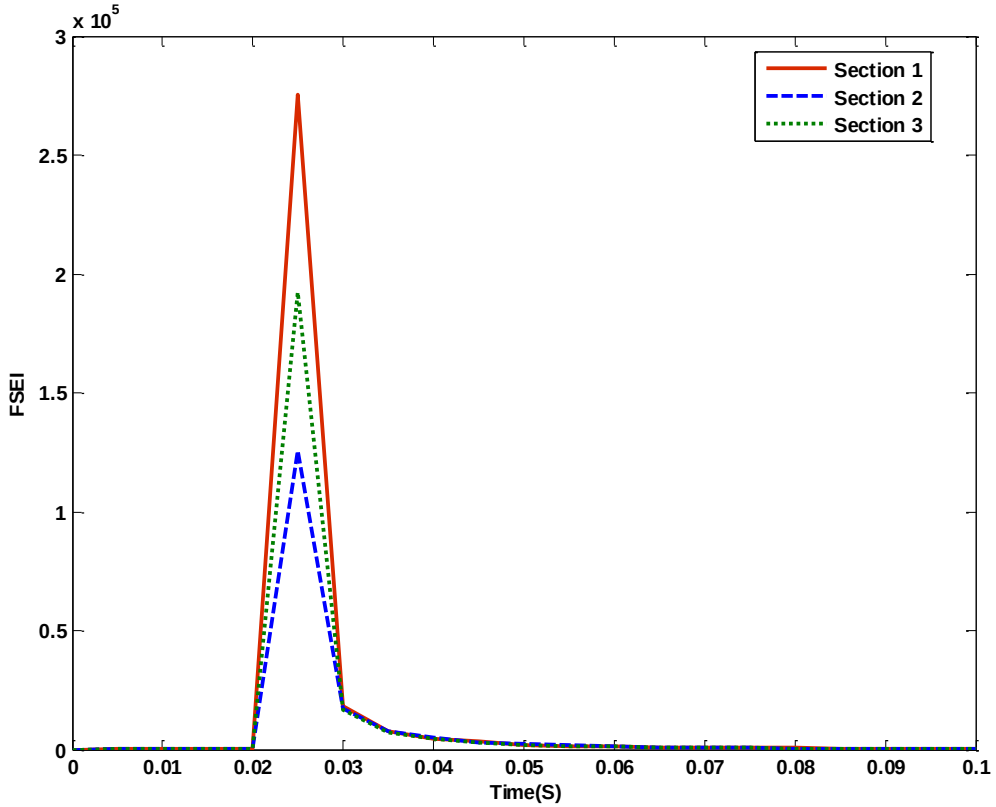

(a) c-a-g fault in section-1 (R_f=50ohms, θ = 90deg)

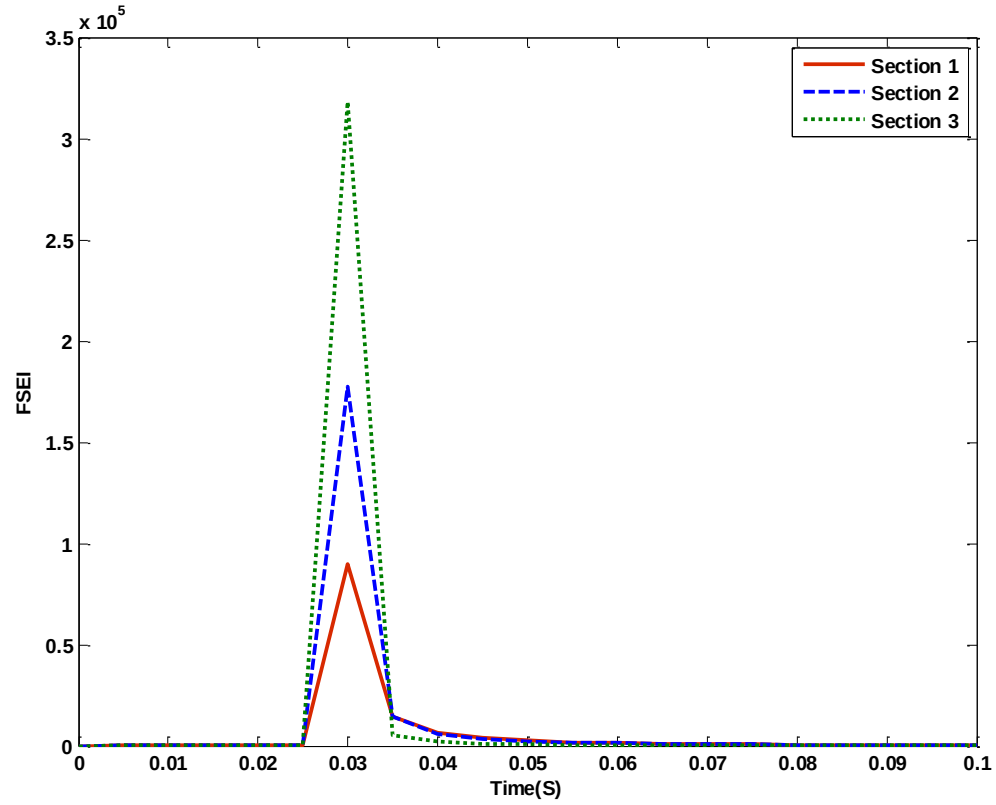

(b) a-b-c fault in section-3 (R_f=50ohms, θ = 90deg)

Fig. 3.8 FSEI variation in asymmetrical teed circuit

Table 3.1: Results of Fault Location in Symmetrical Teed Circuit

Fault Section	Fault Type	Actual Location from source end(km)	Estimated Location for inception angle			
			0^0		90^0	
			$R_f = 0\Omega$	$R_f = 50\Omega$	$R_f = 0\Omega$	$R_f = 50\Omega$
1	a-g	20	20.3167	19.9714	20.0490	20.0265
		40	40.1083	39.9864	39.8323	39.9767
		60	60.5571	59.9866	60.0676	60.0389
		80	80.5447	79.9954	79.9331	80.0181
1	a-b	20	20.2918	19.9780	19.7731	20.0097
		40	40.2086	39.9768	39.5799	40.0166
		60	60.2190	59.9954	60.0633	60.0292
		80	79.5496	79.9932	79.7208	80.0042
2	b-g	20	20.0519	19.9648	19.9583	19.7455
		40	39.4241	39.9847	40.0691	40.0550
		60	60.0325	59.9934	60.0100	59.9716
		80	80.0440	80.0146	80.0622	79.9807
2	a-b-g	20	19.9941	20.1356	19.9532	19.9988
		40	40.1477	40.0346	39.9164	40.0192
		60	60.0831	59.9699	60.8850	60.0049
		80	79.8326	80.0128	79.9706	79.9900
3	c-g	20	19.7891	19.9642	19.7164	20.0617
		40	40.0286	40.0544	39.8101	39.9906
		60	60.0466	59.9831	60.0204	60.0034
		80	79.9542	79.9923	79.0659	80.0057
3	a-b-c	20	20.8410	20.0101	19.2772	19.9920
		40	40.5420	39.9929	39.5806	40.0000
		60	59.7500	59.9916	59.4418	59.9966
		80	81.0455	79.9938	79.5471	79.9954

After identifying the fault section, the fault location is estimated using the accurate fault location method mentioned earlier. In all the cases, the location is accurately found for various types of faults with different incidence angles and fault resistances. Table 3.1 shows the fault location results for various types of faults occurring in different sections of the symmetrical teed circuit.

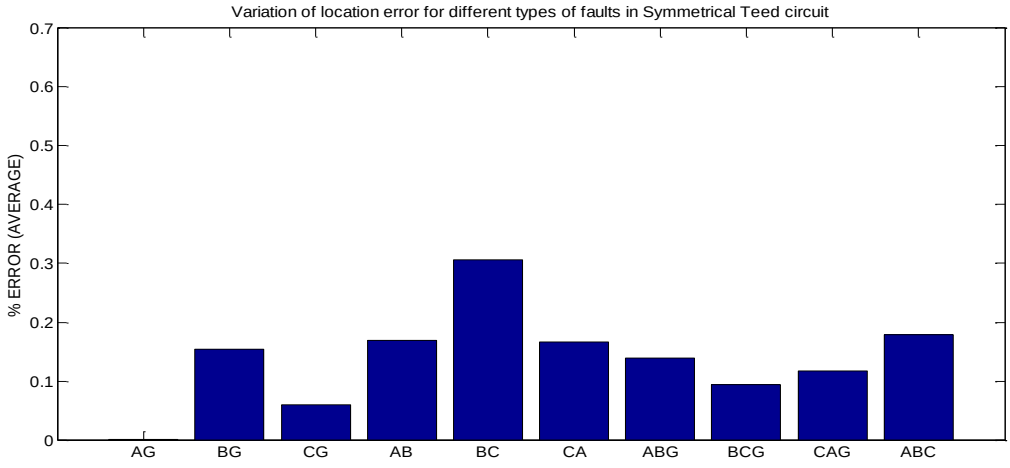

Fig. 3.9 Percentage Error for Different Faults in Symmetrical Circuit

In all the cases presented, the fault detection & section identification are correctly made by the scheme. Fig.3.9 shows the overall percentage error for different types of faults and the maximum error is nearly 0.3% for BC faults.

The asymmetrical teed circuit shown in Fig.2.3(b) is simulated for 1800 different faults in different sections for varying incidence angle and fault resistance. Table 3.2 presents some of the fault location results showing the accuracy attained. The results obtained for asymmetrical teed circuits are also found to be accurate and not influenced by nature of asymmetry. Fig.3.10 shows the overall percentage error for a different type of faults and is below 0.6% for all types.

Table 3.2: Results of Fault Location in Asymmetrical Teed Circuit

Fault Section	**Fault Type**	**Actual Location from source end(km)**	**Estimated Location for inception angle**			
			0^0		90^0	
			$R_f = 0\Omega$	$R_f = 50\Omega$	$R_f = 0\Omega$	$R_f = 50\Omega$
1	a-g	20	20.0050	19.9793	20.0589	20.0125
		40	40.2887	39.9831	39.9013	40.0125
		60	60.1623	59.9931	59.9904	59.9702
		80	80.1367	80.0002	80.0221	79.9766
		100	99.6762	100.0074	99.9910	100.0220
2	b-c	20	20.2033	19.9989	19.4498	20.0059
		40	39.9791	39.9993	39.8480	40.0024
		60	59.8461	59.9988	59.8979	59.9988
3	c-a-g	10	10.0583	9.9850	9.7212	10.0515
		20	20.1129	19.9602	19.7986	20.0332

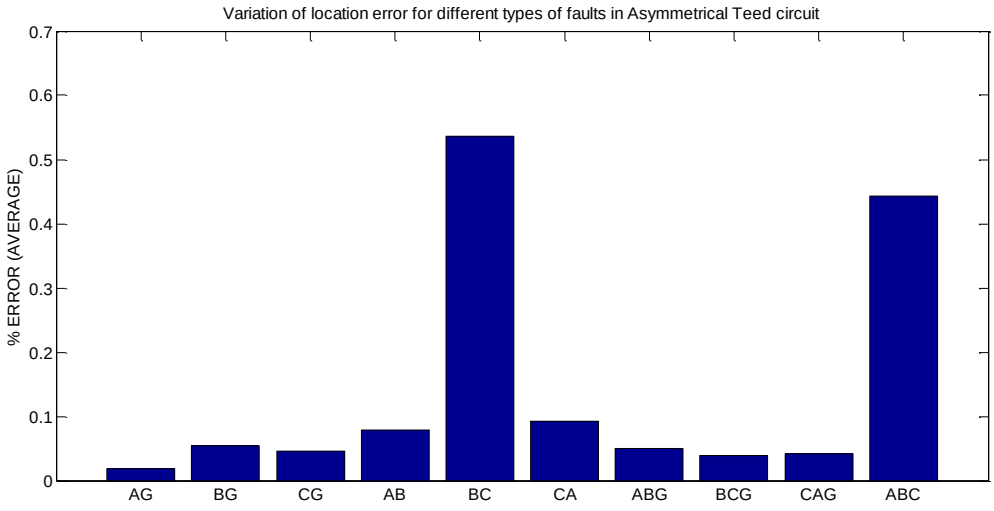

Fig. 3.10 Percentage Error for Different Faults in Asymmetrical circuit

3.4 Travelling Wave based Fault Location in Teed Circuits Using S-Transform & Neural Networks

Application of artificial intelligence (AI) is proven to be a feasible solution for many problems in power system operation, control and protection. Many recent applications involved artificial neural networks (ANN) in areas such as load forecasting, security assessment, transformer protection and transmission line fault classification. All these applications exploit the classification abilities of neural networks. However, the ANNs can also be used for function approximation problems. In this section, a neural network solution for fault location in teed circuits is presented.

The proposed algorithm uses two neural networks, one for identifying the faulted section and the other for finding the exact location in the faulted section. The scheme requires measurement of voltages at the three ends of the line and the locator takes these signals as inputs through communication channels. Then, Clarke's modal transformation [12] is applied to the voltage signals to avoid inter-phase coupling effects. By processing the mode-1 signal with S-transform, the arrival times of the travelling waves at the three ends are obtained.

3.4.1 Conventional TW based Fault Location in Teed Circuits

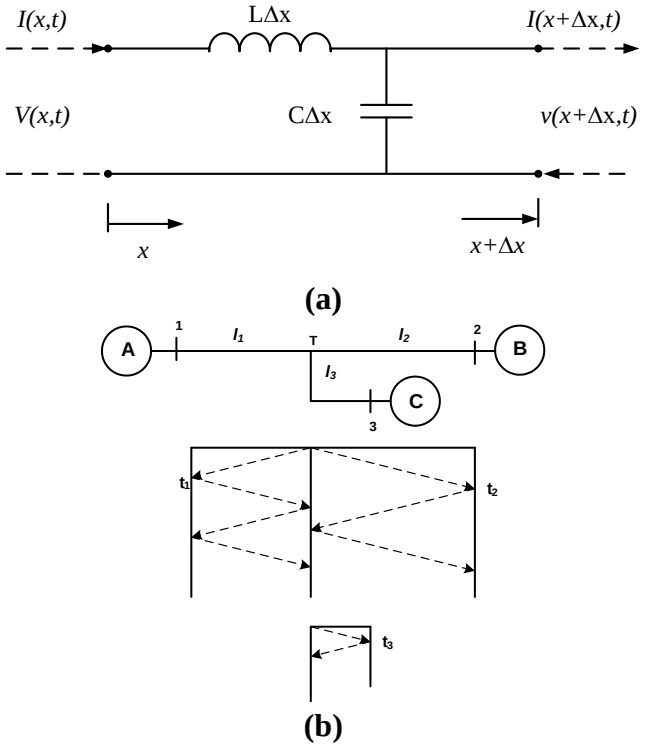

Fig. 3.11 (a) Section of the distributed parameter model of a transmission line
(b) Bewley's Lattice Diagram for Three-Terminal Lines

In a long transmission line the voltage and current at any instant vary significantly with the distance along the transmission line in such lines distribution parameter models are used for accuracy. Fig. 3.11(a) shows a section of the distributed parameter model of a transmission line where L is inductance per unit length and C is capacitance per unit length.

In a loss less line (ignoring series resistance and shunt admittance), the propagation of signals can be analyzed by solving the basic equations.

The voltage and current distributions can be expressed by

$$v = V(x,t) \;\&\; i = I(x,t) \tag{3.25}$$

Considering two points at x and x+Δx, the capacitive current in the section Δx is

$$I(x,t) - I(x+\Delta x,t) = \int_{x}^{x+\Delta x} C.\frac{\partial v}{\partial t}.dx \tag{3.26}$$

If Δx→0

$$\lim_{\Delta x \to 0} \int_{x}^{x+\Delta x} C.\frac{\partial v}{\partial t}.dx = \Delta x.C.\frac{\partial v}{\partial t} \tag{3.27}$$

Therefore

$$\lim_{\Delta x \to 0} \frac{I(x,t) - I(x+\Delta x,t)}{\Delta x} = C.\frac{\partial v}{\partial t} \tag{3.28}$$

$$\frac{\partial i}{\partial x} = -C.\frac{\partial v}{\partial t} \tag{3.29}$$

Similarly the potential difference is

$$V(x,t) - V(x+\Delta x,t) = \int_{x}^{x+\Delta x} L.\frac{\partial i}{\partial t}.dx \tag{3.30}$$

and

$$\frac{\partial v}{\partial x} = -L.\frac{\partial i}{\partial t} \tag{3.31}$$

Using time differentiation of above

$$\frac{\partial^2 i}{\partial t \partial x} = -C.\frac{\partial^2 v}{\partial t^2} \tag{3.32}$$

and

$$\frac{\partial^2 v}{\partial t \partial x} = -C.\frac{\partial^2 i}{\partial x \partial t} \tag{3.33}$$

From the above, it can be written as

$$\frac{\partial^2 v}{\partial x^2} = LC.\frac{\partial^2 v}{\partial^2 t} \tag{3.34}$$

and

$$\frac{\partial^2 i}{\partial x^2} = LC.\frac{\partial^2 i}{\partial^2 t} \tag{3.35}$$

Solving above wave equations by using dAlemberts method

$$v(x,t) = f_1(x-at) - f_2(x+at) \tag{3.36}$$

$$i(x,t) = \frac{1}{Z_c} f_1(x-at) - \frac{1}{Z_c} f_2(x+at) \tag{3.37}$$

Where $f_1(x-at)$ and $f_2(x+at)$ represent travelling waves in positive *x* direction and negative *x* direction respectively. These speed of these travelling waves is *a* and $Z_c = \sqrt{\frac{L}{C}}$

In case of the transmission line with losses, the model includes inductance L in series with a resistance R and a shunt capacitance C in parallel with a conductance G.
Writing wave equations for this line,

$$\frac{\partial^2 v}{\partial x^2} = \gamma^2 v \tag{3.38}$$

and

$$\frac{\partial^2 i}{\partial x^2} = \gamma^2 i \tag{3.39}$$

Where γ is the propagation constant given by $\sqrt{(R+j\omega L)(G+j\omega C)}$

The solution for above equations can be obtained as

$$v(x,t) = A_1(t)e^{\gamma x} + A_2(t)e^{-\gamma x} \tag{3.40}$$

$$i(x,t) = -\frac{1}{Z_c}[A_1(t)e^{\gamma x} - A_2(t)e^{-\gamma x}] \tag{3.41}$$

Where $Z_c = \sqrt{\frac{(R + j\omega L)}{(G + j\omega C)}}$

Travelling wave based fault location in teed circuits mainly involves two steps. In the first step, the faulted section needs to be identified correctly. Then, by processing the measured transient voltage or current signals at the terminals, the forward wave arrival times at the three ends are extracted. These arrival times t_1, t_2 and t_3 as mentioned in Fig.3.11 (b) depend on the location of fault and wave propagation velocity which depends on the system parameters. To extract the arrival times, the fault signals are first transformed into their modal signals by using Clark's Model to eliminate inter-phase coupling. The Clark's transformation is given by

$$\begin{bmatrix} V_1 \\ V_2 \\ V_3 \end{bmatrix} = \frac{1}{\sqrt{3}} \begin{bmatrix} 1 & 1 & 1 \\ \sqrt{2} & \frac{-1}{\sqrt{2}} & \frac{-1}{\sqrt{2}} \\ 0 & \frac{\sqrt{3}}{\sqrt{2}} & \frac{-\sqrt{3}}{\sqrt{2}} \end{bmatrix} \begin{bmatrix} V_a \\ V_b \\ V_c \end{bmatrix} \tag{3.42}$$

The first mode (mode-0), called the ground mode is significant only during faults having a path to ground. Hence, this component cannot be used for all types of faults. The second mode (mode-1) known as the aerial mode is, however, present for all kinds of faults. Therefore, the wave arrival times are extracted by processing aerial mode signals. The aerial mode-1 voltage detail coefficients are obtained by using Wavelet transform in the proposed algorithm. The first peak of the squared wavelet transform coefficients corresponds to the wave arrival time. Given the arrival times t_1, t_2 and t_3, the fault distance '*x*' can be obtained using the following equations

$$\begin{aligned} x &= v_1(t_1 - t_0), \\ l_1 - x + l_2 &= v_1(t_2 - t_0), \\ l_1 - x + l_3 &= v_1(t_3 - t_0). \end{aligned} \tag{3.43}$$

Where t_0 is fault inception time, l_1, l_2 and l_3 are the line lengths of the three sections as shown in Fig.3.11 and v_1 is aerial mode propagation velocity. By eliminating t_0 in the above equations, the fault location can be calculated by

$$x = \frac{(l_1 + l_2) - v_1(t_2 - t_1)}{2} \quad or \quad x = \frac{(l_1 + l_3) - v_1(t_3 - t_1)}{2} \tag{3.44}$$

Any of the above relations can be used for estimating *x*. The fault distance *x* is correctly estimated if the wave arrival times are accurately found.

3.4.2 Uncertainty in Arrival Time Measurements

The necessity of using ANNs for travelling wave based fault location arises because of the uncertainties in the arrival times at the line ends. Many signal processing techniques like Wavelet transform and S-transform are used for finding wave arrival times. These methods fail to accurately estimate the wave arrival times in certain situations for example, during faults with zero inception angles. If errors in arrival times are negligible, the fault location accuracy with conventional deterministic approaches will be acceptable. But, in the case of large errors in arrival times, the estimated fault location may deviate very much from the true location. In order to observe these uncertainties, the system given in Fig. 2.10 is simulated for extracting the arrival times using S-transform. The Figs.3.12 to 3.14 shown below depict the errors in arrival times at the three ends, which vary with fault conditions. These errors are possibly due to the inexact time-frequency localization nature of signal transforms and failure in peak detection.

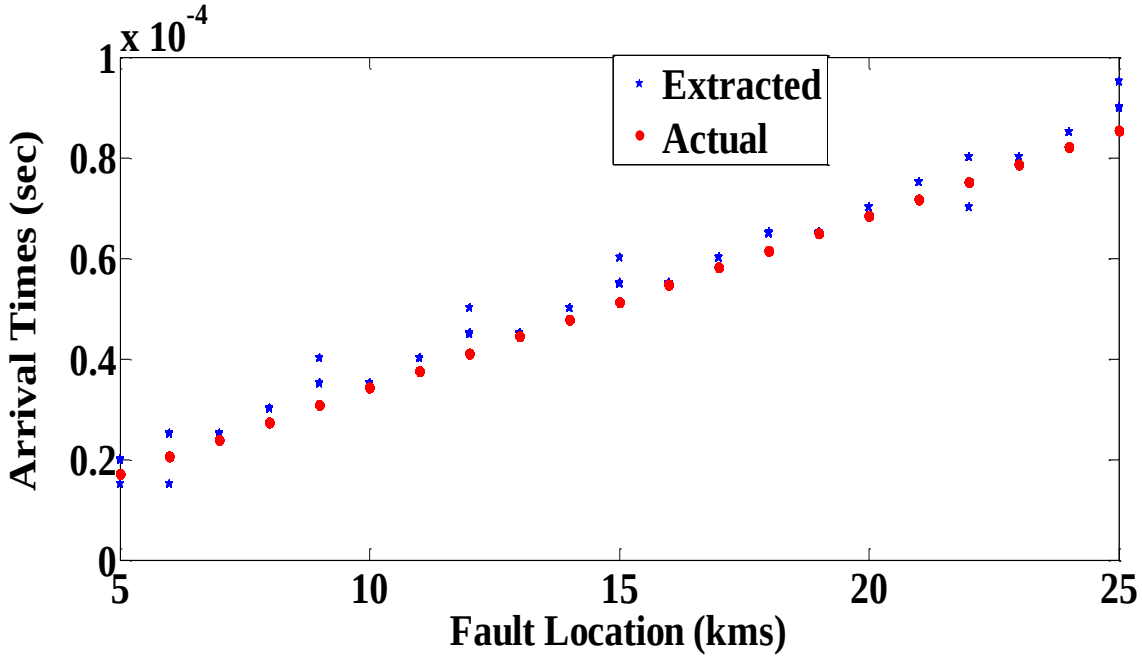

Fig. 3.12 Travelling Wave Arrival Times at End-1

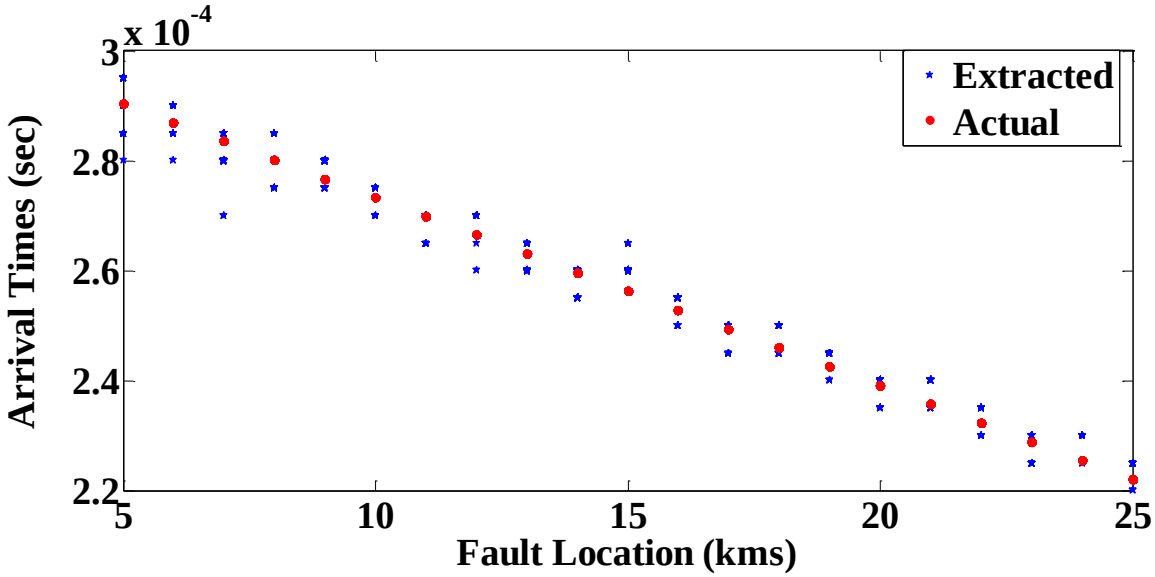

Fig. 3.13 Travelling Wave Arrival Times at End-2

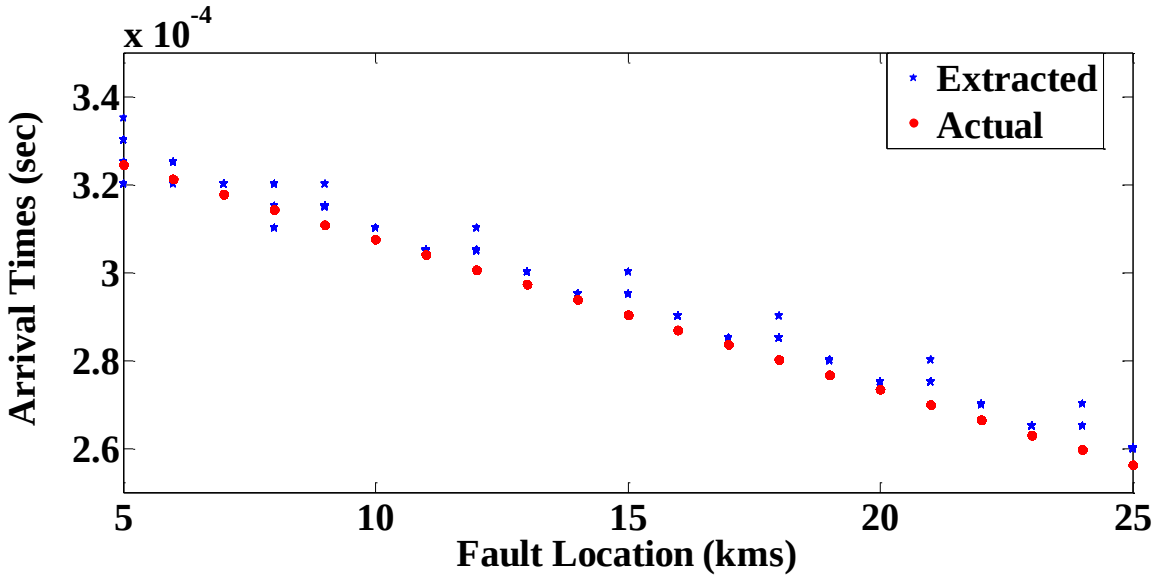

Fig. 3.14 Travelling Wave Arrival Times at End-3

Hence, to tackle the problems with erroneous arrival times, an ANN based technique becomes a feasible solution. The proposed method uses two trained neural networks for fault location. The inputs for these neural networks are the wave arrival times for both faulted section identification and exact fault location.

The following tools are generally used for extracting wave arrival times in travelling wave based fault location.

- Wavelet Transform
- Park's Transformation
- Time-Time Transform

- S-Transform

The wavelet transform which is described in the earlier chapter has been used in many schemes developed previously. Other transforms are being implemented in recent times and they are briefly presented below.

Park's Transformation:

In this approach, the modal voltage signals using Clarke's transformation matrix are converted into two components of direct and quadrature axis components given by equation

$$\begin{bmatrix} V_d \\ V_q \end{bmatrix} = \frac{2}{3}\begin{bmatrix} \cos(\varnothing) & \cos(\varnothing - \frac{2\pi}{3}) & \cos(\varnothing + \frac{2\pi}{3}) \\ -\sin(\varnothing) & -\sin(\varnothing - \frac{2\pi}{3}) & -\sin(\varnothing + \frac{2\pi}{3}) \end{bmatrix}\begin{bmatrix} V_{mg} \\ V_{ma1} \\ V_{ma2} \end{bmatrix} \quad (3.45)$$

where V_{mg}, V_{ma1} & V_{ma2} represents the modal signals, V_d & V_q are the direct and quadrature axis components and $\emptyset = k\omega\Delta t + \theta$, where ω is the angular frequency, Δt is the sampling time and θ is the angle of V_d. Assuming V_d and V_q signals are to be in phase, θ becomes zero degrees. After calculating the direct and quadrature components of voltage signals, the 'C' coefficients of direct and quadrature are computed by using moving data window with new samples using equation 3.29 & 3.30.

$$C_{vd}(k) = V_d(k) - V_d(k-1) \quad (3.46)$$

$$\xi_{vd}(k) = \sum_{n=k-\Delta k_{EN}+1}^{k} [C_{vd}(n)]^2 \quad (3.47)$$

where, $V_d(k)$ is the kth sample of the direct axis component, $C_{vd}(k)$ is the Kth sample of the incremental quantity, $\xi_{vd}(k)$ is the energy of the kth C_{vd} data window, and Δk_{EN} is the number of samples within a quarter cycle. The energy calculated for direct or quadrature components are used to analyse the fault transients in order to capture the travelling wave arrival time.

Time-Time (TT) Transform:

TT transform is a two-dimensional representation of a one dimensional time series to get a local time view of a scaled window. Unlike wavelet transform which needs a mother wavelet, this transform needs no choosing of any function and its output has only one level. Another advantage of this T-T transform is its ability to amplify high frequency components. Therefore, the fault generated high frequency components can be detected by this transform.

Starting from the ST, the TT-transform can be developed based on the inverse Fourier transform of the ST with respect to its frequency component. It is defined as

$$TT(t,\tau) = \int_{-\infty}^{\infty} S(\tau, f) e^{j2\pi ft} df \tag{3.48}$$

The matrices obtained in TT and S-transform contain redundant information, with the ST being in the time-frequency domain where as the TT-transform is in time–time domain.

In this work, the arrival times are extracted by using S-transform which is proven to be an effective signal processing tool. In the following section, S-transform and Generalized Regression Neural Networks are briefly explained.

3.4.3 S-Transform & Generalized Regression Neural Networks

Short Time Fourier Transform (STFT), Wavelet transform (WT) and S-transform [60] are very powerful tools available for non-stationary signal analysis giving the information of transients both in time and frequency domains. The STFT is a localized time-frequency representation of a time series which uses a windowing function to localize the time and the Fourier transform to localize the frequency. Because of the fixed width of the window function, STFT has poor time frequency resolution. On the other hand, the WT uses a basis function which dilates and contracts with scale and it does not retain the absolute phase information. The visual analysis of the time scale plots that are produced by the WT is intricate. A time-frequency representation which combines the good features of STFT and WT is called the S-transform. It can be interpreted as a frequency dependent STFT or a phase corrected Wavelet. The choice of windowing function in S-transform is not limited to the Gaussian function but others functions may also be used.

The S-Transform (ST)

The *S*-transform can be viewed as an intermediate step between the short-time Fourier transform (STFT) and the wavelet transform that enables the use of the frequency variable as well as the multi-resolution strategy of the wavelets. Furthermore, it maintains a direct connection with the Fourier transform which is equal to the *S*-transform's time integral. But, while the *S*-transform formulation is very similar to the short-time Fourier transform, in practice, the multi-resolution strategy used makes it much closer to the wavelet transform.

The *S*-transform of a continuous time signal $x(t)$ is defined as

$$S(\tau, f) = \int_{-\infty}^{\infty} x(t) w(\tau - t, f) e^{-i2\pi ft} dt. \tag{3.49}$$

Although other windows are possible, the window function, $w(\cdot,\cdot)$ is generally chosen to be positive and Gaussian:

$$w(\tau - t, f) = \frac{|f|}{k\sqrt{2\pi}} e^{-\frac{1}{2}\left(\frac{f(\tau - t)}{k}\right)^2} \forall k > 0 \tag{3.50}$$

Where f is the frequency, t is the time, τ is the delay, and k is the scaling factor which controls the time-frequency resolution. It is important to emphasize that in order to have an invertible *S*-transform, any window used must be normalized, so that

$$\int_{-\infty}^{\infty} w(t, f) dt = 1 \forall f \in \square. \tag{3.51}$$

The *S*-transform can also be computed directly from $\hat{x}(f)$, the Fourier transform of $x(t)$. To do so, first (3.32) has to be rewritten as a convolution

$$S(\tau, f) = x(t) e^{-i2\pi ft} * w(t, f). \tag{3.52}$$

Then, applying the convolution property of the Fourier transform, we get

$$S(\tau, f) = F^{-1}\{\hat{u}(\alpha + f) w(\alpha, f)\} \tag{3.53}$$

Where F^{-1} is the inverse Fourier transform and α the Fourier transform pair of t. For the Gaussian window case (3.33) this expression becomes

$$S(\tau, f) = \int_{-\infty}^{\infty} \hat{x}(\alpha + f) e^{-2\left(\frac{\pi k \alpha}{f}\right)^2} e^{i2\pi\alpha\tau} d\alpha. \tag{3.54}$$

One of the main characteristics of the *S*-transform is that summing $S(\tau, f)$ over τ yields the spectrum of x, i.e., using expression (3.32) we obtain

$$\hat{x}(f) = \int_{-\infty}^{\infty} \int x(t) w(\tau - t, f) e^{-i2\pi ft} dt d\tau. \tag{3.55}$$

If $|\hat{x}(f)| < \infty$, the above expression reduces to a simple Fourier transform. As a result, $|\hat{x}(f)|$ can be estimated by the following equation:

$$\hat{x}(f) = \int_{-\infty}^{\infty} S(\tau, f) d\tau. \tag{3.56}$$

This spectrum property enables the definition of an inverse *S*-transform through the inverse Fourier transform of the spectrum of $x(t)$. It gives great flexibility in the window function selection, as it just has to fulfill the normalization property (3.34).

The discrete S-transform of $x[k]$ is given by

$$S[iT, \tfrac{n}{NT}] = \sum_{m=0}^{N-1} X[\tfrac{m+n}{NT}] e^{\left(\frac{-2\pi^2 m^2}{n^2}\right)} e^{\left(\frac{j2\pi im}{NT}\right)} \quad for \quad i = 1, 2, ..., N \;\&\; n = 1, 2, ..., N. \tag{3.57}$$

Where *X* denotes the discrete Fourier transform (DFT) of the original signal, *N* is the size of the data window, and *T* is the sampling time. The S-transform converts a 1-D time series representation into a 2-D map of time–frequency localization of spectral information. The output from the S-Transform $S[i, n]$ is a matrix called the S-matrix. The elements of the S-matrix are complex valued where the row corresponds to the frequency and the column corresponds to the time. Only the absolute values of these complex values are utilized and the best row from S-matrix is selected through simulation studies [43] for more accurate time localization. This time–frequency location feature of the S-transform has made it a better tool for fault-location applications. Further, the S-transform is more stable in noise conditions.

Generalized Regression Neural Networks (GRNN):

A generalized regression neural network (GRNN) is often used for function approximation and is capable of approximating any linear or nonlinear mathematical function to relate input and output variables. A GRNN is similar in form to the PNN. The GRNN estimates values for continuous dependent variables where as the PNN finds decision boundaries between categories of patterns. Both use the non-parametric estimators of probability density functions. The advantages of GRNN are fast-learning and convergence to the Bayes optimal regression surface with the increasing training data. It is particularly advantageous with sparse data in the real-time environment.

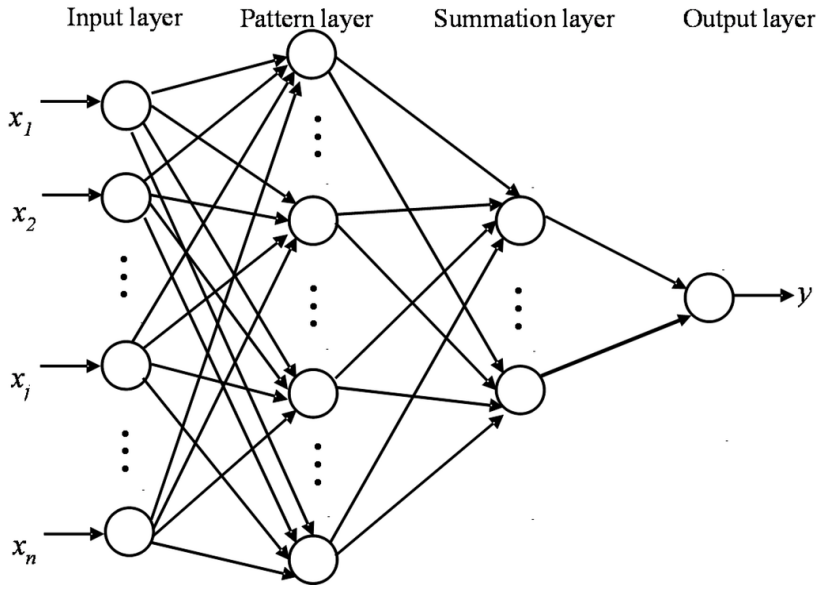

Fig. 3.15 The GRNN Network Architecture

The architecture for the GRNN is shown in Fig.3.15. It is similar to the radial basis network, but has a slightly different second layer. The learning methodology of GRNN does not require any iterative process and its learning process can be completed in one pass. The GRNN algorithm processes the training data by a nonlinear function to find the output probability density functions.

The GRNN consists of four layers: the input layer, pattern layer, summation layer, and output layer. The first layer is fully connected to the second pattern layer, in which each unit represents a training input pattern and its output is a measure of the distance of the input from the stored patterns. Each pattern layer unit is connected to the two neurons in the summation layer: the S-summation neuron and the D-summation neuron. The S-summation neuron computes the sum of the weighted outputs of the pattern layer, whereas the D-summation neuron calculates the un-weighted outputs of the pattern neurons.

The main advantages of a GRNN are its extremely rapid training, which does not require an iterative training procedure, and it can approximate any arbitrary function between input and output vectors, drawing the function estimate directly from the training data. Furthermore, it is consistent: that is, as the training set size becomes large, the estimation error approaches zero, with only mild restrictions on the function. GRNN is particularly advantageous with sparse data in real-time environments because the regression surface is quickly defined everywhere, even with just one sample. The output layer merely divides the output of each S-summation neuron by that of each D-summation neuron, yielding the predicted value to an unknown input vector x as

$$Y_i = \frac{\sum_{i=1}^{n} y_i \exp[-D(x, x_i)]}{\sum_{i=1}^{n} \exp[-D(x, x_i)]} \tag{3.58}$$

where n = number of training patterns and D is the Gaussian function defined as

$$D(x, x_i) = \sum_{k=1}^{m} \left(\frac{x_k - x_{ik}}{\sigma} \right)^2 \tag{3.59}$$

and y_i = weight gain between the ith neuron in the pattern layer and the S-summation neuron; n = number of training patterns; m = size of the input vector; and x_k and x_{ik} are the jth element of x and x_i respectively. The σ is the spread (or width), which determines the generalization performance of the GRNN. In general, a large σ value may result in better generalization; its optimal value is determined through trial and error. In conventional GRNN applications, all units in the pattern layer have the same spread.

Another advantage of GRNNs is that they involve a one-pass learning algorithm and are consequently much faster to train than the well-known back-propagation algorithm. Furthermore, they differ from traditional neural networks in that every weight is replaced by a distribution of weights. They are closely related to Radial Basis Function Neural Networks which are based on a standard statistical technique called Gaussian kernel regression. The GRNN can be treated as a normalized RBFNN in which there is a hidden unit centered at every training case. These units are called “kernels” and are usually probability-density functions.

In the present application, the GRNN is used to model the relationship of the transmission line fault location and travelling wave arrival times. The arrival times calculated by S-Transform (ST) are given as training inputs to GRNN. The overall procedure is depicted in the flowchart shown below in Fig.3.16.

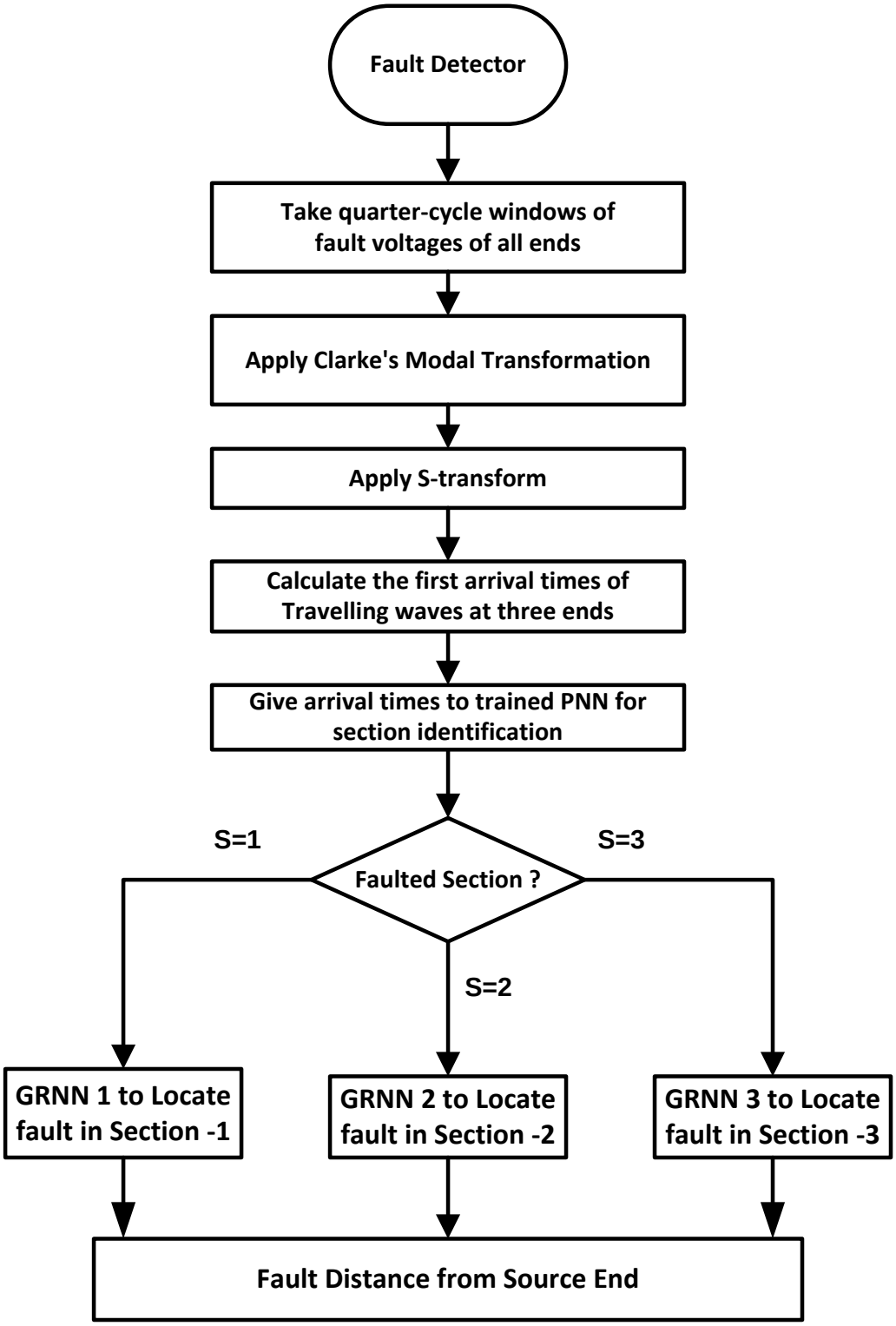

Fig. 3.16 Flowchart for Fault location using S-Transform & Neural Networks

3.4.4 Simulation Results

The proposed method is verified by simulating the system described in Fig.2.10 of chapter-2. The long line model considering distributed parameters is used in MATLAB/SIMULINK simulations. The sampling frequency is chosen to be 200 kHz and a

voltage signal window of 1000 samples is processed for extracting the arrival times. From the instant of fault detection, the voltage signal windows are formed by including 500 samples of pre-fault and post-fault signals each for all the three phases. Extensive simulations are carried out by varying the fault location for different combinations of fault section, fault type, fault resistance and inception angle.

Firstly, the PNN and the three GRNNs are trained by 11,970 generated arrival time patterns for different fault locations. These patterns are generated under the conditions specified in Table-3.3.

Table 3.3: Fault Conditions Considered

Condition	Range
Fault type	AG, BG, CG, AB, BC, CA, ABG, BCG, CAG, ABC
Fault Resistance	0Ω and 50Ω
Fault Inception Angle	0^0 to 180^0 in steps of 45^0
Fault Location	Every 1 KM in each section

The performance of the proposed algorithm is now tested for different arbitrary fault locations. It is observed that in general, the section identification accuracy is very high and in all the simulated cases the section identification is correctly made. The Table-3.4 shows the results of section identification for a set of 36 representative cases.

Once the fault section is identified, the corresponding GRNN is activated to find the exact location in that section. The GRNN takes the same arrival time information as input and produces the estimate of fault location. Table-3.5 lists the results of fault location for a few test cases and a comparison is made with the conventional travelling wave based approach. In most of the tested cases, the performance of the GRNN is much better than the conventional approach. Figs.3.17 to 3.19 show the plots of the mean location error for different faults with respect to the fault location in all the three sections. It can be observed that the GRNN tends to be very effective whenever the direct TW method gives an estimate with a large error. Hence, the arrival time uncertainties can be dealt with by the use of neural networks to mitigate location errors.

Table 3.4: Results of Section Identification

Sl. No	Fault type	Fault location	Fault inception angle	R_f (ohms)	Actual Fault Section	Detected Fault section
Section-1						
1	AG	5.5	40	0	1	1
2	BG	15.2	160	60	1	1
3	CG	22.7	30	130	1	1
4	ABG	6.3	150	10	1	1
5	BCG	14.1	0	45	1	1
6	ACG	23.2	180	80	1	1
7	AB	8.3	60	25	1	1
8	BC	12.9	120	65	1	1
9	AC	21.2	90	100	1	1
10	ABC	9.6	135	15	1	1
11	ACG	17.3	10	90	1	1
12	CG	20.4	100	120	1	1
Section-2						
1	AG	7.6	40	0	2	2
2	BG	33.2	160	60	2	2
3	CG	53.7	30	130	2	2
4	ABG	9.9	150	10	2	2
5	BCG	29.1	0	45	2	2
6	ACG	49.6	180	80	2	2
7	AB	10.1	60	25	2	2
8	BC	41.3	120	65	2	2
9	AC	51.5	90	100	2	2
10	ABC	14.1	135	15	2	2
11	ACG	39.5	10	90	2	2
12	CG	54.7	100	120	2	2
Section-3						
1	AG	6.2	40	0	3	3
2	BG	32.6	160	60	3	3
3	CG	63.8	30	130	3	3
4	ABG	8.1	150	10	3	3
5	BCG	37.7	0	45	3	3
6	ACG	60.3	180	80	3	3
7	AB	11.4	60	25	3	3
8	BC	38.6	120	65	3	3
9	AC	59.5	90	100	3	3
10	ABC	15.9	135	15	3	3
11	ACG	28.3	10	90	3	3
12	CG	61.2	100	120	3	3

Table 3.5: Results of Fault Location

Sl. No	Fault type	Fault inception angle	R_f (ohms)	Actual Fault location (km)	Estimated location	
					Conventional TW	GRNN
Section-1						
1	AG	40	0	5.5	4.74	5.34
2	BG	160	60	15.2	16.45	15.79
3	CG	30	130	22.7	22.31	22.22
4	ABG	150	10	6.3	6.94	6.06
5	BCG	0	45	14.1	14.26	13.99
6	ACG	180	80	23.2	23.77	22.90
7	AB	60	25	8.3	8.40	8.77
8	BC	120	65	12.9	12.79	12.92
9	AC	90	100	21.2	20.84	20.94
10	ABC	135	15	9.6	10.60	9.58
11	ACG	10	90	17.3	17.18	16.89
12	CG	100	120	20.4	21.58	20.96
Section-2						
1	AG	40	0	7.6	8.40	7.28
2	BG	160	60	33.2	34.02	33.01
3	CG	30	130	53.7	55.24	53.88
4	ABG	150	10	9.9	11.33	9.97
5	BCG	0	45	29.1	28.89	28.30
6	ACG	180	80	49.4	50.12	48.97
7	AB	60	25	10.8	12.06	11.38
8	BC	120	65	41.3	42.07	41.07
9	AC	0	100	51.5	53.05	51.99
10	ABC	135	15	14.1	14.99	13.79
11	ACG	10	90	39.5	40.60	39.76
12	CG	100	120	54.7	55.97	54.96
Section-3						
1	AG	40	0	6.2	6.81	6.18
2	BG	160	60	32.6	33.89	32.86
3	CG	30	130	63.8	64.63	63.52
4	ABG	150	10	8.1	10.47	8.77
5	BCG	0	45	37.7	37.55	36.90
6	ACG	180	80	60.3	61.71	60.63
7	AB	60	25	11.4	12.67	11.54
8	BC	120	65	38.6	39.75	38.52
9	AC	90	100	59.5	60.24	59.34
10	ABC	135	15	15.9	17.06	15.70
11	ACG	10	90	28.3	29.50	28.46
12	CG	100	120	61.2	61.71	60.65

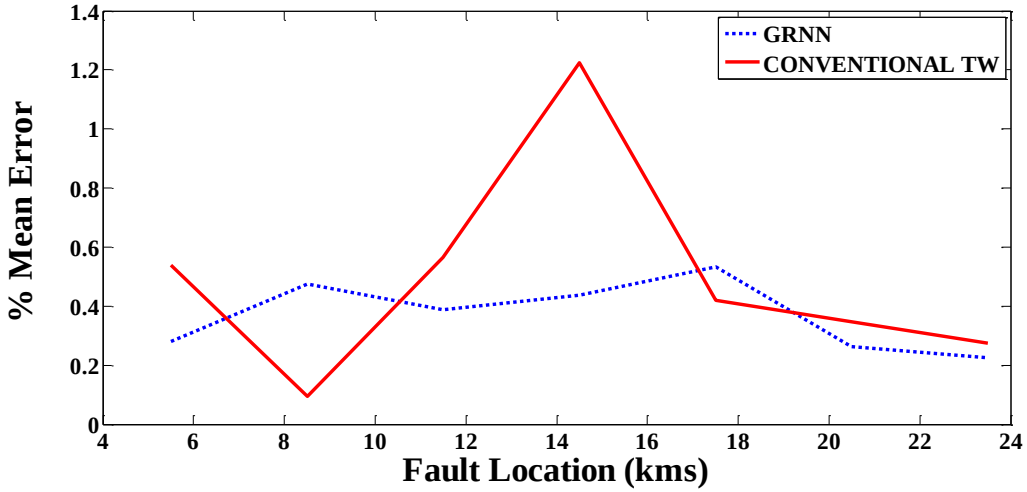

Fig. 3.17 % Mean Error Plot in Section-1

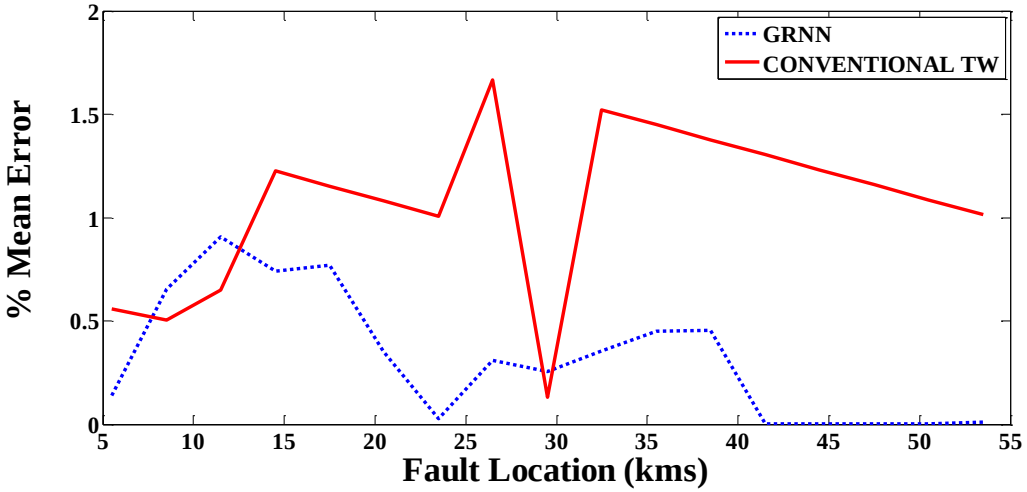

Fig. 3.18 % Mean Error Plot in Section-2

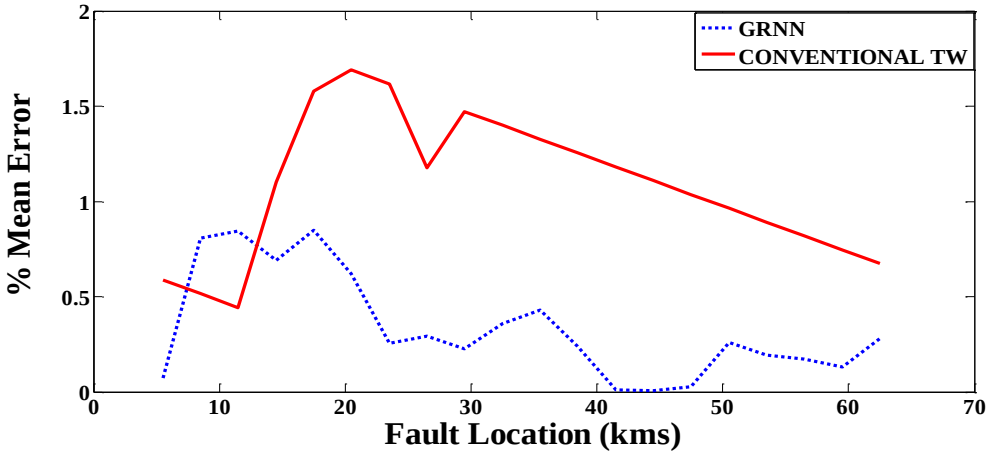

Fig. 3.19 % Mean Error Plot in Section-3

3.5 Conclusions

This chapter presented two approaches for fault location in teed circuits with improved accuracy. The first method uses both transient and steady-state information while the second one is based on travelling waves and neural networks. From the results of the simulation, the following conclusions can be drawn.

The hybrid location approach using transients for section identification and phasors for an exact location is accurate. The location error is well below 1% in all the simulated cases. The scheme is applicable for both symmetrical and asymmetrical teed circuits and is not sensitive to varying fault conditions.

The section identification procedure by using modal voltage signals is very effective and even, faults very nearer to the T-junction are correctly segregated. Modified DFT is employed for phasor estimation and is found to be very effective in fault location.

The other ANN based technique employing S-Transform is able to improve the accuracy compared to conventional traveling wave method. The PNN application is proven to be useful in teed circuits and its performance in section identification is very accurate. The GRNN is capable of locating faults exactly even when the extracted arrival times are erroneous. Exhaustive simulation studies revealed the efficacy of the method under different fault conditions.

Chapter 4

Fault Location in Multi-Terminal Transmission Lines

4.1 Introduction to Multi-Terminal Transmission Lines

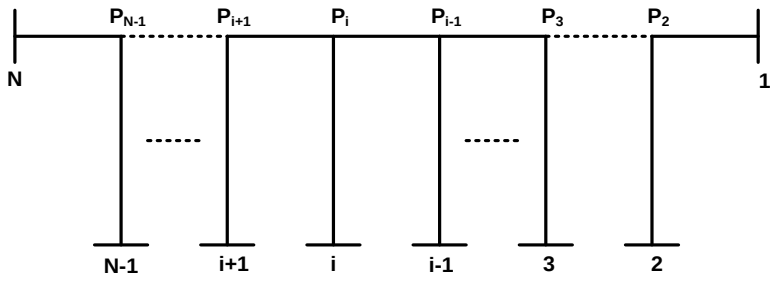

Fig. 4.1 General Multi-terminal Line Configuration

With quick rise in demand for power in modern power systems, the transmission system is becoming more complicated. Such complexity sometimes arises due to many taps taken from the existing lines thus creating multi-terminal lines as shown in Fig.4.1. Multi-terminal power transmission lines have four or more terminals with substantial generation behind them and tap at other locations along the line that serve only as the load. Though a three-terminal line can also be considered as a multi-terminal line, such lines are dealt with separately by calling them teed or tapped lines. The multi-terminal configuration in transmission lines is formed in power systems for different reasons. Mainly, they offer considerable economic advantages in power systems, particularly in low-power density areas. In some cases, it is more economical to serve a growing load with a tapped line at least for a limited period of time until the growth of load justifies the erection of a substation. Sometimes, due to the difficulty in obtaining the right of way for new transmission lines, a multi-terminal line is the only feasible solution. Protection of such multi-terminal lines requires additional considerations because of the possibility of multiple sources feeding faults and no measurements at tap points. The ability to locate the fault accurately in a complex power network is one of the important features of a modern power transmission line protection scheme.

4.2 Fault Location in Multi-Terminal Transmission Lines

In multi-terminal lines, any fault location technique involves two aspects, i.e., identifying the faulted section and locating fault within the faulted section. When compared to three-terminal a line, fault location in multi-terminal lines becomes further complicated as it involves several line sections without any measurements at the ends. The main difficulty is identifying the faulted line section.

From the literature survey in section 1.4, it is observed that the two methods [37,38] require synchronized phasor measurements and exact source impedance must be known for accurate fault location. The techniques are developed for short lines and influence of shunt capacitance needs to be explored further. In the method presented in [39], the computational burden is less and does not require the iterative procedure. Results of simulation indicated an error well below one percent. Despite these advantages, the method needs synchronized phasor measurements and effect of FIA is not reported in the results presented. In another algorithm [40] based on voltage and current phasors, higher fault resistances influenced the accuracy of the location. Reference [41] presented a method that uses both impedance and travelling wave principles. Influence of FIA, phasor accuracy and high sampling frequency are of concern in this method.

A current traveling wave based fault location scheme presented in [42] used Fast Intrinsic Mode Decomposition (FIMD) and Teager Energy Operator (TEO) to detect the arrival time of the traveling wave at each terminal. However, the influence of FIA is not reported and use of 2 MHz sampling frequency is of concern. Recently another transient based technique [43] is proposed by employing S-transform for locating faults in multi-terminal lines. S-transform is applied to aerial mode signals for finding the arrival times of current travelling waves. This approach needs synchronized measurements and shunt capacitance is not considered in simulation studies.

From the above discussion, it can be concluded that many existing techniques are phasor based and they all need synchronized voltage & current phasors. Shunt capacitance of transmission lines is not considered in simulation studies. In the case of traveling wave based approaches, the influence of FIA needs further investigation.

Therefore, the accuracy of phasors needs to be high and synchronization errors between different terminals must be taken into consideration. In the following sections, two accurate fault location algorithms for multi-terminal lines are developed by using transients as

well as fundamental phasors of the fault signals. The first one is a hybrid method whereas the second one uses only phasors with synchronization errors.

4.3 A Hybrid Method for Fault Location in EHV Multi-terminal Lines

In this section, a new fault location scheme for four terminal multi-terminal circuits is presented which is based on the transient fault voltage and current signals from all the ends. This scheme is an extension of the method developed in Section-3.3 earlier for three terminal lines. The multi-resolution analysis using wavelet transform is applied to obtain the fault induced high frequency components of the measured voltage signals and a modal voltage signal is used to detect the fault and identify the faulted section of the multi-terminal circuit. The location of the fault within the faulted section is identified by an accurate fault locator method using phasors. The fundamental voltage and current phasors are estimated using a Discrete Fourier Transform based modified algorithm which mitigates the effects of exponentially decaying DC offsets. This method is termed as 'hybrid' because it is based on processing both the transient high frequency as well as the fundamental frequency components of the fault signals.

The proposed scheme collects sampled data signals of all measured synchronized phase voltages and currents from the four relaying ends S1, S2, S3 and S4 of the circuit shown in Fig.4.2. The synchronized voltage and current signals are obtained by using global positioning system (GPS) based communication systems installed at the relaying ends of the circuit.

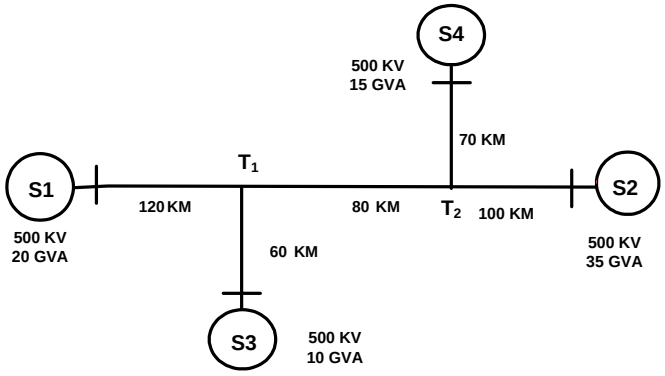

Fig.4.2 Four Terminal Line

4.3.1 Fault Section Identification & Location of Fault

In the proposed scheme, voltage signals at the four relaying ends are used for detection and section identification. A modal voltage signal used earlier for three-terminal lines is formed for each end. A fault section energy index (FSEI) value is evaluated for each end and the fault is detected whenever the FSEI value of any end exceeds a threshold as explained earlier for teed circuits. After detecting the fault, the faulted section is identified by a relative comparison of the FSEI values of the four ends. In the case of faults in sections having source ends, the FSEI value of the faulted section will be much higher than other values. But for faults in the middle section (T1-T2), the index values of nearby sections (sections connected to a common junction) do not differ appreciably.

Once the faulted section is identified, the location procedure explained earlier for three-terminal lines is extended to the multi-terminal circuit shown in Fig.4.2. After identifying the faulted section, the voltage and current phasors for the two ends of it are obtained by utilizing the phasor information of all relay ends. For example, if the fault is in section S1-T1, the phasors at T1 are calculated from the phasor information of S2, S3 and S4 ends. Phasors at S1 are any way directly available. Similarly, if the fault is in section T1-T2, phasors at T1 are calculated from S1 & S3 phasors and phasors at T2 are calculated from S2 & S4 phasors. The phasor estimation is done by applying the modified DFT mentioned earlier.

The fault location procedure is based on the theory of natural modes. The phase voltages and currents are decoupled to simplify calculations. The following transformation is used.

$$\begin{bmatrix} I_a \\ I_b \\ I_c \end{bmatrix} = [Q] \begin{bmatrix} I_0 \\ I_1 \\ I_2 \end{bmatrix} \qquad \begin{bmatrix} V_a \\ V_b \\ V_c \end{bmatrix} = [S] \begin{bmatrix} V_0 \\ V_1 \\ V_2 \end{bmatrix}$$

where subscripts 0, 1 and 2 correspond to earth mode and two aerial modes respectively. The transformation matrices for transposed lines become identical as given by

$$[Q] = [S] = \begin{bmatrix} 1 & 1 & 1 \\ 1 & 0 & -2 \\ 1 & -1 & 1 \end{bmatrix}$$

By using the modal signals the fault distance can be calculated using either ground mode or

aerial mode. For example if the fault is in the middle section (T1-T2) the voltage and current phasors at the two junctions (T1 & T2) are calculated from the phasor information estimate at the four ends.

The fault distance x from T1 is expressed as (based on two terminal line model)

$$x = \left[\tanh^{-1}\left(-\frac{B_k}{A_k} \right) \right] / \gamma_k$$

$$\begin{aligned} \text{where } A_k &= Z_{ok}Cosh(\gamma_k L)I_{T2k} - Sinh(\gamma_k L)V_{T2k} + Z_{ok}I_{T1k}, \\ B_k &= Cosh(\gamma_k L)V_{T2k} - Z_{ok}Sinh(\gamma_k L)I_{T2k} - V_{T1k}, \\ \gamma_k &= Modal\ \ propagation\ constant,\ Z_{ok} = Modal\ surge\ impedance, \\ L &= Length\ of\ \ the\ \ faulted\ \ section. \end{aligned}$$

The quantities V_{T1}& I_{T1} and V_{T2} & I_{T2} are voltage and current phasors of the two junctions T1 and T2. Depending on the type of fault, a suitable mode is selected for locating the fault.

4.3.2 Simulation Results

The scheme is evaluated using a 500 kV, 50 Hz transmission system shown in Fig.4.2 whose line parameters are R_0 = 0.1888 Ω/km, R_1=0.02 Ω/km, L_0 = 3.5 mH/km, L_1 = 0.94 mH/km, C_0 =0.0083 μF/km & C_1 = 0.012 μF/km. The system is modeled in MATLAB Simpower Systems environment. The distributed parameter long line model is used for simulations to represent the wave propagation phenomena and line end reflections with a better accuracy.

A sampling frequency of 200 kHz is chosen to capture the high frequency content of voltage and current signals around the centre frequency of 75 kHz. Adoption of such high sampling frequency avoids the use of anti-aliasing filter thus reducing some delay. At this sampling frequency, each quarter-cycle data window contains 1000 samples.

The network shown in Fig.4.2 is simulated for various fault situations. Fig.4.3 and Fig.4.4 show the waveforms of modal voltage signals of four ends and the corresponding detail coefficients respectively for b-g fault in section S1-T1 at 40 km from the source end.

Exhaustive simulations are carried out for different types of faults occurring in different sections at various locations within the circuit. For each type of fault at a particular

location, the fault inception angle is widely varied to evaluate the performance of the proposed scheme. Influence of fault resistance is also evaluated by considering a fault resistance value of 50 ohms.

The performance of the scheme in detecting faults and section for various types of faults i.e. line-to-ground, line-to-line, double line-to-ground, three phase faults is evaluated. In all the cases studied, the scheme can correctly detect the fault and identify the faulted section. The fault incidence angle is varied from 0^0 to 180^0 for all types of faults.

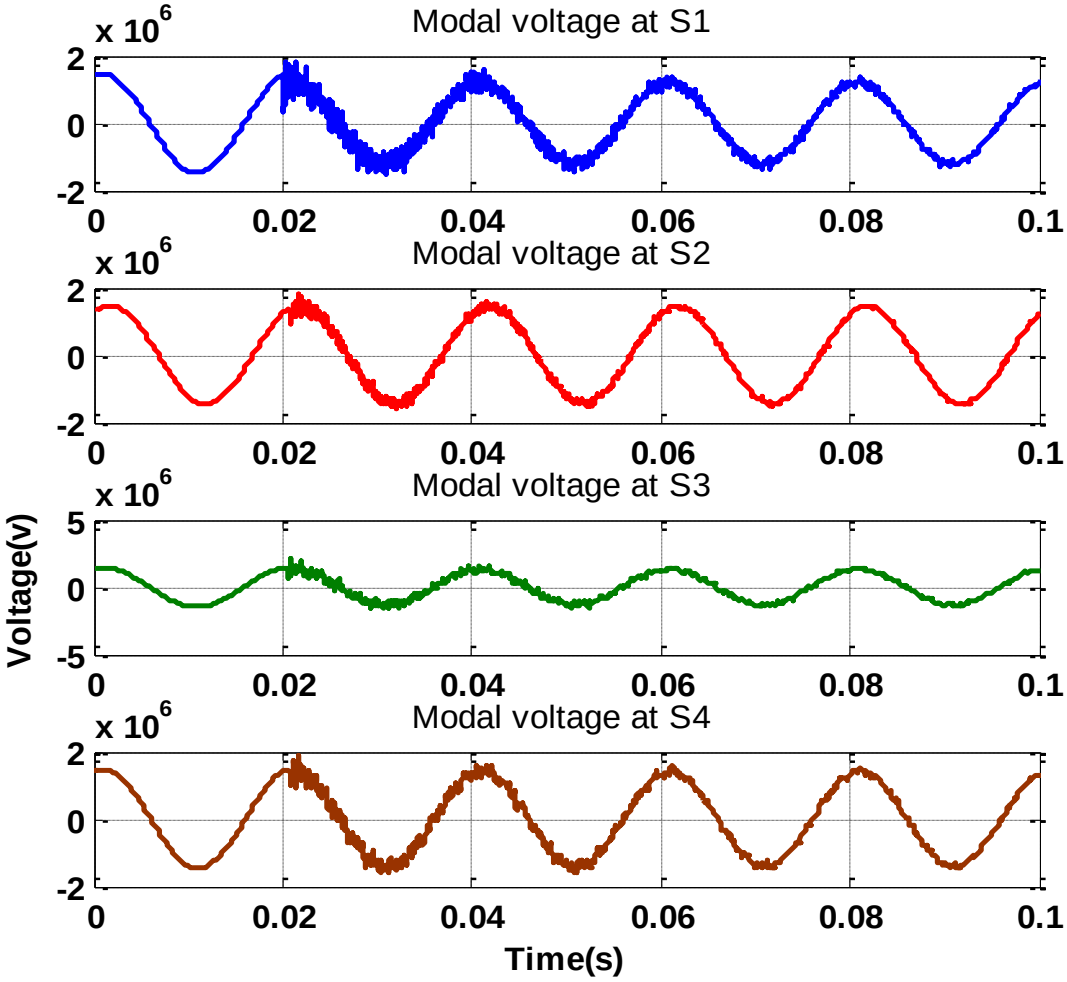

Fig. 4.3 Modal voltages for b-g in fault section S1-T1 at 40 km from S1

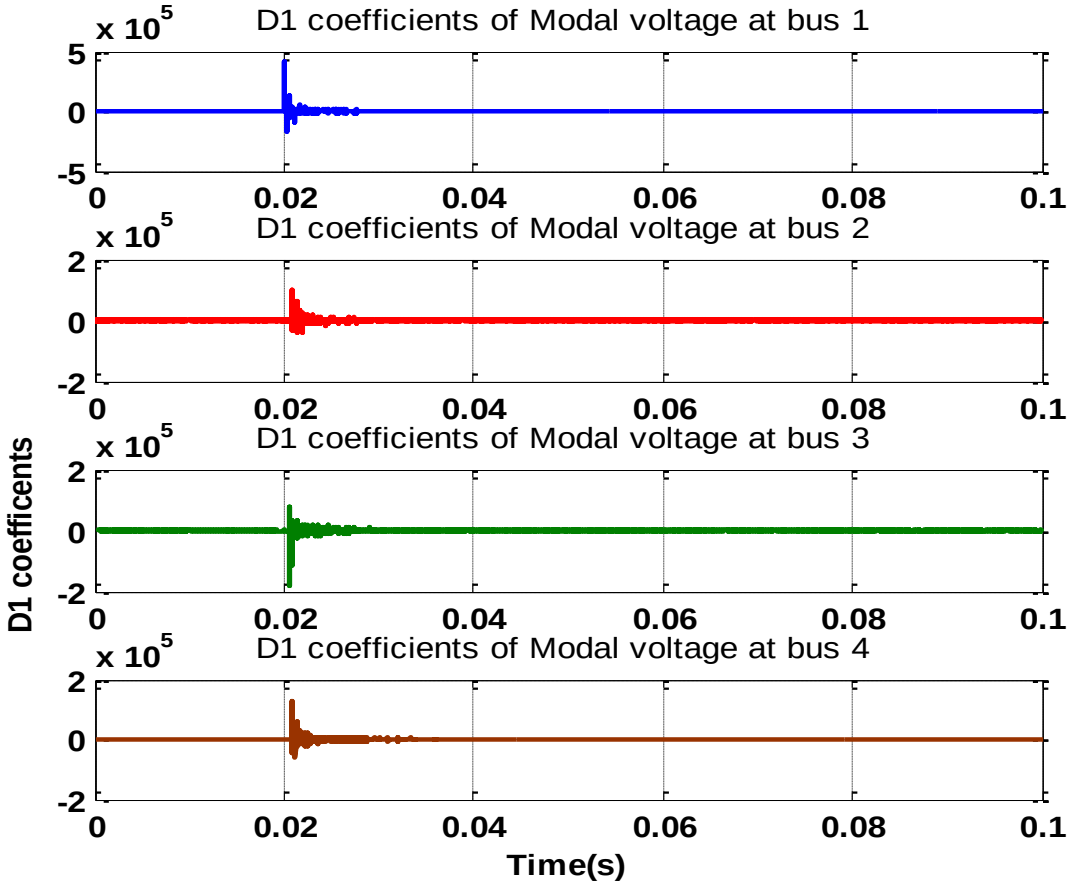

Fig. 4.4 D1 coefficients for b-g fault in section S1-T1 at 40 km from S1

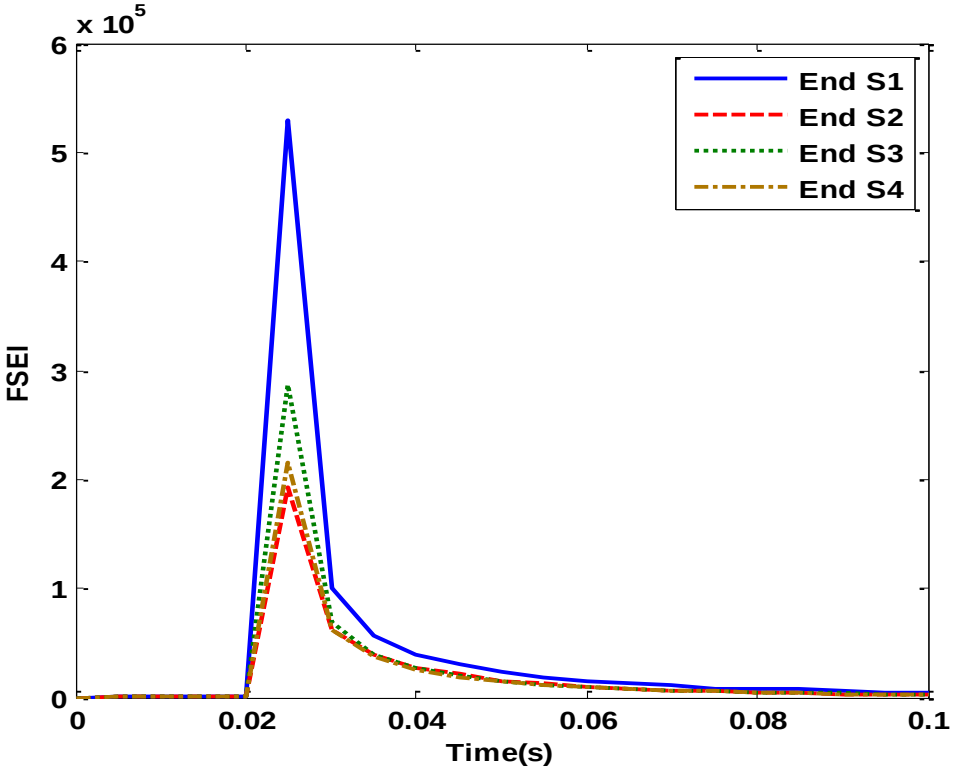

Fig. 4.5 FSEI variation for b-g fault in section S1-T1 at 40 km from S1

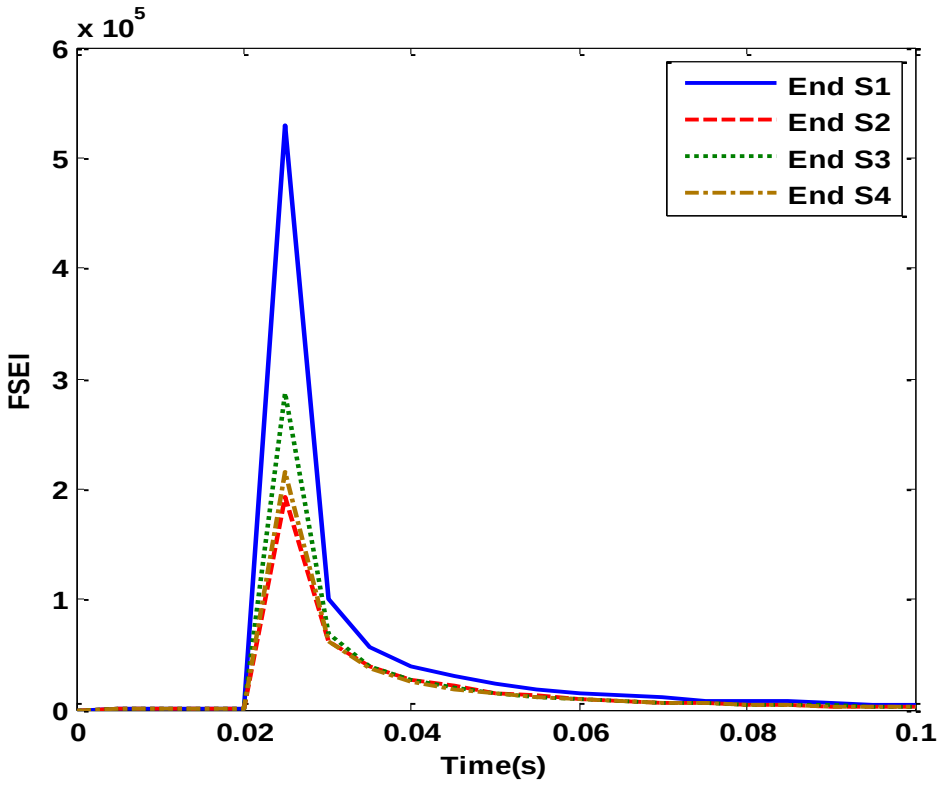

Fig. 4.6 FSEI variation for a-b fault in section S1-T1 at 100 km from S1

In the case of faults in sections with source ends, it is observed from simulation results that the faulted section FSEI value is at least 25% higher than the values of the remaining sections with source ends. Also, it is observed that FSEI values for relay ends far away from faulted section are very small compared to the value of the nearby end. This variation is due to the fact that the fault induced transients have to propagate through two junctions (T1 & T2). This distinctive feature is used to identify the faulted section in such cases correctly. Fig.4.5 and Fig.4.6 show the variation of FSEI values at the four ends with a b-g fault in section S1-T1 at 40 km and an a-b fault in section S1-T1 at 100 km respectively from the source ends.

For faults in the middle section (T1-T2), the difference between FSEI values of nearby sections (sections connected to a common junction) would be very small or negligible. Therefore it is possible to segregate such a fault effectively. Fig.4.7 and Fig.4.8 show the variation of FSEI values at the four ends with a b-c-g fault at 30 km and an a-b-c fault at 60 km respectively in the section T1-T2.

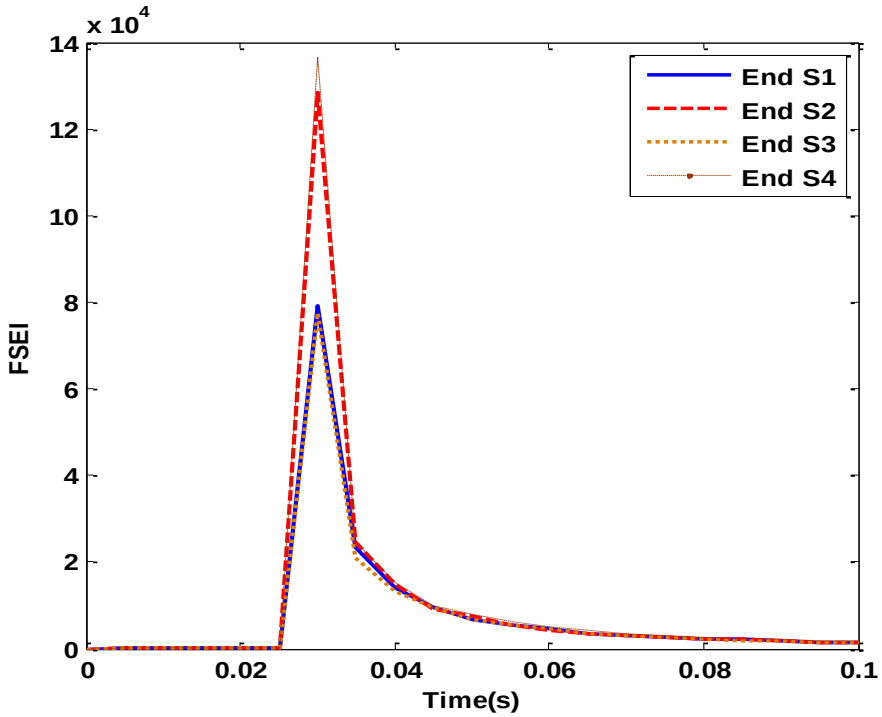

Fig. 4.7 FSEI variation for b-c-g fault in section T1-T2 at 30 km from T1

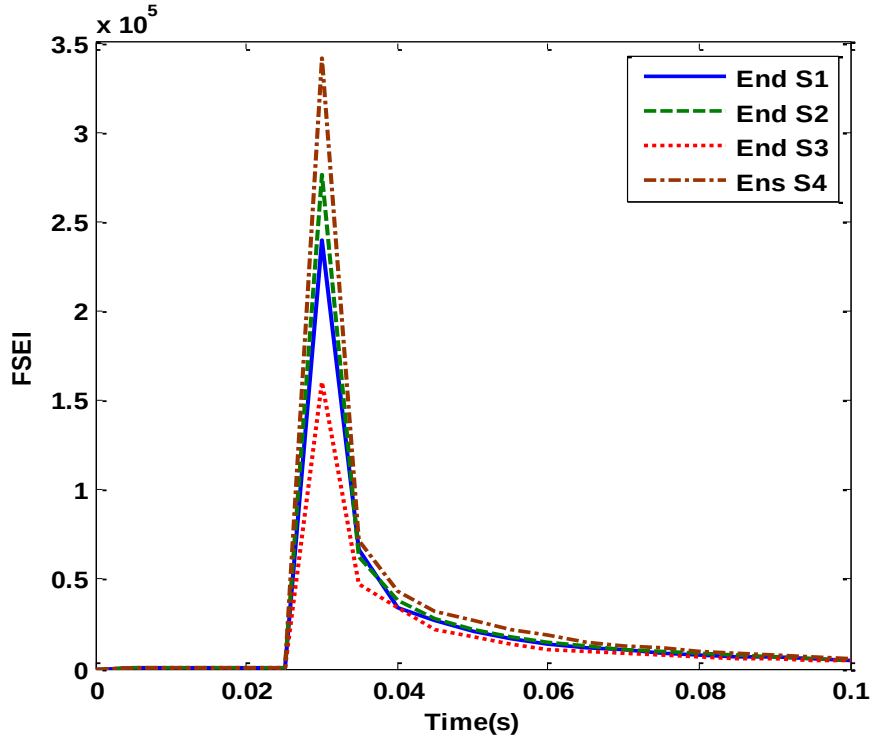

Fig. 4.8 FSEI variation for a-b-c fault in section T1-T2 at 60 km from T1

After identifying the fault section, the fault location is estimated by the accurate fault location method presented earlier. The location is accurately found for various types of faults with different incidence angles and fault resistances. Table 4.1 shows the fault location results

for various types of faults occurring in different sections of the circuit. In all the cases presented, the fault detection & section identification is correctly done by the scheme.

Table 4.1: Fault Location Results

Fault		Actual Location from the source end (km)	Estimated Location for inception angle			
Section	*Type*		0^0		90^0	
			$R_f = 0\ \Omega$	$R_f = 50\ \Omega$	$R_f = 0\ \Omega$	$R_f = 50\ \Omega$
S1-T1	a-g	100	101.47	100.02	100.02	100.08
	a-b	100	99.52	100.03	100.46	100.04
	a-b-g	100	100.02	99.98	100.23	99.97
	a-b-c	100	99.37	100.04	99.97	100.02
S2-T2	b-g	20	20.11	19.91	19.89	19.93
	b-c	20	20.22	19.99	18.92	19.99
	b-c-g	20	20.00	19.93	19.86	20.07
	a-b-c	20	20.27	20.01	19.56	19.87
S3-T1	c-g	30	29.50	29.97	29.01	30.06
	c-a	30	29.16	29.98	29.24	29.94
	c-a-g	30	30.27	30.05	29.03	30.16
	a-b-c	30	30.53	29.98	29.25	29.99
S4-T2	a-g	50	50.28	49.94	50.10	49.94
	a-b-g	50	49.82	50.05	49.45	50.00
	b-c	50	50.41	49.93	48.23	50.01
	a-b-c-g	50	50.71	49.99	49.60	50.01
T1-T2	a-g	40	39.62	39.97	40.15	40.03
	b-g	40	40.07	39.85	39.73	39.92
	c-g	40	39.84	39.85	39.84	40.09
	a-b	40	40.09	40.01	39.71	40.02
	b-c	40	40.24	40.02	39.97	40.00
	c-a	40	39.88	39.98	39.67	40.02
	a-b-g	40	40.18	40.01	39.88	40.04
	b-c-g	40	39.95	39.99	39.83	40.02
	c-a-g	40	39.74	39.92	39.80	39.97
	a-b-c	40	40.22	39.98	39.61	40.01

4.4 A Non-iterative Fault Locator for Multi-terminal Transmission Lines using Unsynchronized Phasors

In this section, a fault location procedure for multi terminal lines is presented which is applicable to any single multi terminal transmission line. The method is an extension of a fault location procedure developed for a two terminal line with unsynchronized phasor measurements.

4.4.1 Fault Detection

In fault location schemes, fault detection is the first step to be done accurately. A new current slope based fault detection method developed in [61] is used here to detect the fault prior to fault location procedure in multi terminal lines.

In the current-slope based fault detector, an index is defined as the sum of the slopes of fault current signal over one cycle time. Under normal conditions, the index value will be zero and, with the inception of fault its value changes drastically. This feature is used to detect faults effectively in a short duration of time.

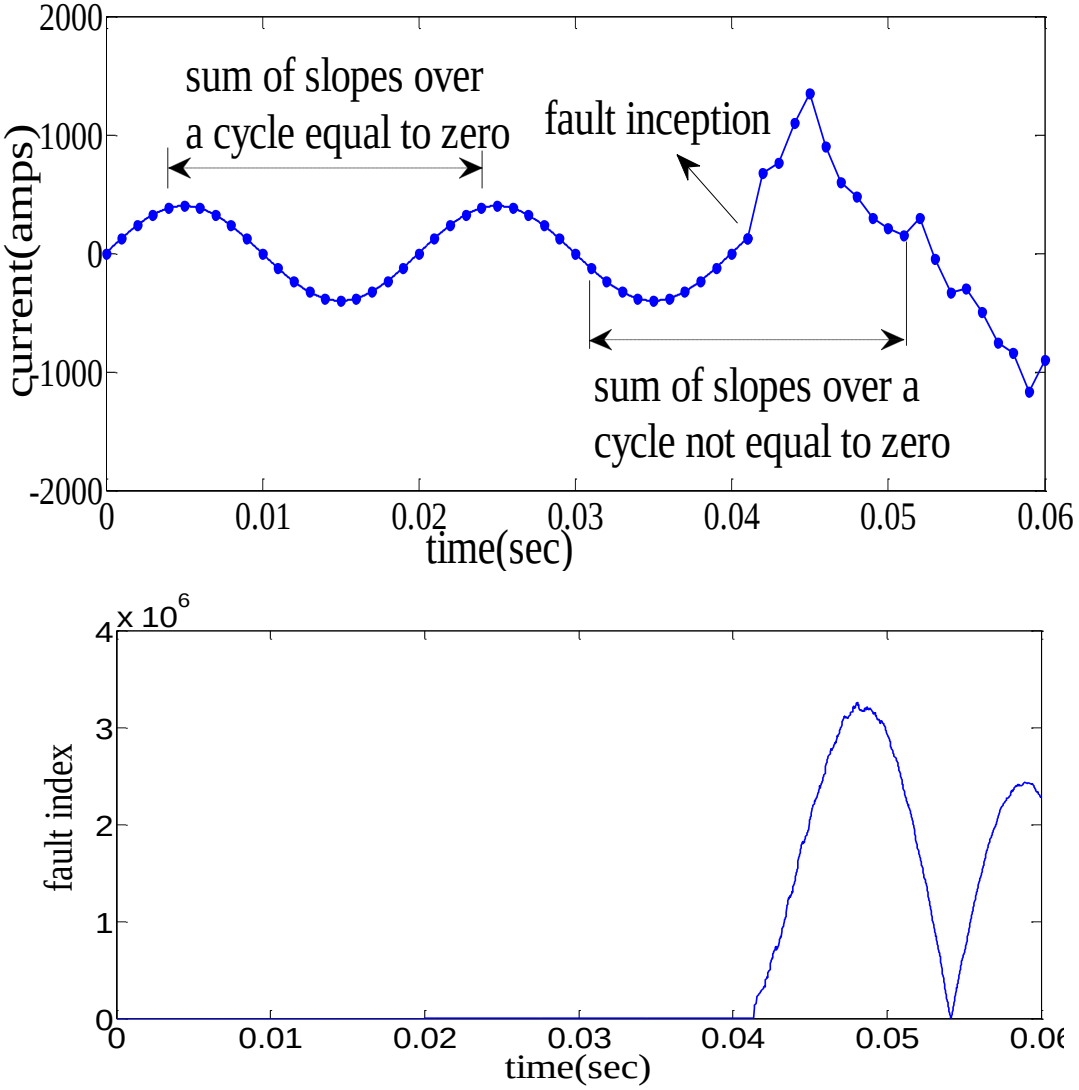

Fig. 4.9 Fault current and Fault detection index

Mathematically,

$$d(k) = [i(k) - i(k-1)] / \Delta t\,, \tag{4.1}$$

$$S(k) = \sum_{l=k-N+1}^{k} d(l)\,, \tag{4.2}$$

Where *d(k)* is the slope of the signal at the instant *k*, Δt is the sampling period, *S(k)* is the index value of the proposed slope sum method, *N* is number of samples per cycle and *i(k)* is the present sample value of the current signal. A fault is registered if,

$$\left|S(k)\right| > T \tag{4.3}$$

Where *T* is a threshold parameter. Equation (4.2) can be written in a recursive form as

$$S(k) = S(k-1) + [i(k) - i(k-1)] / \Delta t\,. \tag{4.4}$$

A proper threshold value is important for any fault detection unit as it should not treat noise signals and sudden load changes as faults. Fig.4.9 shows the current signal with fault incepted at 0.0425 sec and the variation of the fault detection index. It can be seen that with the inception of fault, the index grows to a large value there by allowing us to set a large threshold value which excludes load changes and small frequency deviations as fault conditions.

4.4.2 Analytical Synchronization for Two Terminal Line

Reference [62] proposes an accurate non iterative fault location algorithm on two terminal lines. In this method, both positive and negative sequence voltages and currents are taken to avoid the iterative procedures required for synchronizing the unsynchronized measurements and then to locate the fault. The method is briefly presented here.

In the two-terminal network shown in Fig.4.10, the two end measurements are considered to be unsynchronized by an angle 'δ'. Assume that the line is represented by its distributed parameter model for improved accuracy.

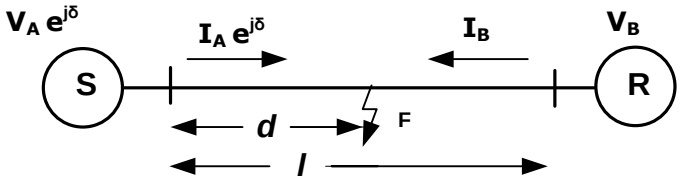

Fig. 4.10 Two Terminal line

The following equations can be written for the voltage at the fault point using source end measurements and line parameters.

$$\mathrm{V_F(A)} = \mathrm{V_A e^{j\delta}} \cosh(\gamma l d) - \mathrm{Z_c I_A e^{j\delta}} \sinh(\gamma l d), \tag{4.5}$$

$$\mathrm{V_F(B)} = \mathrm{V_B} \cosh(\gamma(1-l)\mathrm{d}) - \mathrm{Z_c I_B} \sinh(\gamma(1-l)\mathrm{d}), \tag{4.6}$$

$$V_F(A) = V_F(B). \tag{4.7}$$

Case-1: If the fault is a unsymmetrical fault, obtain an equation for both positive and negative sequence components. The equations for positive sequence is

$$(G_1 e^{j\delta} + H_1)cosh(\gamma ld) + (S_1 e^{j\delta} + T_1)sinh(\gamma ld) = 0 \tag{4.8}$$

where

$$G_1 = V_{A1}; H_1 = Z_{c1} I_{B1} \sinh(\gamma l) - V_{B1} \cosh(\gamma l),$$

$$S_1 = -Z_{c1} I_{A1} \sinh(\gamma l); T_1 = V_{B1} \sinh(\gamma l) - Z_{c1} I_{B1} \cosh(\gamma l).$$

Similarly, the equations for negative-sequence can be written as

$$\left(G_2 e^{j\delta} + H_2\right)\cosh(\gamma ld) + \left(S_2 e^{j\delta} + T_2\right)\sinh(\gamma ld) = 0 \tag{4.9}$$

where

$$G_2 = V_{A2}; H_2 = Z_{c1} I_{B2} \sinh(\gamma l) - V_{B2} \cosh(\gamma l),$$

$$S_2 = -Z_{c1} I_{A2} \sinh(\gamma l); T_2 = V_{B2} \sinh(\gamma l) - Z_{c1} I_{B2} \cosh(\gamma l).$$

Combining the formulae for the positive-sequence (4.8) and the negative-sequence (4.9) yields

$$\left(G_1 e^{j\delta} + H_1\right)\left(S_2 e^{j\delta} + T_2\right) - \left(S_1 e^{j\delta} + T_1\right)\left(G_2 e^{j\delta} + H_2\right) = 0 \tag{4.10}$$

From (4.10), one gets the quadratic formula (4.11) for the synchronization operator, in which the unknown distance to the fault is not involved.

$$K_1(e^{j\delta})^2 + K_2 e^{j\delta} + K_3 = 0 \tag{4.11}$$

where

$K_1 = G_1S_2 - G_2S_1$; $K2 = G_1T_2 + H_1S_2 - G_2T_1 - H_2S_1$; $K_3 = H_1T_2 - H_2T_1$.

Solving the quadratic equation (4.11) gives two solutions for the synchronization operator, and thus two values for the synchronization angle δ_1, δ_2. One of them is valid δ_v, i.e., is consistent with the actual value of the synchronization angle.

Case-2: If the fault is a symmetrical fault, i.e. in the case of three-phase balanced faults, instead of negative-sequence components, the incremental positive sequence components will be used in addition to the positive-sequence components. The positive sequence equations are mentioned earlier and writing equation for incremental positive sequence,

$$\left(G_{\Delta 1}e^{j\delta}+H_{\Delta 1}\right)\cosh\left(\gamma ld\right)+\left(S_{\Delta 1}e^{j\delta}+T_{\Delta 1}\right)\sinh\left(\gamma ld\right)=0 \tag{4.12}$$

where

$$\mathrm{G_{\Delta 1}=V_{A\Delta 1};H_{\Delta 1}=Z_cI_{B\Delta 1}\sinh\left(\gamma l\right)-V_{B\Delta 1}\cosh\left(\gamma l\right)},$$

$$\mathrm{S_{\Delta 1}=-Z_{c1}I_{A\Delta 1};T_{\Delta 1}\ =V_{B\Delta 1}\sinh\left(\gamma l\right)-Z_{c1}I_{B\Delta 1}\cosh\left(\gamma l\right)}$$

Here, $V_{A\Delta 1}=V_{A1}-V_{A1}^{pre}$ is the incremental positive-sequence voltage from the bus A and other incremental positive-sequence quantities are determined analogously. Combining (4.8) and (4.12) yields the following quadratic formula for the synchronization operator, in which again the unknown distance *d* to fault is not involved:

$$K_4(\mathrm{e^{j\delta}})^2+\ \mathrm{K_5e^{j\delta}}+\ \mathrm{K_6}=0 \tag{4.13}$$

where

$\mathrm{K_4 = G_1S_{\Delta 1} - G_{\Delta 1}S_1;\ K_5 = G_1T_{\Delta 1}+H_1S_{\Delta 1}-G_{\Delta 1}T_1-H_{\Delta 1}S_1;\ K_6 = H_1T_{\Delta 1}-H_{\Delta 1}T_1}$

Solution of the quadratic formula (4.11) or (4.13) gives two solutions for the synchronization operator, and thus two values for the synchronization angle δ_1 and δ_2. One of them is valid δ_v, i.e., is consistent with the actual value of the synchronization angle.

Equation (4.11) or (4.113) gives two values of synchronization angle 'δ', out of which valid 'δ_v' is selected from the condition which will depend upon the type of faults,

$$\left|\mathrm{e^{j\delta}}\right|>0.9\ \textit{or}\ \ \left|\mathrm{e^{j\delta}}\right|<1.1 \tag{4.14}$$

Then fault distance '*d*' can be calculated by using equations 4.5-4.7 as given by the following formula [62],

$$d=\frac{1}{\gamma l}\tan h^{-1}\left(\frac{\mathrm{V_B}\cosh\left(\gamma l\right)-\mathrm{Z_cI_B}\sinh\sinh\left(\gamma l\right)-\mathrm{V_Ae^{j\delta}}}{\mathrm{V_B}\sinh\left(\gamma l\right)-\mathrm{Z_cI_B}\cosh\cosh\left(\gamma l\right)-\mathrm{Z_cI_Ae^{j\delta}}}\right). \tag{4.15}$$

4.4.3 Fault Location Method for Multi terminal lines

In this work, the above fault location procedure is extended to a multi-terminal network. Fig.4.11 shows a general multi-terminal network and the fault location procedure is elaborated in the following.

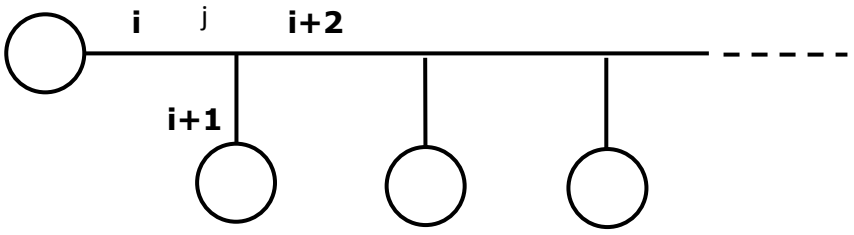

Fig. 4.11 Multi Terminal network

The fault detector algorithm continuously monitors the current signals at all the terminals. Whenever a fault is incepted, it senses the fault and gives a signal to the fault locator. The fault locator starts from the initial pair of sections 'i' and 'i+1' (i=1 initially), compares the voltages at their interconnecting junction 'j' (i.e., V_j^i and V_j^{i+1}). Their absolute values ratio is almost equal to one if the fault is not present in 'i' and 'i+1' sections. Then both sections as shown in Fig. 4.12 are synchronized as follows.

$$e^{j\delta_{(i+1)}} = \frac{(V_j^i)}{(V_j^{i+1})}, \tag{4.16}$$

Where '$\delta_{(i+1)}$' is the synchronization angle of the $(i+1)^{th}$ section with the i^{th} section, V_j^i is the voltage at the j^{th} junction by using the i^{th} section information and V_j^{i+1} is the voltage at the j^{th} junction by using $(i+1)^{th}$ section information. Then the equivalent source at j^{th} junction is calculated as

$$V_j^i = V_{j-1}^i \cosh\left(\gamma l^i\right) - Z_c I^i \sinh\left(l^i\right), \tag{4.17}$$

$$I^j = \left(-Z_c \cosh\left(\gamma l^i\right) V_{j-1}^i + I^i \cosh\left(l^i\right)\right) + \left(-Z_c \cosh\left(\gamma l^{i+1}\right) V_{j-1}^{i+1} + I^{i+1} \cosh\left(l^{i+1}\right)\right) * e^{j\delta_{i+1}}, \tag{4.18}$$

Where l^i is the line length of the i^{th} section, I^i is the current in the i^{th} section and I^j is the equivalent source current at the j^{th} junction.

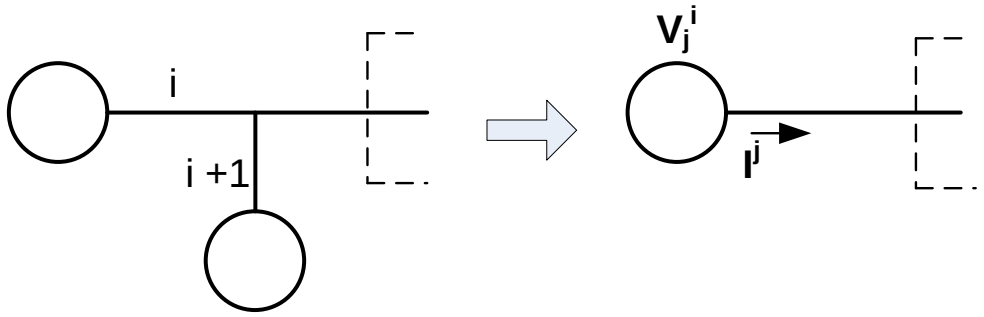

Fig. 4.12 Synchronization and equivalent source formation of 2 sections.

Now proceed in the same way for the next two sections. If their absolute values ratio is not equal, the fault might be present in i^{th} or $(i+1)^{th}$ section. It can be confirmed by synchronizing and combining from the other end up to $(j+1)^{th}$ junction and comparing the j^{th} junction voltage calculated using i^{th} and $(i+1)^{th}$ sections with that calculated using $(i+2)^{th}$ section information(i.e. V_j^i and V_j^{i+1} with V_j^{i+2}). In case V_j^i / V_j^{i+1} not equal to one, synchronize ith or (i+1)th sections with the (i+2)th section obtained by simplifying the network from the other end as shown in Fig. 4.13.

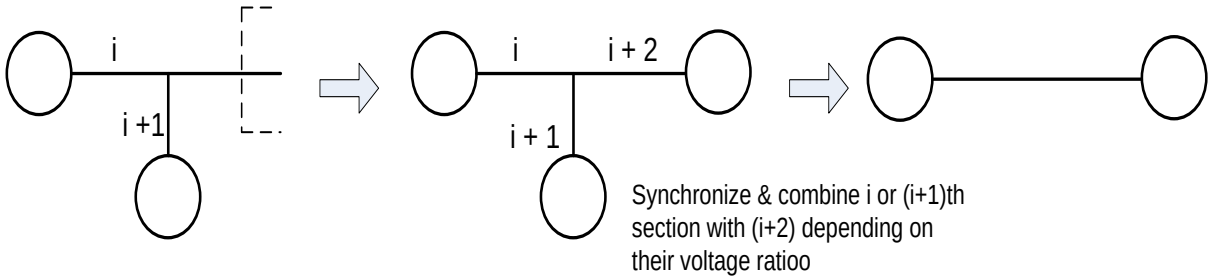

Fig. 4.13 Simplification procedure in case V_j^i / V_j^{i+1} not equal to one.

In this way, the multi terminal network is reduced to an equivalent two terminal network and the fault distance is calculated using (4.10). This procedure can be extended to any number of lines and gives accurate results as any iterative procedures are not involved. The flow chart in Fig.4.14 explains the scheme of identifying the faulted section and the fault distance.

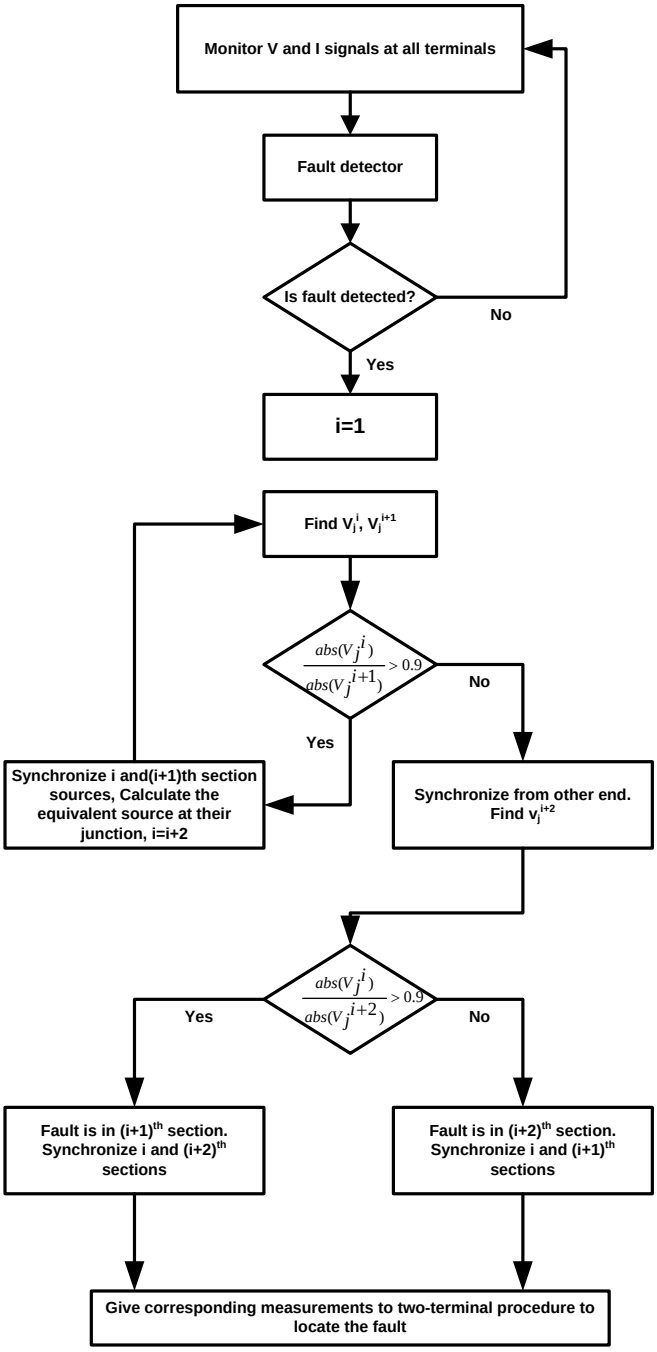

Fig. 4.14 Flow Chart for the proposed method

4.4.4 Simulation Results

The five terminal network shown in Fig.4.15 is considered for evaluating the proposed method in MATLAB/SIMULINK environment. The distributed parameter model is taken into account for all line sections and the parameters are given in Table 4.2. This model is based on the Bergeron's traveling wave method and the distributed parameter line represents the wave propagation phenomena and line end reflections with a better accuracy.

The terminal source data is given in Table 4.3 and the load L3 is taken to be 138kv, 40 MVA, 0.8 PF lagging. The measurements at different source terminals are assumed to be unsynchronized by small angles as given in Table 4.3.

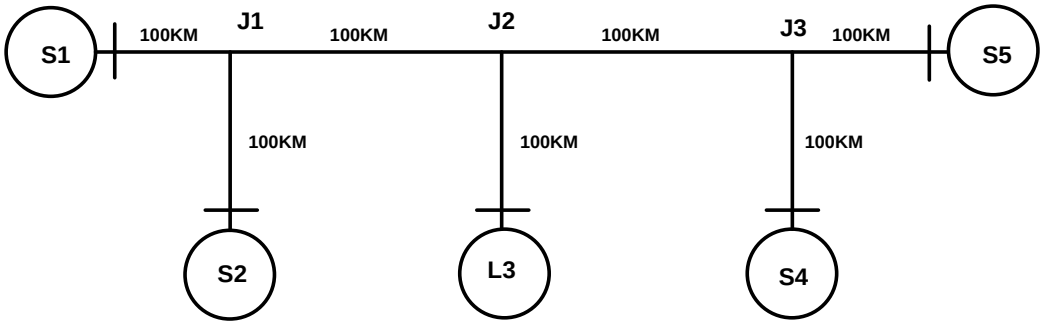

Fig.4.15. Five-terminal transmission network.

Table 4.2: Line Parameters

Section	*R1*	*L1*	*C1*	*R0*	*L0*	*C0*	*Length*
S1-J1	0.011	0.8658e-3	0.012e-6	0.309	4.1e-3	0.0083e-6	100kms
S2-J1	0.028	1.3e-3	0.012e-6	0.213	3.4e-3	0.0083e-6	80kms
J1-J2	0.022	1.1e-3	0.012e-6	0.306	4.2e-3	0.0083e-6	100kms
S3-J2	0.022	1.1e-3	0.012e-6	0.314	4.2e-3	0.0083e-6	80kms
J2-J3	0.023	1.1e-3	0.012e-6	0.310	4.2e-3	0.0083e-6	100kms
S4-J3	0.022	1.1e-3	0.012e-6	0.314	4.2e-3	0.0083e-6	80kms
S5-J3	0.023	1.1e-3	0.012e-6	0.310	4.2e-3	0.0083e-6	60kms

Table 4.3: *Source Data*

Component	**Sequence impedances**		**Voltage**	**Phase**
	Z1(Ω/km)	Z0(Ω/km)	**(kv)**	**(Deg)**
Source S1	1.8967+j18.0456	0.356+j10.1938	138	1
Source S2	2.0279+j19.2937	0.2801+j10.6963	138	3
Source S3	1.8651+j21.3186	0.2906+j11.0962	138	4
Source S5	1.4206+j16.238	0.4187+j9.5909	138	0

The considered model is extensively checked for different faults under varying fault conditions with varying fault resistance and fault inception angles. The simulation results indicated that the faults are detected very quickly (within 3ms) and are also located accurately. The results of the algorithm are presented in Tables 4.4 - 4.10. It is observed that

the accuracy of fault location is quite satisfactory for all types of faults under varying fault conditions in different sections of the multi-terminal line.

Table.4.4: Fault Location Results in Section S1-J1

Sl. No	Type of fault	Fault resistance (ohms)	Fault inception angle (deg)	Actual distance (km)	Estimated distance (km)
01	AG	0	90	20	19.310
		10	60	40	39.373
02	BG	0	30	80	78.478
		10	90	60	59.067
03	CG	5	30	20	19.274
		0	90	60	59.800
04	ABG	10	70	40	38.391
		5	60	60	59.665
05	BCG	0	0	80	78.062
		10	20	60	59.544
06	CAG	5	50	40	39.150
		0	45	60	60.689
07	AB	5	10	40	39.074
		10	60	60	59.675
08	BC	0	10	60	60.362
		5	10	40	39.632
09	CA	0	90	80	80.608
		10	60	40	38.868
10	ABC	5	90	60	60.200
		10	0	40	40.325

Table 4.5: Fault Location Results in Section S2-J1

Sl. No	Type of fault	Fault resistance (ohms)	Fault inception angle (deg)	Actual distance (km)	Estimated distance (km)
01	AG	0	90	20	19.4788
		10	60	40	41.4965
02	BG	0	30	20	18.1910
		10	0	40	40.9540
03	CG	5	10	40	39.9196
		0	60	60	61.1161
04	ABG	10	10	40	39.4965
		5	90	60	61.9071
05	BCG	0	0	20	20.2320
		10	10	60	58.5633
06	CAG	5	30	40	41.5230
		0	90	60	60.1311
07	AB	5	90	40	41.3096
		10	10	60	58.8765
08	BC	0	0	20	20.2353
		5	40	60	61.7803
09	CA	0	30	40	41.1714
		10	90	60	60.1209
10	ABC	5	60	20	20.0842
		10	0	40	39.9666

Table 4.6: Fault Location Results in Section J1-J2

Sl. No	Type of fault	Fault resistance (ohms)	Fault inception angle (deg)	Actual distance (km)	Estimated distance (km)
01	AG	0	60	40	40.2649
		10	0	80	80.6457
02	BG	0	90	60	61.2238
		10	0	80	80.0437
03	CG	5	30	60	60.8247
		0	30	80	80.1095
04	ABG	10	0	20	19.0122
		5	60	80	79.3342
05	BCG	0	90	20	20.0632
		10	60	80	81.0656
06	CAG	5	30	20	21.5187
		0	0	80	80.0011
07	AB	5	0	20	19.5003
		10	90	60	59.8255
08	BC	0	30	60	59.9193
		5	90	80	79.9912
09	CA	0	60	20	19.9888
		10	30	80	79.9792
10	ABC	5	90	60	59.9098
		10	90	80	79.8063

Table 4.7: Fault Location Results in Section L3-J2

Sl. No	Type of fault	Fault resistance (ohms)	Fault inception angle (deg)	Actual distance (km)	Estimated distance (km)
01	AG	0	60	40	40.8294
		10	60	20	20.7361
02	BG	0	0	40	41.3276
		10	90	60	61.1829
03	CG	5	30	45	45.9135
		0	30	60	61.1730
04	ABG	10	90	20	19.3582
		5	30	55	56.5742
05	BCG	0	0	20	18.2442
		10	60	40	39.1145
06	CAG	5	0	20	19.9556
		0	10	35	34.8649
07	AB	5	80	20	18.1681
		10	30	35	36.4596
08	BC	0	60	20	18.8264
		5	0	60	58.5899
09	CA	0	90	20	19.3175
		5	0	30	31.5471
10	ABC	0	10	15	17.0737
		10	30	60	61.1868

Table 4.8: Fault Location Results in Section J2-J3

Sl. No	Type of fault	Fault resistance (ohms)	Fault inception angle (deg)	Actual distance (km)	Estimated distance (km)
01	AG	0	60	20	20.9075
		10	20	40	41.2309
02	BG	0	0	20	20.9005
		10	15	40	38.8104
03	CG	5	60	40	40.6290
		0	10	35	33.5993
04	ABG	10	30	20	20.4764
		5	60	60	60.0188
05	BCG	0	90	20	20.3533
		10	90	40	40.2098
06	CAG	5	30	60	60.1010
		0	30	80	80.0616
07	AB	5	10	35	35.5015
		10	60	60	60.0036
08	BC	0	90	60	60.0974
		5	90	80	80.0365
09	CA	0	30	60	60.0966
		10	30	80	80.0360
10	ABC	0	10	55	55.0454
		10	60	60	59.7804

Table 4.9: Fault Location Results in Section S4-J3

Sl. No	Type of fault	Fault resistance (ohms)	Fault inception angle (deg)	Actual distance (km)	Estimated distance (km)
01	AG	0	90	20	18.8624
		10	60	60	60.0798
02	BG	0	30	25	26.5487
		10	0	40	40.7964
03	CG	5	40	20	21.5647
		0	60	40	41.8026
04	ABG	10	30	20	18.5433
		5	30	60	60.2914
05	BCG	0	60	20	18.5880
		10	30	40	38.3428
06	CAG	5	90	20	18.5384
		0	20	55	56.4723
07	AB	5	30	40	41.8213
		10	60	60	59.1848
08	BC	0	40	20	18.6351
		5	60	40	41.6443
09	CA	0	30	20	21.1974
		10	80	60	59.1901
10	ABC	5	50	20	20.7852
		10	30	40	41.5468

Table 4.10: Fault Location Results in Section S5-J3

Sl. No	Type of fault	Fault resistance (ohms)	Fault inception angle (deg)	Actual distance (km)	Estimated distance (km)
01	AG	10	60	15	13.5482
		0	0	40	40.9660
02	BG	5	20	30	31.5119
		10	90	40	41.4350
03	CG	5	80	25	24.1254
		0	30	40	38.9809
04	ABG	5	20	30	32.0831
		0	60	40	39.6327
05	BCG	5	10	55	54.0981
		10	40	40	39.5517
06	CAG	0	90	20	21.9516
		5	20	50	51.8146
07	AB	10	70	20	19.9589
		0	30	40	41.0787
08	BC	5	10	35	34.0672
		10	20	40	38.7170
09	CA	5	90	20	22.0239
		0	60	40	39.0981
10	ABC	5	70	20	21.1989
		10	90	40	41.0936

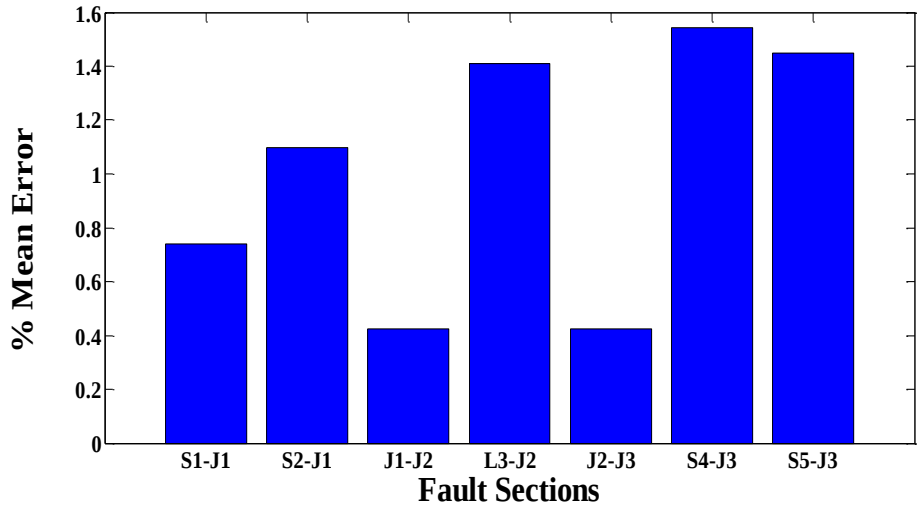

Fig. 4.16 Fault Location Error in Different sections

Fig.4.16 shows the mean percentage error with faults occurring in different sections of the line. When compared to fault location accuracy in three-terminal lines, the error seems to be slightly higher because of error compounding due to multiple synchronization requirements.

4.5 Conclusions

In this chapter, two fault location methods are presented for multi-terminal transmission lines. The first method is applicable to a four terminal line and it uses a hybrid procedure to locate the fault. Fault section is identified by using transients and exact location is carried out by using phasor information. The section identification procedure by using modal voltage signal transients is found to be effective for the four terminal line. Results of simulation demonstrate the accuracy and method is not sensitive to fault conditions.

The second method is for a general multi-terminal network where the measurements are considered to be unsynchronized. It is based on an analytical synchronization procedure developed for two terminal lines. Simulation results obtained indicate satisfactory accuracy.

Chapter 5

Summary & Conclusions

In this work, an attempt is made to develop protection algorithms for EHV teed and multi-terminal transmission circuits with a focus on fault classification and location problems. Protection and fault location in such circuits is complicated mainly because of no measurements at tap points. Conventional phasor based approaches like distance relaying face zone setting problems and their speed is not satisfactory for modern power systems. Therefore, new methods for quick & reliable fault detection and classification in such transmission lines are very much essential to maintain grid integrity. In view of the protection speed requirements, the transient based approach is considered to be a feasible solution for fault detection and classification in this work. Unlike phasor based schemes, transient based techniques use short post-fault data windows to enhance the speed of response.

In addition, a fault location feature is very useful for making post fault repairs in case of permanent faults. Accurate fault location in teed and multi-terminal lines requires correct identification of faulted section first which is then followed by exact calculation of fault distance. Lack of synchronization between measured voltage and current signals at various terminals is another point of concern. Based on these issues, work is done to develop effective fault section identification methods and improve accuracy with fault location. Both phasor and travelling wave methods are explored to develop improved location techniques. Further, to deal with the problems of deterministic fault classification and location methods, artificial intelligence solutions using ANNs are also proposed for teed circuits.

In this thesis work, the following contributions have been made in the development of protection algorithms for teed and multi-terminal transmission circuits.

- Transient Based Fault Classification in EHV Teed Circuits using Wavelet Transform
- Transient and Probabilistic Neural Network Based Fault Classification in EHV Three-Terminal Lines
- Fault Location In Teed Circuits Using Modified DFT Phasor Estimation
- Travelling Wave Based Fault Location In Teed Circuits Using S-Transform & Neural Networks

- A Hybrid Method for Fault Location in EHV Multi-Terminal Circuit with Four terminals.
- A Non-iterative Fault Locator for Multi-terminal Transmission Lines using Unsynchronized Phasors

All the above algorithms are verified exhaustively by simulation in MATLAB environment considering different fault conditions. The following observations and conclusions can be drawn from the results obtained.

- The direct transient based fault classification technique is accurate for all faults except double-line-ground faults. Accuracy with such faults is only around 80% because of misleading transient patterns generated in fault voltages.
- Simple transient based fault detection using modal signal is found to be very fast and effective. Uses only a quarter-cycle window of voltage signals for processing with Wavelet transform.
- Transient & PNN based scheme is accurate, simple, requires one threshold and insensitive to fault conditions. The overall accuracy is 99.88% with the use of transient energy from three ends and performance is much better compared to other methods.
- A PNN based solution for double-line-ground faults is found to be very effective. Use of PNN only for such faults reduces network complexity and training.
- The scheme can also be used with only single end transient energy to enhance dependability without much reduction in accuracy. Failure of a classifier at one end mostly will not influence the overall classification result.
- Fault location in teed circuits using modified DFT is very effective and the hybrid approach using transients for section identification and phasors for an exact location is accurate. The location error is well below 1% in all simulated cases.
- The technique is applicable to both symmetrical and asymmetrical teed circuits and method is not sensitive to fault conditions.
- Travelling wave based location in teed circuits is affected by the uncertainties in extracted wave arrival times. Application of neural networks to resolve this problem in fault location is found to be feasible.
- PNN is very effective in section identification and GRNN is able to locate fault accurately compared to the conventional travelling wave based approach in many situations. The mean error is below 1% for all simulated faults tested.

- Wave arrival time extraction by using S-transform is found to be accurate when compared to other methods like wavelet transform.
- Fault location in four terminal line is done accurately by extending the transient based section identification procedure used for three terminal lines.
- The non-iterative synchronization procedure is extended to a general multi-terminal transmission line and is found to be useful for accurate fault location.
- Fault location using analytical non-iterative synchronization procedure is very useful for multi-terminal lines which involve several unsynchronized measurements. The method avoids the necessity of synchronized measurements which is expensive.

Future Scope:

High speed transient based non-unit protection scheme for three terminal lines is sensitive to measurement noise. Further improvements for noise tolerance may be explored.

The knowledge based methods can be extended to the protection of general multi-terminal lines. Other avenues include a hardware implementation of protection algorithms using DSP and FPGA.

Published Papers

1. Varma R K Bhupatiraju and Ramana Rao V Pulipaka, "A Wavelet Based Protection Scheme for EHV Asymmetrical Teed Circuits," 9th International Power & Energy Conference (IPEC 2010), Singapore, October 2010.
2. B.R.K. Varma and P.V.R. Rao, "A hybrid method for fault location in EHV multi-terminal-circuits," 16th National Power Systems Conference (NPSC-2010), Hyderabad, December 2010.
3. B.R.K. Varma, Karri Nagaraju, D.V.S.S. Siva Sarma and P.V. Ramana Rao, "A Non-iterative Fault Locator for Multi-terminal Transmission Lines using Unsynchronized Phasors," 17th National Power Systems Conference (NPSC-2012) IIT (BHU) Varanasi, December 2012.

Submitted Papers

1. B.R.K.Varma, D.V.S.S. Siva Sarma and P.V. Ramana Rao, "Transient and Probabilistic Neural Network Based Fault Classification in EHV Three-Terminal Lines," *Turkish Journal Of Electrical Engineering & Computer Sciences* (Under review)
2. B.R.K Varma, D.V.S.S. Siva Sarma and P.V. Ramana Rao, "Fault Classification and Location in EHV Teed Circuits using Wavelet Transform and Modified DFT", *International Journal on Electrical Engineering and Informatics*. (Under review)

References

[1] NPTEL e-Learning Course on web: nptel.ac.in/downloads/108101040

[2] N.Zhang, M.Kezunovic, "Transmission Line Boundary Protection using Wavelet Transform and Neural Network," *IEEE Trans. on Power Del.,* vol. 22, no. 2, pp. 859-869, Apr. 2007.

[3] NERC, A technical document prepared by the systems protection and control task force of the NERC planning committee- "The complexity of protecting three terminal transmission line," 2006. [online]. Available: www.nerc.com

[4] R.K.Aggarwal and A.T. Johns, "The development of a new high speed three terminal line protection scheme," *IEEE Trans. Power Del.,* vol. 1, no. 1, pp. 125-134, Jan. 1986.

[5] R.K.Aggarwal and A.T. Johns, "Digital differential relaying scheme for teed circuits based on voltage and current signal comparison," *IEE Proceedings C Gen., Tran. and Distr.,* vol. 137, no. 6, pp. 414-423, Nov. 1990.

[6] R.K.Aggarwal, A.H. Husseini and M.A. Redfern "Design and testing of a new microprocessor-based current differential relay for EHV teed feeders," *IEEE Trans. Power Del.,* vol.6, no.3**,** Jul.1991

[7] A.Girgis, D. Hart and W. Peterson, "A new fault location technique for two-and three-terminal lines", *IEEE Trans. Power Del*.,vol.7, no.1,pp. 98-107, Jan. 1992.

[8] R.K.Aggarwal, D.V.Coury, A.T.Johns and A.Kalam, "A practical approach to accurate fault location on extra high voltage teed feeders," *IEEE Trans., Power Del.,* vol.8, no.3, pp.874-883, Jul. 1993.

[9] A.M. Carter, A.T. Johns, R.K. Aggarwal, Z.Q. Bo., "Computer-aided design of a new non-unit protection scheme for EHV teed circuits," *IEE Proc., Gener. Trans Dist*. 143, no. 2 pp. 142-150, Mar. 1996.

[10] Ying-Hong Lin, Chih-wen Liu and Chi-shan Yu "A New Fault Locator for Three-Terminal Transmission Lines – Using Two-Terminal Synchronized Voltage and Current Phasors," *IEEE Trans., Power Del.*, vol. 17, no. 2, pp. 452-459, Apr. 2002.

[11] M.M. Eissa, "A new digital relaying scheme for EHV three terminal transmission lines," *Electric Power System Research*, vol. 73, no. 2, pp.107-112, Feb. 2005.

[12] C.Y. Evrenosoglu and Ali Abur, "Travelling Wave Based Fault Location for Teed Circuits", *IEEE Trans. Power Del.*, vol. 20, no. 2, April 2005.

[13] J.Izykowski, E.Rosolowski et al, "A Fault-Location method for application with current differential relays of three-terminal lines" *IEEE Trans. Power Del.*, vol. 22, no. 4, pp. 2099-2107, Oct. 2007

[14] M.da.Silva, M. Oleskovicz, D.V. Coury, "A hybrid fault locator for three– Terminal lines based on wavelet transforms," *Electric Power System Research*, vol. 78, no.11, pp. 1980-1988, Nov. 2008.

[15] B.Bhalja and R.P. Maheswari, "New differential protection scheme for tapped transmission line," IET Gen. Trans. Distri., vol. 2, no. 2, pp. 271-279, Mar. 2008.

[16] M.M.Eissa, **"**A new digital teed circuit protection using directional element," *IEEE Trans. Power Del.*, vol. 24, no. 2, pp. 531–541, Apr. 2009.

[17] P.Jafarian and M.Sanaye-Pasand, "High-Frequency Transients-Based Protection of Multi-terminal Transmission Lines Using the SVM Technique," *IEEE Trans. Power Del.*, vol. 28, no. 1, pp. 188-196, Jan. 2013.

[18] M. Khodadadi and S.M. Shahrtash, "A New non-communication based protection scheme for three-terminal transmission lines employing mathematical morphology-based filters," *IEEE Trans. Power Del.*, vol. 28, no. 1, pp. 347-356, Jan. 2013.

[19] H.Livani and C.Yaman Evrensoglu, "A fault classification and localization method for three-terminal circuits using machine learning," *IEEE Trans. Power Del.*, vol. 28, no. 4, pp. 2282-2290, Oct. 2013.

[20] A.Ahmadimanesh and S. Mohammad Shahrtash, "Time-time transform based fault location algorithm for three-terminal transmission lines," *IET Gen., Trans. and Distr.*, vol. 7, no. 5, pp 464-473, May 2013.

[21] B.Mahamedi and J.Guo Zhu "Fault classification and faulted phase selection based on the symmetrical components of reactive power for single-circuit transmission lines," *IEEE Trans. Power Delivery,* vol. 28, no.4, pp. 2326-2332, Oct. 2014.

[22] Z.He, L.Fu, S.Lin, and Z.Bo, "Fault detection and classification in EHV transmission line based on wavelet singular entropy," *IEEE Trans. Power Del.*, vol. 25, no. 4, pp. 2156-2163, Oct. 2010.

[23] S.P.Valsan, K.S.Swarup, "Wavelet transform based digital protection for transmission lines," *Electrical Power and Energy Systems*, vol. 31, no. 7, pp. 379-388, Sep. 2009.

[24] X.Dong, W.Kong, and T.Cui, "Fault classification and faulted-phase selection based on the initial current traveling wave," *IEEE Trans. Power Del.*, vol. 24, no. 2, pp.552-559, Apr. 2009.

[25] O.A.Youssef, "Combined fuzzy-logic wavelet-based fault classification technique for power system relaying", *IEEE Trans. Power Del.*, vol. 19, no. 2, pp. 582-589, Apr. 2004.

[26] M.J.Reddy, D.K.Mohanta, "A wavelt-fuzzy combined approach for classification and location of transmission line faults," *International Journal of Electric Power and Energy Systems*, vol. 29, no. 9, pp. 669-678, Nov. 2007.

[27] S.Vasilic, M.Kezunovic, "Fuzzy ART neural network algorithm for classifying the power system faults," *IEEE Trans. Power Del*., vol. 20, no. 2, pp.1306-1314, Apr 2005.

[28] K.M.Silva, B.A.Souza, N.S.D. Brito "Fault detection and classification in transmission lines based on wavelet transform and ANN," *IEEE Trans. Power Del.*, vol. 21, no. 4, pp. 2058-2063, Oct. 2006.

[29] P.K.Dash, S.R.Samantaray, G.Panda " Fault classification and section identification of an advanced series-compensated transmission line using Support Vector Machine," *IEEE Trans. Power Del.*, vol. 22, no. 1, pp. 67-73, Jan. 2007.

[30] J.A. Jiang, C.L.Chuang, Y.C. Wang, C.H. Hung, J.Y. Wang, C.H.Lee, Y.T Hsiao "A hybrid framework for fault detection, classification, and location—Part-I: Concept, structure and methodology," *IEEE Trans. Power Del.*, vol. 26, no. 3, pp. 1988-1998, Jul. 2011.

[31] A.Jamehbozorg, S.M.Shahrtash "A decision-tree-based method for fault classification in single-circuit transmission lines," *IEEE Trans Power Del.*, vol. 25, no. 4, pp. 2190-2196, Oct. 2010.

[32] J.Upendar, C.P.Gupta, G.K.Singh "Statistical decision-tree based fault classification scheme for protection of power transmission lines," *International Journal of Electrical Power and Energy Systems*, vol. 36, no. 1, pp.1–12, Mar. 2012.

[33] Z.He, S.Lin, Y.Deng, X.Li, Q.Qian "A rough membership neural network approach for fault classification in transmission lines," *International Journal of Electrical Power and Energy Systems*, vol. 61, pp. 429–439, Oct. 2014.

[34] T. Nagasawa, M. Abe, N. Otsuzuki, T. Emura, Y. Jikihara, and M. Takeuchi, "Development of a new fault location algorithm for multi-terminal two parallel transmission lines," *IEEE Trans. Power Del*., vol.7, no. 3, pp. 1516–1532, Jul. 1992.

[35] M.Abe, N. Otsuzuki, T.Emura and M.Takeuchi "Development of a new fault location system for multi-terminal single transmission lines" *IEEE Trans. Power Del.*, vol. 10, no. 1, pp.159-168, Jan. 1995.

[36] T. Funabashi, H. Otoguro, Y. Mizuma, L. Dube, and A. Ametani, "Digital fault location for parallel double-circuit multi-terminal transmission lines," *IEEE Trans. Power Del.*, vol. 15, no. 2, pp. 531–537, Apr. 2000.

[37] S.M. Brahma, "Fault location scheme for a multi-terminal transmission line using synchronized voltage measurements," *IEEE Trans. Power Del.*, vol. 20, no. 2, pp 1325-1331, Apr. 2005.

[38] S.M. Brahma "New fault-location method for a single multi-terminal transmission line using synchronized phasor measurements," *IEEE Trans. Power Del.*, vol. 21, no. 3, pp.1148-1153, Jul. 2006.

[39] C.W. Liu, K. P. Lien, C. S. Chen and J. A. Jiang, "A universal fault location technique for N-terminal (N>3) transmission lines", *IEEE Trans.Power Del.*, vol. 23, no. 3, pp. 1373–1386, Jul. 2008.

[40] G. Manassero, E.C.Singer, R.M.Nakagoni, E.L.Pellini, and E.C.N.Rodrigues, "Fault-location system for multi-terminal transmission lines," *IEEE Trans. on Power Del*., vol. 21, no. 3, pp. 1148–1153, Jul. 2010.

[41] E.E.Ngu, K.Ramar "A combined impedance and traveling wave based fault location method for multi-terminal transmission lines," *International Journal of Electrical Power and Energy Systems*, vol. 33, no. 10, pp. 1767–1775, Oct. 2011.

[42] Y. Zhu, X.Fan "Fault location scheme for a multi-terminal transmission line based on current travelling waves," *International Journal of Electrical Power and Energy Systems*, vol. 53, pp. 367-374, Dec. 2013.

[43] A.Ahmadimanesh, S.M.Shahrtash "Transient-based fault-location method for multi-terminal lines employing S-transform," *IEEE Trans. Power Del.*, vol. 28, no. 3, pp.1373-1380, July 2013.

[44] I.Daubechies "The wavelet transform, time-frequency localization and signal analysis," *IEEE Trans. Inf. Theory*, vol. 36, no. 5, pp. 961-1005, Sep. 1990.

[45] S. Mallat, *A Wavelet Tour of Signal Processing*. New York: Academic, 1999.

[46] A.G.Shaik, P.V.Ramana Rao, "A new wavelet based fault detection, classification and location in transmission lines," *International Journal of Electrical Power and Energy Systems*, vol. 64, pp. 35-40, Jan. 2015.

[47] A.M.Carter, R.K.Aggarwal, A.T.Johns, and Z.Q.Bo, "Computer-aided design of a new nonunit protection scheme for EHV teed circuits", *IEE Proc.-Gener.Transm. Distrib.*, vol. 143, no.2, pp. 140-150, Mar. 1996.

[48] S.M.Brahma, P.L.De Leon, R.G.Kavasseri, "Investigating the option of removing the antialiasing filter from digital relays," *IEEE Trans Power Del.*, vol. 24, no. 4, pp. 1864-1868, Oct. 2009.

[49] F.B. Costa, B.A. Souza, and N.S.D. Brito, "Effects of the fault inception angle in fault-induced transients," *IET Gener. Trans. Distrib*., vol. 6, no. 5, pp. 463–471, May 2012.

[50] S.M.Brahma, "Distance relay with out-of-step blocking function using wavelet transform," *IEEE Trans. Power Del.*, vol. 22, no. 3, pp. 1360-1366, Jul. 2007.

[51] W.Chen, O.P.Malik, X.Yin, D.Chen, Z.Zhang "Study of wavelet-based ultra high speed directional transmission line protection," *IEEE Trans. Power Del.* Vol. 18, no. 4, pp. 1134-1139, Oct. 2003.

[52] A.H.Osman, O.Malik "Transmission line distance protection based on Wavelet transform," *IEEE Trans.Power Del.*, vol. 19,no. 2, pp. 515-523, Apr. 2004.

[53] D.F.Specht, "Probabilistic neural networks," *Neural Netw*., vol. 3, no. 1, pp. 109-118, Dec. 1990.

[54] N.Perera, A.D. Rajapakse "Recognition of fault transients using a probabilistic neural network classifier," *IEEE Trans. Power Del.*, vol. 26, no.1, pp. 410-419, Jan. 2011.

[55] MATLAB SimPowerSystems Simulink Blockset

[56] Protection System Reliability: Redundancy of Protection System Elements, *NERC System Protection and Control Task Force Technical Paper*, Nov, 2008.

[57] A.T.Johns and S.Jamali, "Accurate fault location technique for power transmission lines," *In IEE Proc. C-Gen., Trans. and Dis.,* vol.137, no.6, pp. 395-402, Nov. 1990.

[58] S.H.Kang, D.G. Lee, S.R. Nam, P.A. Crossley, and Y.C. Kang " Fourier transform-based modified phasor estimation method immune to the effect of the DC Offsets," *IEEE Trans. Power Del.,* vol. 24, no. 3, pp.1104-1111, Jul. 2009.

[59] Donald F Specht "A General Regression Neural Network," *IEEE Trans. Neural Net.,* vol. 2, no. 6, pp. 568-576, Nov 1991.

[60] R.G. Stockwell, L. Mansinha, and R.P. Lowe "Localization of Complex Spectrum: The S-Transform," *IEEE Trans. Signal Processing*, vol. 44, no. 4, pp. 998-1001, Apr. 1996.

[61] K.Nagaraju, P.S.V. Sivateja Varma, Bh. R.K. Varma "A Current-Slope based Fault Detector for Digital Relays," *Proceedings of IEEE India's annual conference,* INDICON-2011, Hyderabad, India, pp. 1-4, Dec. 2011.

[62] J. Izykowski, E. Rosolowski, P. Balcerek, M. Fulczyk and M.M. Saha, "Accurate non iterative fault location algorithm utilizing two-end unsynchronized measurements," *IEEE Trans. Power Del*., vol. 26, no. 2, pp. 547-555, Apr. 2011.

[63] A.d.Souza Gomes, M.A.Costa, T.G.A.de Faria, and W.M.Caminhas, "Detection and classification of faults in power transmission lines using functional analysis and computational intelligence," *IEEE Trans.Power Del.,* vol. 28, no. 3, pp.1402-1413 Jul. 2013.

[64] M.R. Noori and S.M. Shahrtash "Combined fault detector and faulted phase selector for transmission lines based on adaptive cumulative sum method," *IEEE Trans. Power Del.,* vol.28, no.3, pp.1779-1787, Jul. 2013.

[65] G.E. Alexander and J.G. Andrichak, "Application of phase and ground distance relays to three terminal lines," store. Gedigotalenergy.com /faq.documentr/alps/GER-3964.pdf.

[66] A.T.Johns, R.K.Aggarwal, and Z.Q.Bo "Non-unit Protection Technique for EHV Transmission Systems Based on Fault Generated Noise. Part-1: *Signal Measurement," IEE Proc.-Gen., Trans. and Dist.* vol. 141, no. 2, pp.133-140, Mar. 1994.

[67] R.K.Aggarwal, A.T.Johns, and Z.Q.Bo ''Non-unit Protection Technique for EHV Transmission Systems Based on Fault Generated Noise. Part-2: *Signal processing," IEE Proc.-Gen., Trans. and Dist.* vol. 141, no. 2, pp 141-147, Mar. 1994.

[68] Arun G. Phadke, James S. Thorp "Computer Relaying for Power Systems" *Research Studies Press Ltd.,* England, 1994.

[69] V. Cook "Analysis of Distance Protection," *Research Studies Press Ltd.,* England, 1985.

[70] A.T. Johns, J.R. Platts "Digital Protection for Power Systems" *IEE Power Series* 15, 1995.

[71] IEEE Power system Relaying Committee "Protection aspects of multi-terminal lines," IEEE Publication Number. 79 TH0056-2-PWR 1979, pp 1-17

[72] S.Rajendra and P.G.McLarenm, "Travelling wave techniques applied to the protection of teed circuits: Multi-phase/multi-circuit system," *IEEE Trans. Power App. Syst.*, vol. PAS-104, no.12, pp.3551-3557, Dec.1985.

[73] C.Yu, C.Liu, and Y.Lin, "A fault location algorithm for transmission lines with tapped leg--PMU based approach," In *proc. IEEE Power Eng. Soc. Summer Meeting*, Vancouver, BC, Canada, vol. 2, pp. 915-920, Jul. 2001.

[74] M.M.Saha, J.Izykowski, E.Rosolowski "Fault Location on Power Networks." Springer-Verlag London Limited 2010.

[75] S.El Safty, A.El-Zonkoly "Applying wavelet entropy principle in fault classification", *International Journal of Electrical Power & Energy Systems*, vol. 31, no. 10, pp. 604-607, Dec. 2009.

[76] F.V. Lopes, D. Fernandes, Jr., and W.L.A. Neves, "A Travelling-Wave detection method based on Park's transformation for fault locators," *IEEE Trans. Power Del.*, vol. 28, no. 3, pp. 1626-1634, July. 2013.

[77] F.H. Magnago and A. Abur "Fault location using Wavelets," *IEEE Trans. Power Del.*, vol. 13, no. 4, pp. 1475-1480, Oct. 1998.

[78] J. Gracia, A. J. Mazón, "Best ANN Structures for Fault Location in Single & Double-Circuit Transmission Lines," *IEEE Trans. Power Del.*, vol. 20, no. 4, pp. 2389-2395, Oct. 2005.

[79] D.C. Robertson, O.I. Camps, J.S. Mayer, and W.B. Gish, "Wavelets and electromagnetic power system transients," *IEEE Trans. Power Del.*, vol. 11, no. 2, pp. 1050–1056, Apr. 1996.

[80] A.W. Galli, G.T. Heydt, and P.F. Ribeiro, "Exploring the power of wavelet analysis," *IEEE Comput. Appl. Power*, vol. 9, no. 4, pp. 37–41,Oct. 1996.

[81] C.H. Kim, H.Kim, Y- H. Ko, S.H. Byun, R.K. Aggarwal, and A.T. Johns, "A novel fault–detection technique of high–impedance arcing faults in transmission lines using the wavelet transform," *IEEE Trans. Power Del.*, vol.17,no.4,pp. 921-928, Oct. 2002.

[82] D.J. Zhang, Q.H. Wu, and Z.Q. Bo, "Transient positional protection of transmission lines using complex wavelets analysis," *IEEE Trans. Power Del.*, Vol. 18, no. 3, pp. 705-710, Jul. 2003.

[83] A.I. Megahed, A.M. Moussa, and A.E. Bayoumy, "Usage of wavelet transform in the protection of series–compensated transmission lines," *IEEE Trans. Power Del.*, vol. 21, no. 3, pp. 1213-1221, Jul. 2006.

[84] F. Liang and B. Jeyasurya, "Transmission line distance protection using wavelet transform algorithm," *IEEE Trans. Power Del.*, vol. 19, no. 2, pp. 545-553, Apr. 2004.

[85] P.K.Dash, B.K.Panigrahi, and G. Panda, "Power quality analysis using S-transform," *IEEE Trans. Power Del.,* vol. 18, no. 2, pp.406-411, Apr. 2003.

[86] D.Chanda, N.K.Kishore, A.K.Sinha "A wavelet multiresolution analysis for location of faults on transmission lines," *International Journal of Electrical Power & Energy Systems,* vol. 25, no. 1, pp. 59–69, Jan. 2003.

[87] P. M. Anderson, *Power System Protection*. New York: IEEE Press, 1999, pp.539-540.

[88] P.Jafarian and M.S.Pasand, "A traveling wave based protection technique using wavelet/PCA analysis," *IEEE Trans. Power Del.*, vol.25, no. 2, pp. 588–599, Apr. 2010.

[89] M. Kezunovic and I. Rikalo, "Detect and classify transmission line faults using neural nets," *IEEE Comput. Appl. Power,* vol. 9, no. 4, pp. 42–47, Oct. 1996.

[90] A.A.Hajjar "A high speed noncommunication protection scheme for power transmission lines based on wavelet transform," *Electric Power Systems Research,* vol. 96, pp. 194-200, Mar. 2013.

[91] Z.Q.Bo "A new noncommunication protection technique for transmission lines," *IEEE Trans. Power Del.,* vol. 13, no. 4, pp. 1073–1078, Oct. 1998.

[92] W.A.Wilkinson and M. D. Cox, "Discrete wavelet analysis of power system transients," *IEEE Trans. Power Sys.*, vol. 11, no. 4, pp. 2038-44, Nov. 1996.

[93] O.Youssef, "New algorithm to phase selection based on wavelet transforms," *IEEE Trans. Power Del.,* vol. 17, no. 4, pp. 908–914, Oct. 2002.

[94] M. Kezunovic, "A survey of neural net application to protective relaying and fault analysis," *Eng. Intell. Syst.*, vol. 5, no. 4, pp. 185–192, Dec . 1997.

[95] H.A. Darwish, M.Hesham, A.MI. Taalab, and N.M.Mansour " Close Accord on DWT Performance and Real-Time Implementation for Protection Applications," *IEEE Trans Power Del.*, vol. 25, no. 4, Oct. 2010.

[96] S.Ekici, S.Yildirim, M.Poyraz, "A transmission line fault locator based on Elman recurrent networks," *Applied Soft Computing,* vol. 9, no. 1, pp. 341–347, Jan. 2009.

[97] D. F. Peelo, F. Rahmatian, M. Nagpal, And D. Sydor , "Real-time Monitoring and Capture of Power System Transients", 21, rue d'Artois, F-75008 PARIS B3-101 CIGRE 2012 http://www.cigre.org.

[98] J.Sadeh and H.Afradi "A new and accurate fault location algorithm for combined transmission lines using adaptive network-based fuzzy inference system," *Electr. Power Syst. Res.*, vol.79, no. 11, pp. 1538-1545, Nov. 2009.

[99] G. N. Korres, C. A. Apostolopoulos, "Precise fault location algorithm for double circuit transmission lines using unsynchronized measurements from two anti-parallel ends", *IET Gen., Trans., and Dist.*, vol. 4, no. 7, pp. 824-835, Jul. 2010.

[100] C.A.Apostolopoulos, G.N.Korres "A novel algorithm for locating faults on transposed/untransposed transmission lines without utilizing line parameters," *IEEE Trans. Power Del.*, vol. 25, no.4, pp. 2328-2338, Oct. 2010.

[101] C.A.Apostolopoulos, G.N.Korres, "A novel fault-location algorithm for double-circuit transmission lines without utilizing line parameters," *IEEE Trans. Power Del.*, vol. 26, no.3, pp.1467-1478, Jul. 2011.

[102] C.A.Apostolopoulos, G.N.Korres "Accurate fault location algorithm for double-circuit series compensated lines using a limited number of two-end synchronized measurements," *International Journal of Electrical Power and Energy Systems*, vol. 42, no.1, pp. 495-507, Nov. 2012.

[103] N.Kang and Y.Liao "Double-circuit transmission-line fault location with the availability of limited voltage measurements," *IEEE Trans. Power Del.*, vol. 27, no. 1, pp. 325-336, Jan. 2012.

[104] M.Korkali, H. Lev-Ari, A. Abur, "Traveling-wave-based fault-location technique for transmission grids via wide-area synchronized voltage measurements," *IEEE Trans. Power Del.*,vol.27, no. 2, pp. 1003-1011. May 2012.

[105] D.A.G.Vieira, D.B.Oliveira, and A.C.Lisboa "A closed-form solution for un-transposed transmission-lines fault location with non-synchronized terminals," *IEEE Trans. Power Del*., vol. 28, no. 1, pp. 524-525, Jan. 2013.

[106] V.Terzija, Z.M.Radojevii, G.Preston,"Flexible synchronized measurement technology-based fault locator, " *IEEE Trans. Smart Grid*, vol. 6, no. 2, pp. 866-873, Mar. 2015.

[107] A. Salehi-Dobakhshari and A. M. Ranjbar "Robust fault location of transmission lines by synchronized and unsynchronized wide-area current measurements," *IET Gen., Trans. and Distr.*, vol. 8, no. 9, pp. 1561-1571, Sept. 2014.

[108] P.Chaiwan, N. Kang, Y. Liao, "New accurate fault location algorithm for parallel transmission lines using local measurements," *Electr. Power Syst. Res*. vol. 108, pp.68-73, Mar. 2014.

[109] P.Dutta, A. Esmaeilian, M. Kezunovic "Transmission-line fault analysis using synchronized sampling," *IEEE Trans. Power Del.*, vol. 29, no. 2, pp. 942-950, Apr. 2014.

[110] N. Kang, J. Chen, Y. Liao "A fault-location algorithm for series-compensated double-circuit transmission lines using the distributed parameter line model," *IEEE Trans. Power Delivery*, vol. 30, no. 1, pp. 360-367, Feb. 2015.

[111] X.Jiao and Yuan Liao "Accurate fault location for un-transposed/transposed transmission lines using sparse wide area measurements," *IEEE Trans. Power Del.*, vol. 31, no. 4, pp.1797-1805, Aug. 2016.

[112] S.G. Di Santo, and de Morais Pereira, "Fault location method applied to transmission lines of general configuration", *International Journal of Electrical Power & Energy Systems,* vol. 69, pp. 287-294, Jul. 2015.

[113] A. Yadav and A. Swetapadma "A single ended directional fault section identifier and fault locator for double circuit transmission lines using combined wavelet and ANN approach," *International Journal of Electrical Power & Energy systems*, vol. 69, pp. 27-33, Jul. 2015.

[114] A.Swetapadma and A. Yadav "lmproved fault location algorithm for multi-location faults, transforming faults and shunt faults in thyristor controlled series capacitor compensated transmission line," *IET Gen., Trans. & Dist.*, vol. 9, no. 13, pp. 1597-1607, May 2015.

[115] A.S.Dobakhshari and A.M.Ranjbar "A novel method for fault location of transmission lines by wide-area voltage measurements considering measurement errors," *IEEE Trans. Smart Grid*, vol. 6, no. 2, pp.874-884, Mar. 2015.

[116] A.Yadav and A.Swetapadma "Enhancing the performance of transmission line directional relaying, fault classification and fault location schemes using fuzzy inference system," *IET Gen., Trans. & Dist.*, vol. 9, no. 6, pp. 580-591, Feb. 2015.

[117] N.Roy and K.Bhattacharya "Detection, classification, and estimation of fault Location on an overhead transmission line using S-transform and neural network," *Electric Power Components and Systems*, vol. 43, no, 4, pp.461-472, Feb. 2015.

[118] B.Mahamedi, M.S.Pasand, S.Azizi, J.G.Zhu "Unsynchronized fault-location technique for three-terminal lines," *IET Gen., Trans. & Dist.*, vol 9, no. 15, pp. 2099-2107, Jun. 2015.

[119] C.Fan, K. K. Li, W. L. Chan, W. Yu "Study of protection scheme for transmission line based on wavelet transient energy," *International Journal of Electrical Power & Energy Systems*, vol. 28, no. 7, pp. 459-470, Sep. 2006.

[120] H.Gao and P.A.Crossley, "A new current differential protection scheme for teed transmission lines," *IEEE Power Engineering Society General Meeting*, pp. 6-pp, Jun. 2006.

[121] B.Bhalja and R.P.Maheshwari, "Wavelet-based relaying scheme for tapped transmission line", *Electric Power Components and Systems*, vol. 37, no. 8, pp. 879-893, Jun. 2009.

[122] S.R. Samanta Ray "A systematic fuzzy rule based approach for fault classification in transmission lines," *Applied Soft Computing*, vol. 13, no. 2, pp. 928-938, Feb. 2013.

[123] M.T.N.Dinh, M.Bahadornejad, A.S.Al Shahri, and N.K.C.Nair "Protection schemes and fault location methods for multi-terminal lines: A comprehensive review," in *IEEE innovative Smart Grid Tech*. Asia (ISGT Asia), pp. 1-6, Nov. 2013.

[124] K.Ramar, H.S.Low, E.E.Ngu "One-end impedance based fault location in double-circuit transmission lines with different configurations," *International Journal of Electrical Power and Energy Systems*, vo. 64, pp. 1159-1165, Jan. 2015.